A Dissertation for the Degree of Doctor of Philosophy

Pulse Frequency Dependency of Photobiomodulation on Osteogenic Differentiation of Human Dental Pulp Stem Cells

펄스변조 광생물조절이
치수줄기세포의 골형성 분화에
미치는 효과 연구

February 2018

Hong Bae Kim

Department of Biosystems &
Biomaterials Science and Engineering
Major in Biosystems Engineering
Seoul National University

Pulse Frequency Dependency of Photobiomodulation on Osteogenic Differentiation of Human Dental Pulp Stem Cells

Advisor: Prof. Jong Hoon Chung

Submitting a Ph.D. Dissertation
of Public Administration

February 2018

Department of Biosystems &
Biomaterials Science and Engineering
Seoul National University
Major in Biosystems Engineering

Hong Bae Kim

Confirming the Ph.D. Dissertation written by
Hong Bae Kim

Chair	김 기 석
Vice Chair	정 종 훈
Examiner	정 준 호
Examiner	주 철 민
Examiner	임 기 택

Abstract

Photobiomodulation (PBM) therapy contributes to pain relief, wound healing, and tissue regeneration. The pulsed wave (PW) mode has been reported to be more effective than the continuous wave (CW) mode when applying PBM to many biological systems. However, the reason for the higher effectiveness of PW-PBM is poorly understood. Herein, it suggest using delayed luminescence (DL) as a reporter of mitochondrial activity after PBM treatment. DL originates mainly from mitochondrial electron transport chain systems, which produce reactive oxygen species (ROS) and adenosine triphosphate (ATP). The decay time of DL depends on the pulse frequencies of applied light, which correlate with the biological responses of human dental pulp stem cells (hDPSCs). Using a low-power light whose wavelength is 810 nm and energy density is 38 mJ/cm^2, it find that a 300-Hz pulse frequency prolonged the DL pattern and enhanced alkaline phosphatase activity. In addition, it analyze mitochondrial morphological changes and their volume density and find evidence supporting mitochondrial physiological changes from PBM treatment. Our data suggest a new methodology for determining the effectiveness of PBM and the specific pulse frequency dependency of PBM in the differentiation of hDPSCs.

In addition, duty cycle and pulse frequency of PW were empirically verified based-on-expanded biology experiment. To do such this, it applied 810 nm LPL of 128 μW/cm^2 energy density *in vitro*. Upon this value, CW irradiation did not induce any significant changes for differentiation of hDPSCs. However, the membrane hyperpolarization, alkaline phosphatase activity, and intracellular oxidative stress were largely enhanced in the PW with 30 % of duty cycle and 300-3000 Hz frequencies-LPL in which LED driver work in the form of square wave. After 21 days of daily LPL treatment, Western blot revealed the dentinogenesis in this condition *in vitro*. This study demonstrates that the very low power light at 810 nm enhanced significant differentiation of hDPSCs in the PW mode and there were duty cycle dependency as well as pulsing frequency dependency in the efficiency.

Meanwhile, together with NIR, blue light has been known to induce differentiation of stem cells. In order to enhance the effectiveness of PBM the blue light is incorporated into NIR-PBM. PBM has almost been used in the region of red or near infrared (NIR) whereas the blue light does not frequently due to inducing disrupt cellular processes. Photoacceptor for NIR is

cytochrome c oxidase and is Flavin for blue light in the mitochondrial electron transport chain system. The delayed luminescence (DL), in which radiate light after expose light to cells, originate from cytochrome c oxidase in the region of NIR and from flavins in the region of blue light. Correlation between PBM and NIR and blue light-induced DL for hDPSCs was employed to investigate an optimal excitation to differentiate the cells. The DL showed that the NIR with blue-light-pre-irradiation exerted better excitation than the others (only NIR or blue light) in pulsed wave mode that their energy density was 89 mJ/cm^2. In blocking complex I with rotenone, the DL was all decreased in excitation for NIR, blue light and blue-then-NIR light, while Antimycin A-bloocked-complex III DL was preserved for only NIR. It suggests that photoacceptor of blue light may be in complex I and III simultaneously whereas in complex III for NIR. As for differentiation of hDPSCs, it showed that alkaline phosphatase (ALP) activity was highly expressed for blue-then-NIR light. ROS and RT-PCR data support the result of ALP activity.

Based on the results *in vitro*, PBM was applied to Beagle's teeth in order to verify formation of dentin *in vivo*. A dentin formation was produced to be up to 20 % increment compared to the control that was not exposed to NIR and also induced dense periodontal ligament (PDL) after 8 weeks of exposure of NIR to teeth. It was observed that odontoblast subjected to NIR light exposure was active, generating new tubular dentin along with older dentin. Notably, such active odontoblast was not observed in controls, even though odontoblast-like layer whereby dentin structure was there in SEM analysis. It suggests that such a strategy might facilitate treatments relating to the diseases of dentin and PDL in mature permanent teeth. In summary, PW-PBM was more effective than CW-PWM in differentiating hDPSCs into osteogenesis. Duty cycle 30% and pulse frequency 300 Hz was effective among PW-frequencies. Blue-light-incoporated NIR induced much more differentiation than when only NIR applied. Beagle test verified dentin formation by means of PW-PBM.

Keyword : Photobiomodulation, Pulse frequency, Delayed luminescence, Osteogenic differentiation, Human dental pulp stem cell, Cytochrome c oxidase

Student Number : 2014-30404

Table of Contents

List of Tables

List of Figures

PBM was plotted with theoretical fittings. DL was measured when hDPSCs were in PBS with no treatment **(A),** with pre-treatment in rotenone **(B),** with pre-treatment in AMA **(C),** and with pre-treatment in NAC **(D)**.

Figure 2.4 The temporal trend of the decay probability *P(t)* **(A, C, E, G)** and the degree of excitation *n(t)* **(B, D, F, H)** from the DL shown in Fig. 2.3. Data were analyzed from the DL measured when hDPSCs were in PBS with no treatment **(A, B)**, with pre-treatment in rotenone **(C, D)**, with pre-treatment in AMA **(E, F)**, and with pre-treatment in NAC **(G, H)**. The time scales of the *P(t)* were changed for clear discrimination.

Figure 2.5 Confocal microscopic images of mitochondria in hDPSCs 3 days after PBM treatments. Nuclei were stained with 4',6-diamidino-2-phenylindole (DAPI), and mitochondria were stained with MitoTracker Red. Control hDPSCs **(A–C)**, hDPSCs exposed to 3-Hz PW **(D–F)**, and hDPSCs exposed to 300-Hz PW **(G–I)** were visualized. The scale bar is 10 μm.

Figure 2.6 (A) Representative TEM images of mitochondria in hDPSCs after 7 days of incubation under osteogenic medium, 7 days after PBM treatment. hDPSCs (control, treated with 3-Hz PW-PBM, and treated with 300-Hz PW-PBM) were compared. The areas marked with white rectangles (a, c, e) were magnified (b, d, f). **(B)** Quantitative analyses of the number of mitochondria per area, mitochondrial volume density per cell, and mitochondrial length. **(C)** Magnified TEM image of mitochondria in control cells (a) and cells subjected to 300-Hz PW-PBM.

Figure 3.1 An optical device that carries light energy to objects. **A.** A schematic of the device which is composed of LEDs as a light source, and a reflector, a light-guider and a diffuser to make the exposure light uniform. **B.** A photo of the LED source part, from where light travels through a light-guide and becomes uniform at some distance. **C.** Photos of the device with increasing driving voltage. Samples were put within the marked area with dotted rectangle. The variance of light intensity within this area was under 3.9 %. **D.** LEDs irradiated only near infrared 810 nm light. **E.** Applied voltage was modulated in the form of 1 Hz square waves with different duty cycles.

Figure 3.2 Effects of power and duty cycle of PBM on hDPSC cytoplasmic membrane potential, metabolic activity and ALP activity. **A.** FLIPR fluorescence intensities of hDPSCs relative to control after 1 Hz PW-PBM treatment with different duty cycles 0.3 to 60 % (n = 3 in each experiment and 3 replicates). **B.** FLIPR fluorescence intensities of

hDPSCs relative to control after 77 mJ/cm^2 CW-, 77 mJ/cm^2 PW-, or 2,310 mJ/cm^2 PW-PBM with 30 % duty cycle. The statistical analysis between CW and PW with 77 mJ/cm^2 indicated *P* expressed 0.033 (n = 3 in each experiment and 3 replicates). **C.** WST-1 assay absorbance relative to control after CW and 1 Hz PBM treatment with 30 % duty cycle. *P* values between CW and PW (1 Hz) was all under 0.001 (n = 10 in each experiment and 3 replicates). **D.** ALP activity absorbance relative to control after 77 mJ/cm^2 and 2,310 mJ/cm^2 1Hz PW-PBM applied energy density with 30 % duty cycle. *P* values between 77 mJ/cm^2 and 2.3 J/cm^2 in PW mode was significant (n = 10 in each experiment and 3 replicates).

Figure. 3.3 Effects of frequency of PW-PBM on hDPSC cytoplasmic membrane potential, metabolic activity, and ALP activity. **A.** FLIPR fluorescence intensities of hDPSCs relative to control just after 77 mJ/cm^2 PW-PBM in 1, 3, 30, 300, or 3000 Hz with same 30 % duty cycle (n = 3 in each experiment and 3 replicates). **B.** Metabolic activities of hDPSCs relative to control for 3 days after 77 mJ/cm^2 PW-PBM in 1, 30, 300, or 3000 Hz with same 30 % duty cycle (n = 10 in each experiment and 3 replicates). **C.** ALP activity absorbance relative to control for 7 days after 77 mJ/cm^2 PW-PBM in 1, 30, 300, or 3000 Hz with same 30 % duty cycle. NAC was added for the case of 300 Hz PW-PBM (n = 10 in each experiment and 3 replicates).

Figure. 3.4 Effects of frequency of PW-PBM on intracellular ROS, mitochondrial activity, intracellular ATP of hDPSCs, changes in the nuclear transcriptional levels, and cell cycle cycles. PBM conditions were 1, 3, 30, 300, or 3000 Hz PW-PBM with same 30 % duty cycle and 77 mJ/cm^2 total energy density, and NAC was for the case of 300 Hz PW-PBM. Cells were stained by the following dyes; **A.** H2DCFDA, **B.** MitoSOX, **C.** JC1, and **D.** ATP-luciferase. All the values were expressed as relative intensities to control. Intracellular ROS, mitochondrial membrane potential, and intracellular ATP increased, while mitochondrial superoxide decreased. hDPSCs were treated by PW-PBM of 1, 3, 30, and 300 Hz PW-PBM with 30 % duty cycle daily for 3 days (n = 3 in all each experiment and 3 replicates). **E.** mRNA transcriptional levels for SOD1, SOD2, BAX, and TGF-β1. There was no statistics (n = 3 in each experiment and 3 replicates). **F.** The population ratio in each cell cycle was not changed significantly. Increase of intracellular ROS affects the transcription of redox

contolling genes, however it did not induce apoptosis or cell cycle arrest. There was no statistics (n = 3 in each experiment and 3 replicates).

Figure. 3.5 Dentinogenic differentiation of hDPSCs after 21 days of PBM daily treatment. 300 Hz PW-PBM with duty cycles 30 % and 77 mJ/cm^2 total energy density were applied. **A.** Bright field images of hDPSCs stained with ALP staining kit at 21 after 30 %-3Hz-PBM daily irradiation. **B.** ALP activity absorbance relative to control (n = 3 in each experiment and 3 replicates). **C.** Western blots (W.B.) for ALP, DMP1, OPN, OCN, and BSP. **D.** Bar graph showing mean density relative to beta-actin by analyzing Fig.3.5C. The significance between controls and the PBM was all much lower than 0.05 (n = 3 in each experiment and 3 replicates).

Figure 4.1 PBM system. **(A) (B)** PBM system in incubator. PBM system irradiate NIR light (810 nm) and blue light (405 nm) in separate. LED for NIR light is separated to be 12.5 mm in distance and LED for blue light 25 mm. To aim uniform of lights on the plate, the LED assembly is distant to the plate to be 210 mm. Light from LEDs exposes to cell plate. **(C)** Design for exposing is that NIR is 89, blue and NIR light (BN1) is alternately 1.2 and then 87.8, BN2 is 3.6 and then 85.4, and BN3 is 12 and then 77 mJ/cm^2.

Figure 4.2 DL data from hDPSCs in responses to PBM treatment. The measured DL in the period between 1 s and 18 s after PBM treatment were plotted. DL was measured when hDPSCs were in PBS with no treatment **(A)**, with pre-treatment in antimycin-a **(D)**, with pre-treatment in rotenone **(G)**, and with pre-treatment in NAC **(J)**. The degree of excited level *n(t)* **(B, E, H, K)** and the temporal trend of the decay probability *P(t)* **(C, F, I, L)** from DL. The time scales of the *n(t)* and *P(t)* were changed for clear discrimination.

Figure 4.3 Proliferation and differentiation of hDPSCs by means of PBM treatment. **(A)** Proliferation of hDPSCs was assessed by WST-1 for 3 days. (n=6 per group, two-way ANOVA) **(B)** Alkaline phosphatase activity was measured at 3, 7, and 14 days after PBM treatment. (n=6 per group, two-way ANOVA). **(C)** Calcium deposition during matrix mineralization was assessed by Alizarin Red S (ARS) staining at 14 and 21 days after PBM treatment. **(D)** Quantitative analysis of **(C)** ARS staining was performed with destaining solution for ARS (n=6 per group, two-way ANOVA). *** $P < 0.001$ in one group, #$P < 0.05$,

List of Abbreviations

PBM	Photobiomodulation
LLLT	Low level light therapy
NIR	Near infra-red
LED	Light emitting diode
ATP	Adenosine triphosphate
mtNO	mitochondria synthesize nitric oxide
CCO	Cytochrome c oxidase
MMP	Mitochondrial membrane potential
PW	Pulsed wave
CW	Continuous wave
DL	Delayed luminescence
ROS	Reactive oxygen species
hDPSCs	Human dental pulp stem cells
BN1	Blue light
PDL	Periodontal ligament
cAMP	Cyclic adenosine monophosphate
AP1	Activator protein-1
PKA	Protein kinase A
CREB	cAMP response element-binding protein
CNGC	Cyclic nucleotide-gated channels
NF-kB	Transcription factor nuclear factor kappa B
SHED	Human exfoliated deciduous teeth
SCAP	Stem cells from apical papilla
SNTSCs	Human supernumerary tooth-derived stem cells
CFU-F	Colony-forming unit-fibroblast
AMA	Antimycin-A
DPBS	Dulbecco's phosphate-buffered saline
NAC	N-acetyl cysteine
ALP	Alkaline phosphatase
DAPI	4',6-diamidino-2-phenylindole
TEM	Transmission electron microscopy
UV	Ultraviolet
ETC	Mitochondrial electron transport chain
NADH	Nicotinamide adenine dinucleotide
CMP	Cytoplasmic membrane potential

MMP	Mitochondrial membrane potential
OPN	Osteopontin
DMP1	Dentin matrix protein1
OCN	Osteocalcin
BSP	Bone sialoprotein
SD	Standard deviation
SOD	Superoxide dismutase
Bax	Bcl-2-associated X protein
TGF-β1	Transforming growth factor-beta 1
PCR	Real-time polymerase chain reaction
COL1A	Collagen type 1a
DSP	Dentin sialoprotein
DGP	Dentin glycoprotein
DPP	Dentin phosphoprotein
H&E	Hematoxylin-eosin

Chapter 1

Photobiomodulation

1.1 Light

1.1.1 Brief of light

Light is an electromagnetic field consisting of oscillating electric and magnetic disturbances that can propagate as a wave through a vacuum as well as through a medium. In addition, in terms of the modern quantum theory light has a particle nature as energy packets called photons. This dual-character description of light is represented in Table 1.1. In this particle view of light, the brightness of the light is the number of photons, the color of the light is the energy contained in each photon, and four numbers (X, Y, Z and T) are the polarization, where X, Y, Z are the directions and T is the time.

All electromagnetic waves travel with the same speed in a vacuum. In a medium such a biological material, the speed of an electromagnetic wave, often labeled as ν, is different. The ratio of the two speeds c and ν is called the refractive index, n, of the medium. In other words, c/ν = speed of light in a vacuum / speed of light in a medium = n or $\nu = c/n$. Therefore, n can be viewed as the resistance offered by the medium toward the propagation of light. The higher the refractive index, the lower the speed.

1.1.2. Light as photon particles

The interaction of light with particles of matter involves the exchange of energy as well as momentum. These processes can only be described by assuming that the light also behaves like particles called photons. As described in Table 1.1, a photon for a light of a specific frequency ν has a discrete, fixed energy of value $h\nu$, where h is a constant (Planck's constant) having a magnitude of 6.63×10^{-34} Js. Thus the energy of an electromagnetic wave is quantized (discrete) and is not continuously variable. The smallest energy of an electromagnetic wave is equal to that of a photon. The total energy E is equal to then $Nh\nu$, where N is the number of photons, resulting in the equation $E = Nh\nu$. The quantized energy aspect of a photon is used in the description of absorption, emission, or scattering of light by matter.

Photons as particles also carry momentum (a physical quantity described by the product of the mass and the velocity of the particle). As described in

Table 1.1, the momentum, p, of a photon is given as $p = h/\lambda = h\nu/c$. The momentum aspect of a photon comes into play when a photon changes its direction of propagation while scattered by another particle or when it is refracted at the surface of a medium. This change of direction of photon propagation creates a change in momentum and can produce a force to trap a particle.

1.1.3 Different light sources

The different light sources available are described in Table 1.2.

1.1.4 Nature of interactions

Biological systems are molecular media. For such a medium the interaction with light can be described by the electronic polarization of a molecule subjected to an electric field. The linear field response, which is defined by linear dependence of the dipole moment on the electric field, gives the total molecular dipole as $\mu_T = -er = \mu + \alpha\varepsilon(\nu')$. μ_T is the total electronic dipole moment vector given by the product of the electronic charge e and its position r. The term μ is the permanent dipole term in the absence of any field, and the term $\alpha\varepsilon(\nu')$ is the electric-field-induced dipole moment, μ_m, describing the polarization of the electronic cloud of a molecule in the field. In the case of polarization of the oscillating electric field $\varepsilon(\nu')$ of light, the induced polarization is characterized by the dynamic polarizability term α, which is a second rank tensor that relates the directions of two vectors, the electric field and, as in this case, the resulting dipole, μ_m.

The dipolar interaction V between the molecule and a radiation field can be described as $V = \varepsilon(\nu')\mu + \varepsilon(\nu)\alpha\varepsilon(\nu')$. Here, the first term describes interaction with a photon field of frequency ν leading to the phenonmem of absorption and emission of a photon by the molecule. The second term represents inelastic scattering, Raman scattering, where a photon of frequency is scattered inelastically by a molecule creating a photon of a different frequency ν' and exchanging the energy difference with the molecule. The energy diagrams in Fig. 1.1 describe these processes. The absorption process describes the transition from a quantized lower energy initial level, i, to a higher energy level, f, with the energy gap between them matching the photon energy. For electronic absorption, generally the initial electronic level i is the ground state. If the initial level is an excited level, the resulting absorption is an excited state absorption. The spontaneous emission process describes the retrun of the molecule from the excited state, f, to its lower energy state, i, by

Table 1.1. Dual character of light

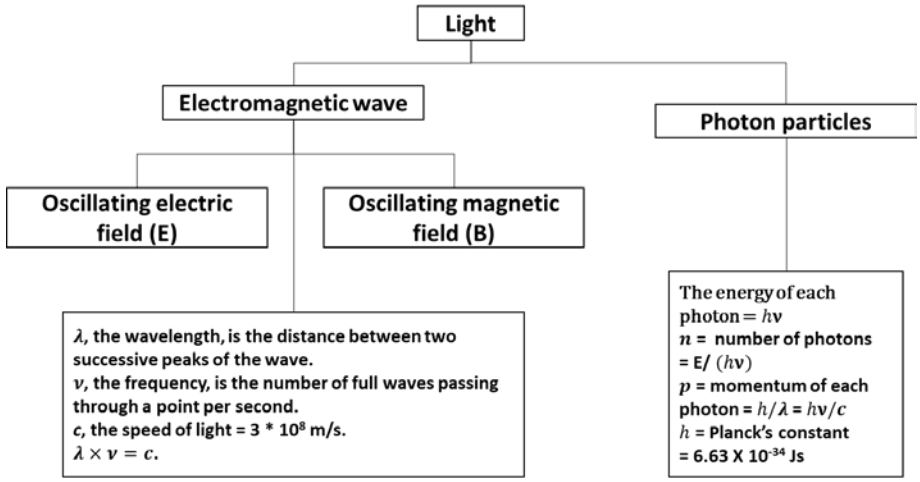

Table 1.2. Different light source and their characteristics

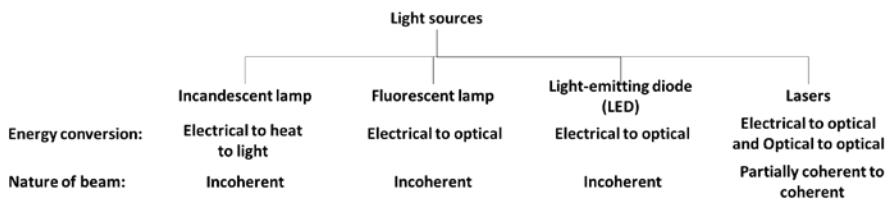

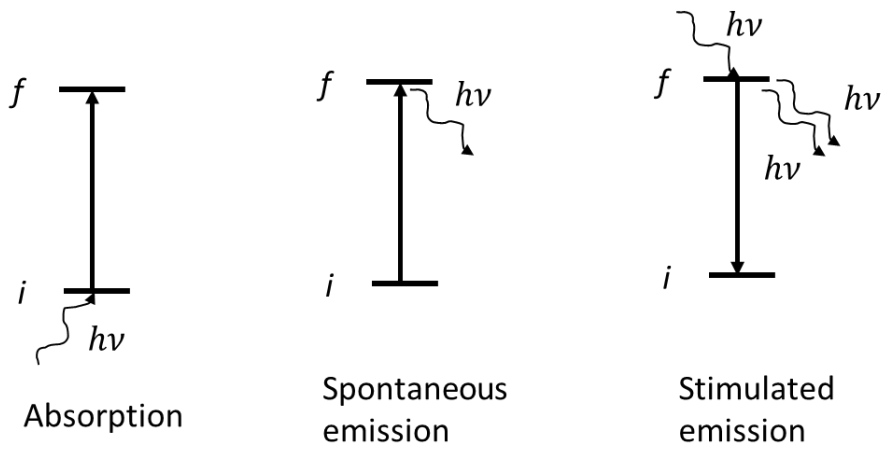

Figure 1.1 Schematics of various light-molecule interaction processes.

emission of a photon of energy corresponding to the energy gap between the two levels. The stimulated emission is a process of emission triggered by an incident photon of an energy corresponding to the energy gap between *i* and *f*. In the absence of an incident photon of same energy, there can be no stimulated emission, but only spontaneous emission. In study, the stimulated emission is to be used in analyzing delayed luminescence (DL).

1.1.5 Fate of excited state

The processes that can take place following an excitation created by light absorption, which takes a molecule to an excited state can be radiative, where a photon is emitted to bring the molecule back to the ground state. They can be nonradiative, where the excited-state energy is dissipated as a heat or in producing a chemical reaction (photochemistry). The return to the ground state may also involve crossing from one electronic level to another of lower energy, with the excess energy converting to vibrational energy by an interaction. Subsequently, the excess vibrational energy is converted to heat by coupling to translation. These processes are schematically represented in Table 1.3. In this table the star sign signifies that A is in the excited state. The processes of energy transfer and excited-state complex formation occur only when more than one molecule are interacting. Therefore, for such processes a minimum size molecular aggregate is a dimer (A2) or a biomolecular (AB) unit. An excimer [an excited-state dimer, (A-A)*] or an exciplex [an excited-state complex, (A-B)*] may return to the ground state radiatively (by emitting light) or nonradiatively.

Exciplexes are excited-state complexes formed between two different molecules (or molecular units), A and B, when one of them is excited. Exciplexes can form between aromatic molecules. Just like in the case of an excimer, the resulting emission from the exciplex (A-B*) is red-shifted, compared to that from A*. Of biological interest has been the exciplex formation between a metalloporphyrin and a nucleic acid or an oligonucleotide, which can provide structural information on the microenvironment of the metalloporphyrin [1, 2]. Exciplex formation has been studied for double-stranded phoynucleotides and natural DNA having regular double-helix structures. In study, the DL that is to be utilized present the light fade of excited state.

1.1.6 Light-dental tissue interaction

Light can interact with a tissue in four key ways: transmission, reflection,

Table 1.3. Schematic representation of processes involved in electronic excitation

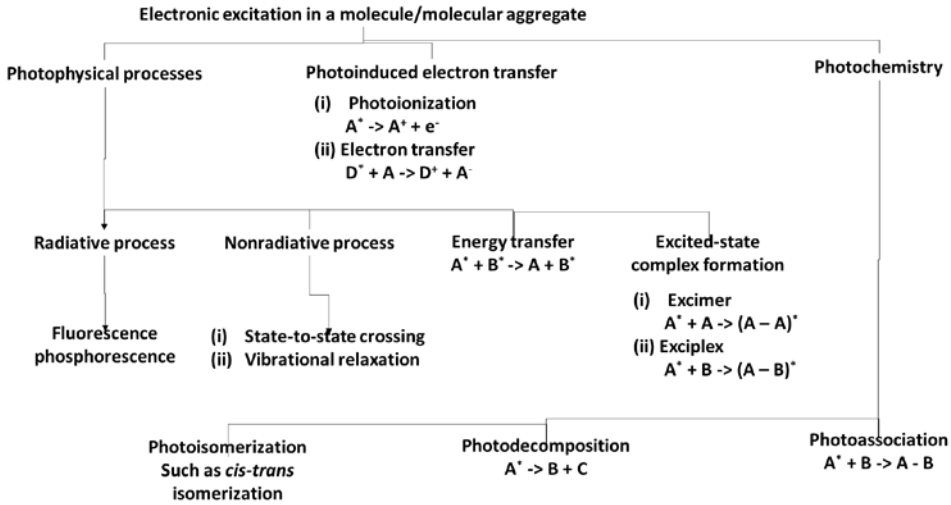

scattering, and absorption. Transmission refers to the passage of light through the tissue without having any effect on that tissue or on the properties of the light. Reflection refers to the repelling of light off the surface of the tissue without an entry into the tissue. Approximately 4 to 7 % of light is reflected off the tissue [3]. The amount of light reflected increases with increasing angle of incidence with the least reflection occurring when the light directed perpendicular to the tissue. Scattering of light occurs after light has entered the tissue. Scattering is due to the heterogenous structure of tissue, with variations in particle size and the index of refraction between different parts of the tissue determining the amount of scatter. Scattering spreads out the light within the tissue, resulting in radiation of larger area than anticipated. Scattering also limits the depth of penetration because it can occur backward as well as forward. Light absorption is the fundamental goal of clinical light. According to the Grothus-Draper law, light must be absorbed by tissue to produce an effect in that tissue. The absorption of the photons of light is responsible for its effects on the tissue. The components of the tissue that absorb the photons preferentially depend on wavelength.

Dental hard tissues are inhomogeneous materials. Dental enamel is an ordered array of inorganic apatite-like crystals surrounded by a protein/lipid/water matrix. The crystals are approximately 30-40 nm in diameter and can be as long as 10 μm. The crystals are clustered together in ~4-μm-diameter rods, which are roughly perpendicular to the tooth surface. Dentin is a complex structure, honeycombed with dentinal tubules 1~3 μm in diameter. Each of these tubules is surrounded by a matrix of needle-shaped, hydroxyapatite-like crystals in a protein matrix largely composed of collagen. Because of the complex nature of these materials, the scattering and absorbing distributions are generally anisotropic and depend on tissue orientation relative to the irradiating light source [4].

Moreover, because of such dental optical properties of scattering and absorption, one of the fundamental challenges in applying light to dentistry is the high optical loss in dental tissue. In dental soft tissue, the 1/e optical penetration depth at which the light intensity drops to the 1/e level (37%) is less than 1 mm for visible and near-infrared radiation [5]. In dental hard tissue, there is not data on optical loss. About real measurement on dental hard tissue, the following chapter is to be dealt.

1.2 Photobiomodulation

1.2.1 Brief of photobiomodulation

Photobiomodulation (PBM), so-called low level light therapy (LLLT) is a form of light treatment that uses visible or near infrared (NIR) light with a power density (irradiance) between 1 mW ~ 5 W/cm^2. Evidence supporting potential uses in a variety of medical, dental, physical therapy and acupuncture have shown efficacy in reducing pain and in treatment of traumatic injuries, among others [6-11]. PBM is currently used clinically in the application of light to a pathology to promote tissue regeneration, reduce inflammation, and relieve pain. However, there is still a lack of consensus over its effectiveness as a clinical treatment. These uncertainties are largely centered over two major domains- biological and device parameters. A lack of thorough understanding of PBM mechanisms has prevented optimization of the large number of device parameters. Some of the key device parameter include wavelength, treatment distance, fluence, time, irradiance, pulsing and polarization [12]. Even though parameters in PBM is very important, it is not defined the effectiveness of PBM on biological systems.

1.2.2 Mechanism of PBM

1.2.2.1 Strategic mechanism of PBM

Most of the effects of PBM can be explained by light absorption within the mitochondria [13, 14]. Cells can contain up to several thousand mitochondria, which generate cellular energy, which is adenosine triphosphate (ATP) from oxygen and pyruvate. In addition, in stressed or ischemic tissues, mitochondria synthesize nitric oxide (mtNO) [15, 16], which competes and can displace oxygen from binding to cytochrome c oxidase (CCO), which is the terminal enzyme in the electron transport chain necessary for energy generation [17]. Here, CCO absorbs red and near-infrared light, mediating the electron transfer from cytochrome c to molecular oxygen. It seems that PBM increase the availability of electrons for the reduction of molecular oxygen in the catalytic center of CCO, increasing the mitochondrial membrane potential (MMP) and the levels of ATP, cAMP and ROS as well [18].

PBM increases the activity of complexes I, II, III, IV and succinate dehydrogenase in the electron transfer chain. CCO is known as complex IV and, as mentioned before, appears to be the primary photoacceptor. This assumption is supported by the increased oxygen consumption during low-

level light irradiation, and by the fact that sodium azide, a CCO inhibitor, prevents the beneficial effect of PBM. Besides ATP and cAMP, nitric oxide level is increased, either by release from metal complexes in CCO or by up-regulation of CCO activity as a nitrite reductase [19]. In fact, it was proposed that PBM might work through the photodissociation of NO from CCO, thereby reversing the mitochondrial inhibition of cellular respiration due to excessive NO binding [20]. NO is photodissociated from its binding sites on the heme iron and copper centers from Cox, where it competes with oxygen and reduces the necessary enzymatic activity. This allows an immediate influx of oxygen and, thus, the resumption of respiration and generation of reactive oxygen species. NO can also be photo-released from other intracellular sites, such as nitrosylated hemoglobin and myoglobin [21].

In addition, the retrograde mitochondrial signaling occurs with light activation in the visible and infrared range (Fig. 1.2). This activation of light increases mitochondrial membrane potential causing an increase in the synthesis of ATP and changes in the concentrations of reactive oxygen species (ROS), Ca2+ and NO. Furthermore, there is a communication between mitochondria and the nucleus, driven by changes in the mitochondria ultrastructure, i.e. changes in the fission-fusion homeostasis in a dynamic mitochondrial network. The alteration in the mitochondrial ultrastructure induces changes in ATP synthesis, in the intracellular redox potential, in the pH and in cyclic adenosine monophosphate (cAMP) levels. Activator protein-1 (AP1) and NF-kB have their activities altered by changes in membrane permeability and ion flux at the cell membrane. Some complementary routes were also suggested by Karu, such as the direct up-regulation of some genes [22].

There are secondary effect after PBM both *in vitro* and *in vivo*. An increase in intracellular ATP is one of the most frequent and significant findings after PBM. The stimulated synthesis of ATP is caused by an increased activity of CCO when activated by light. Extracellular ATP participates in a wide array of signaling pathways [23]. ATP purinergic signaling is mediated by P2Y G-protein-coupled receptors, and P2X ligand-gated ion channels. ATP can be hydrolyzed to adenosine that carries out signals via the P1 G-protein-coupled receptor [24]. Up to the present date extracellular ATP or adenosine can be stimulated by PBM. Several workers have shown an increase in adenosine-3',5'-cyclic-monophosphate (cAMP) after PBM [25]. This increase in cAMP is a direct consequence of the rise in ATP caused by light. cAMP exerts its cellular effects via activation of three different kinds of sensors: cAMP-dependent

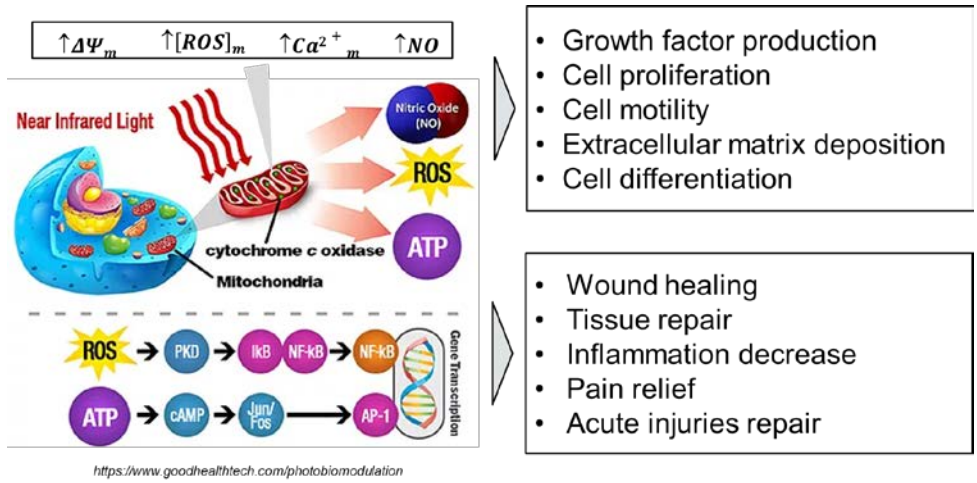

Figure 1.2 Scheme of mitochondrial retrograde signaling pathways.

protein kinase A (PKA) which phosphorylates and activates cAMP response element-binding protein (CREB), which then binds to CRE domain on DNA and in turn activates genes; cyclic nucleotide-gated channels (CNGC) and exchange proteins directly activated by cAMP. PBM can produce mitochondrial ROS leading to activation of the transcription factor nuclear factor kappa B (NF-κB), which can act as a redox-sensor. The fact that the addition of antioxidants inhibits the activation of NF-κB by 810 nm light reinforces this assumption [26]. There are many different cellular systems that are designed by evolution to detect excessive levels of ROS and activate transcription factors to produce extra levels of antioxidant defenses [27]. Hydrogen peroxide and lipid hydroperoxides [28] are thought to be the ROS most likely to carry out beneficial redox signaling by reversible oxidation of cysteine thiols in the sensor protein. Nitric oxide (NO) is often found to be produced after PBM [29] .

These secondary effectors by PBM have their proliferation levels. Keratinocytes showed an enhanced proliferation after 660 nm light irradiation, accompanied by an increased expression of Cyclin D1 and a faster maturation of keratinocytes in migration to the wound sites, via the expression of proteins involved in the epithelial proliferation process, namely p63, CK10 and CK14. This is useful for the improvement of epithelial healing [8]. These effectors also promote migration of cells. Tsai and co-workers evaluated the effect of 660 nm light on rat Achilles tendon-derived tenocytes, and found that dynamin-2 expression was enhanced and the migration was stimulated *in vitro* [30].

It appears that stem cells are particularly sensitive to light. PBM induces stem cell activity shown by increased cell migration, differentiation, proliferation and viability, as well as by activating protein expression [31]. Mesenchymal stem cells, usually derived from bone marrow, dental pulp, periodontal ligament and from adipose tissue, proliferate more after light irradiation (usually with wavelengths ranging from 600 to 700 nm). Min and co-workers reported that the cell viability of adipose-derived stem cells was found to be increased after irradiation with 830 nm light. Their *in vivo* results also revealed elevated numbers of stem cells compared to the control group [32]. Epidermal stem cells can also be influenced by light, as demonstrated by Liao et al. The authors reveal that 632.8 nm light has photobiological effects on cultured human epidermal stem cells, such as an increase in proliferation and migration *in vitro* [33]. Soares observed a similar effect on human periodontal ligament stem cells irradiated with a 660 nm diode laser [34].

1.2.2.2 Parameters of PBM

The light parameters and the does applied are fundamental in PBM. The most important parameters regarding the light source and the light doses are described in Table 1.4 and Table 1.5. PBM refers to the use of light in the red or near-infrared region, with wavelengths usually in the range of 600 to 700 nm and 780 to 1100 nm, and the laser or LEDs typically having an irradiance or power density between 5 mW/cm^2 to 5 W/cm^2. This type of irradiation can be a continuous wave or a pulsed light consisting of a relatively low-density beam (0.04 to 50 J/cm^2), but te output power can vary widely from 1 mW up to 500 mW in order not to allow thermal effects [35]. The wavelength range between 700 and 780 nm has been found to be rather ineffective as it coincides with a trough in the absorption spectrum of cytochrome c oxidase. Moreover red/NIR light is chosen because its penetration through tissue is maximal in this wavelength range, due to lower scattering and absorption by tissue chromophores.

Table 1.4 Description of the irradiation parameters.

Irradiation parameters		
Irradiation parameter	Measurement unit	Description
Wavelength	nm	Light is an electromagnetic form of energy with a wave-like behavior. Its wavelength is measured in nanometers (nm), and it is visible within the 400 ~ 700 nm range.
Irradiaance	W/cm^2	It can also be called Power Density or Intensity, and corresponds to the power (in W) divided by the area (in cm-2)
Pulse Structure	Peak power (W) Pulse frequency (Hz) Pulse width (s) Duty cycle (%)	If the beam is pulsed, the Power should be called Average power, which is calculated as follows: Arrange power (W) = Peak power (W) * pulse width (s) x pulse frequency (Hz)
Coherence	Coherence length Depends on special bandwidth	Cohereent light produces laser speckle, which is belived to paly an important role on photobiomodulation interaction with cells and organells
Polarization	Linear polarized or circular polarization	Polarized light is known to lose its polarity in highly scattering media such a biological tissues, therefore, this property is not considered very often on the effects of PBM

Table 1.5 Description of the light dose parameters.

Light dose parameters		
Irradiation parameter	Measurement unit	Description
Energy	Joules (J)	It cannot be mistook as dose, as it assumes reciprocity (the invserse relationship between power and time). It is calculated as: Energy (J) = power (W) X Time (s)
Energy density	J/cm^2	This is an important descriptor of dose, but it could be unreliable when we consider that it assumes a reciprocity relationship between irradiance and time
Irradiance time	s	Possibly the best way to prescribe and to record PBM would be to define the four parameters of table 1 and then define the irradiation time as the real "dose"
Treatment interval	Hours, days or weeks	Different time intervals may result in different outcomes, but more data need to be gathered in order to define the extent of the differences between them.

1.2.3 Application of PBM to dentistry

1.2.3.1 Oral and maxillofacial indications of PBM

Many trials of PBM relating to oral and maxillofacial indications were performed (Table 1.6).

Table 1.6 Oral and maxillofacial indications of PBM [36].

Oral specialty	Application	PBM effect
Endodontics	Dentinal hypersensitivity	Reduced tactile and thermal sensitivity
	Pulp	Improved dentin formation in the dental pulp
		Promotion of HDP cell mineralization
Maxillofacial	Bisphosphonate related osteonecrosis of the jaw	Reduced pain, reduced edema, pus and fistulas,
		improved healing
	Mandibular distraction	Improved bone trabeculation and ossification
	Mandibular advancement	Improved bone formation in condylar region
		Improved osteogenesis
	Temporo-mandibular joint disorder	Reduced pain
		Improved range of mandibular movement
	Trauma to the mandibular	Improved bone healing
Oral pathology	Burning mouth syndrome	Reduced symptoms, reduced pain
	HSV	Improved healing and reduced reoccurrence
	Lichen planus	Reduced lesion size, less pain
		As effective as corticosteroids
	Oral mucositis	Reduced incidence, duration and severity
	Xerostomia/dryness	Regeneration of salivary duct epithelial cells
		Improved salivary flow, improved antimicrobial
		characteristics
Oral surgery	Healing	Improved healing after gingivectomy, reduced gingival
		Inflammation
	Paresthesia/alveolar nerve	Improved mechanical sensory perception
	Third molar extraction	Reduced pain, reduced swelling, improved trismus
Orthodontics	Orthodontic pain	Reduced pain
		Faster remodeling
	Titanium implants	Improved healing
		Improved attachment
		Improved osseointegration
	Tooth movement	Accelerated tooth movement
		Improved osteoblast/osteoclast activity
		Improved collagen deposition
Pediatric	Cavity preparation	Reduced pain
	Mandibular distraction	Faster healing
	Gingivitis	
Periodontics	Chronic gingivitis	Reduced inflammation
		Improved healing
	Periodontal ligament	Increased early hyalinization
	Periodontitis	Improved pocket depth
		Less inflammation
Prosthodontics	Denture stomatitis	Reduced yeast colonies
		Reduced palatal inflammation
	Implants	Faster bone formation
		Improved bone–implant interface strength
		Improved osseointegration

1.2.3.2 Human dental pulp-derived stem cells

In 2000, dental pulp stem cells (DPSCs) were discovered stem cells in human dental pulp tissues of extracted impacted third molars for the first time in the world [37]. It was identified other types of human dental pulp-derived stem cells from dental pulp of human exfoliated deciduous teeth, root apical papilla of human teeth, and dental pulp of human supernumerary teeth, namely stem cells from human exfoliated deciduous teeth (SHED) [38], stem cells from apical papilla (SCAP) [39], and human supernumerary tooth-derived stem cells (SNTSCs) [40]. These all types of such cells commonly share characteristics as mesenchymal stem cells; self-renewal capacity, colony-forming unit-fibroblast (CFU-F) forming ability, high proliferation activity, expression of cell-surface markers-CD34, CD45, CD14, multipotency, *in vivo* tissue regeneration capacity, and immunomodulation.

1.2.3.3 Multipotency of human dental pulp-derived stem cell

Human dental pulp-derived stem cells are known to differentiate into mesenchymal lineage cells including onotoblasts, osteoblasts, chondrocytes, adipocytes, and myocytes [37-41]. Recent advantage of stem cell technology enables to induce human dental pulp-derived stem cells both into ectodermal lineage cells, such neural cells [37-40], and into endodermal lineage cells, such vascular endothelial cells [41], hepatocytes and pancreatic islet-insulin-producing beta cells [42] in Fig. 1.3.

1.2.3.4 Application of PBM to human dental pulp-derived stem cell

A few studies on hDPSCs of PBM were performed to proliferate. hDPSCs that were irraddated with the 20 mW (6 sec and 3 J/cm^2) setting presented significantly higher MTT activity at 72 hours, compared to control group [43]. Similarly, the dental pulp stem cells irradiated with an energy density of 1.0 J/cm^2 and power of 30 mW, exhibited an increase of cell proliferation, compared to the control group at 72 and 96 hours [44]. However, there was no significant difference in cell proliferation between 1.0 J/cm^2 and 0.5 J/cm^2 [44]. Contrary to the other experiments, Pereira et al., using different energy densities (0.05, 0.3, 7 and 42 J/cm^2), did not observe an increase in proliferation or odonto-osteogenic differentiation of hDPSCs isolated from patients with normal and inflamed dental pulps [45]. In addition, hDPSCs were differentiated into osteogenesis, chondrocyte and adipogenesis. PBM irradiation influences the *in vitro* increases the expression of essential proteins for bone formation [46]. Dose response analysis at 20-second

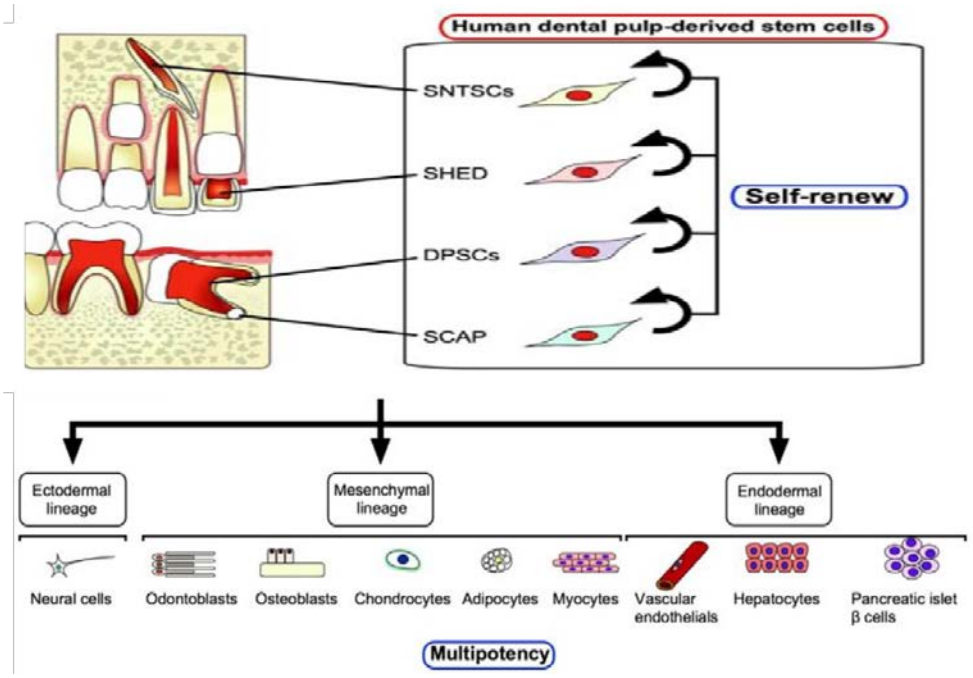

Figure 1.3 Origin, multipotency, and immunomodulatory function of human dental pulp-derived stem cells

intervals up to 120 seconds demonstrated that PBM significantly increased levels of *in vitro* mineralization at 21 days post-irradiation with 40 (149 mJ/cm^2) and 60 (224 mJ/cm^2) seconds of radiant exposure. This result was associated with significantly increased ATP, nitric oxide and mitochondrial metabolic activity [47]. The number of calcified nodules was increased by 1.0 W/cm^2 irradiation [48]. Characterization of PBM is listed up in Table 1.7. All together, these results pose challenges to define irradiation conditions to derive better effectiveness of PBM on biological systems.

Table 1.7 Characterisation of PBM on the proliferation of the hDPSCs.

Laser type (medium) /wavelength (nm)	Stem cells source	Power (mW)	Energy density (J/cm^2)	Number/duration of irradiation
InGaAIP/660	Human deciduous dental pulp	20 and 40	3	2 irradiations (0 and 6 h) 40 mW (3s) and 20 mW (6s)
InGaAiP/660	Human periodontal ligament	30	0.5 and 1.0	2 irradiation (0 and 48 h) after cell plating 16 s (0.5 j/cm^2) and 33 s (1.0 J/cm^2)
InGaAIP/660	Healthy and inflamed human dental pulp	28	0.05, 0.3, 7, and 42	Single irradiation, cells irradiated with a 1 mm dentin interposition between the cells and laser beam [10 s(0.05 J/cm^2) and 60 s (0.3 J/cm^2)] or irradiated directly [10s (7 J/cm^2) and 60 s (42 J/cm^2)].
InGaAIP/660	Human dental pulp	30	0.5 and 1.0	2 irradiations 90 and 48 h)
InGaAsP/810	Human dental pulp	60	0.1, 0.2, or 0.3	7 irradiations within 7 consecutive days, 6h after cell plating. The cells were irradiated every 24 h (each well for 60 s)
Non-specified diode laser/980	Human dental pulp	100	3	Single irradiation: 100 mW (60s)

1.3 Delayed luminescence

1.3.1 Delayed luminescence

Delayed luminescence (DL), so-called the photo-induced ultra-weak luminescence emitted by biological systems for long time (up to minutes) after the illumination source has been switched off, seems to be an excellent means for monitoring an optical status of biological systems, while fluorescence refers to light emission that rapidly fades within an extremely short time in the order of nanoseconds or picoseconds. The DL has a spectral emission lying from the optical range to near infrared and its intensity is various orders of magnitude ($10^3 \sim 10^5$) lower than the usual fluorescence. The DL connects to the repopulation of the excited singlet state via back reaction from an undefined metastable state, where the energy, lower than the excited singlet state, is stabilized. This connection gives DL emission to the formation of soliton states inside the quasi unidimensional polymeric chains that constitute the cytoskeleton. Moreover, the DL from solid state systems have confirmed this close connection between DL and structure of the emitting systems [49]. This connection brought DL in application to biological systems. The DL showed the possibility to discriminate between normal and tumor conditions [50-52] and to perform *in vivo* measurements of the mitochondrial oxygen tension [53-55].

The DL time trend generally follows a power law [56] and allows measuring this phenomenon until several seconds (or minutes in the case of biological systems provided with photosystem and/or longer illumination durations) after the stimulation end. Based on such trend, DL was modeled and explained DL data from experiment. The model is related to a large variety of biomolecules to be excited by incident light with diversity wavelength. Such biomolecules act as endogenous luminescence, demonstrating the mitochondrial origin of the DL signal [55, 57]. Mitochondria play a key role into controlling life and death, representing an essential component of many apoptotic pathways by releasing cytochrome c into the cytosol [58], in addition to their established role in generating energy for the cell. This support that DL is mainly produced within the mitochondrial electron transfer system (ETC). For theoretical approach of DL, it is dealt in chapter 2 for detail.

1.3.2 PBM and DL

PBM and DL share some interesting factors: visible and NIR photons, the mitochondrial electron transport chain, and the generation of ROS (oxygen tension). PBM can promote cellular metabolism via photostimulation of

elements of the mitochondrial electron transport chain [59]. PBM is thought to result in electron-excited states and the increased generation of ROS [60]. The mitochondrial ROS generation is likely one of the primary mechanisms involved in PBM. In human fibroblasts, PBM-induced proliferation was associated with real time transient increases in ROS production [60]. Antioxidant mechanisms have been shown to inhibit such PBM effects, further implicating the role of ROS in PBM signal transduction [61].

Moreover, a major source of DL is in the ETC. In fact, the metabolic processes involved in producing electronically excited states in DL-producing molecules are generally derived from oxidative metabolism accompanied by the production of ROS. With increasing generation of ROS by the mitochondrial electron transport chain, DL intensity increases. PBM can be used to induce the well-described oxidative burst in neutrophils, which occurs *in vivo* during phagocytosis [62]. During neutrophil phagocytosis and oxidative burst, the generation of ROS, involving excited singlet oxygen and excited carbonyl groups, leads to luminescence [62]. This luminescence has been investigated for its potential role in optically mediated neutrophil interactions [63].

1.4 Measurement of intensity into pulp chamber

Dental hard tissues are consisted of dental enamel, dentin and cementum. The primary mineral of enamel is hydroxyapatite, which is a crystalline calcium phosphate. Dentin consists of the mineral hydroxyapatite, which weighting 70% of one, while the rest is organic material. Cementum is slightly softer than enamel or dentin and consisted of nearly hydroxyapatite of half one. The hydroxyapatite as consisting mineral almost in dental hard tissues has higher refractive index among their composites: mineral, collagen, protein, and water [4]. An incident light toward such hard tissue undergoes severe scattering and absorbing including slightly transmitting. Despite there are a few theoretical approach for calculating these optical properties, such data does not reflect on *in situ*. For getting a measurement-based-optimal data of PBM toward *in vitro*, it is required to know the light intensity approaching at pulp chamber via enamel and dentin tissues. In order to measure the power density, second molars were got from out-patients after getting permission of Institutional Review Board Approval at the Seoul National University Hospital. These samples were measured with Vernier calipers for shortly width, length between shortly surface of the crown and site of pulp chamber. (Fig. 1.4-1.5 Table 1.8). To measure of the power penetrating the bilateral side of crown of a tooth to pulp

chamber via enamel and dentin tissue, a tip of optical fiber was inserted into pulp chamber through a hole that was made by driller with about 2-mm in diameter at one of both bilateral sides and another end of the fiber was vertically linked onto a sensor of power meter (PM100USB, Thorlabs, USA). Using a light source of LED (package size, 2 mm in diameter) in wavelength of 810 nm, measurements of the power was made in intensity of modulating the light source at one of bilateral sides of crown and pulp chamber in the ambient humidity at room temperature. Then, at end of both bilateral sides of top of the crown, the power was measured in intensity dependent manner. Then, the power loss at the pulp chamber *in vivo* was calculated from referencing a value whom the light was measured at bilateral side of the top of the crown *in vivo*.

The power density at the pulp chamber was revealed to be an average of about 18.4 times to that of both bilateral sides of the top of crown using the LED given above (Table 1.8). Thus *in vivo* power density in the pulp chamber through enamel and dentin material was computatively 426 ± 35.2 $\mu W/cm^2$ after calculating based on the density at opposite site of the light source (Table 1.9). This value is able to increase if utilizing brighter than that. This value gave us a determinant of light intensity for examining *in vitro*. Based on this measurement, the backlight produces emitting from diffuser to be power density of 426 ± 35.2 $\mu W/cm^2$. Under this condition, all the cell examinations were conducted

Table 1.8. Samples utilized in this study and ratio of power density at pulp chamber to short surface

Number	Age (years)	Distance of ① (mm)	Power density at ⓐ (uW/cm^2)	Power density at ⓑ (uW/cm^2)	Ratio of power density at pulp chamber to short width
1	40	5.01	32.18	1.86	17.30
2	45	5.82	29.78	1.20	24.81
3	49	5.02	31.47	1.80	17.48
4	45	4.8	31.75	1.95	16.28
5	45	4.62	32.46	1.95	16.64
6	47	4.92	31.47	1.72	18.30

Table 1.9. In situ samples utilized in this study and calculated power density at pulp chamber

Number	Age (years)	Short width of ② (uW/cm^2)	Ratio of power density	Calculated power density at pulp chamber in situ
1	45	25.25	18.4	464.6
2	46	24.50		450.8
3	48	19.95		367.08
4	48	24.20		445.28
5	42	23.00		423.2
6	49	22.30		410.32

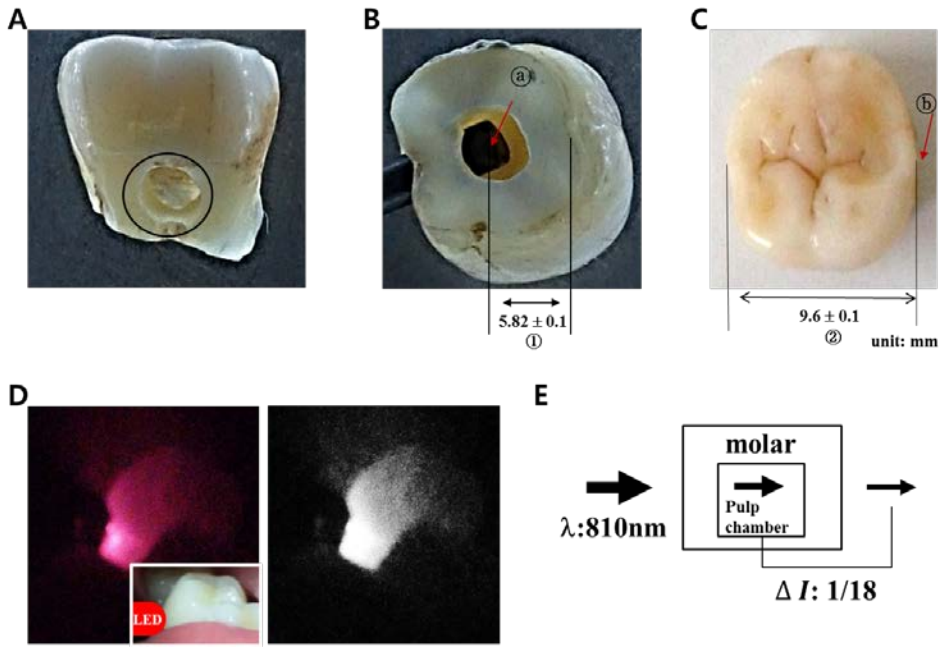

Figure 1.4. Representative optical characterization of second molar. A. A hole (circled) for inserting an optical fiber. B. Inserted an optical fiber and its site (indicated with ⓐ) in the pulp chamber for measuring NIR signals passing through dentin and pulp tissue. The optical fiber was linked with an optical sensor to measure intensity. ① indicates a width between center of the pulp chamber and a shortly surface of the bilateral side of crown. C. short-axis-length of the sample examined. ⓑ and ② indicates the site of contacting NIR's led for examination and a shortly width of the sample, respectively. D. NIR penetration into in situ the second molar (Left) and its inverse image (Right). LED site on the second molar (in box). E. The power density (intensity) of NIR is gradually weakened as passing through enamel and dentin layer. The final intensity of NIR traveling out to at the site of pulp chamber is one twenty-two.

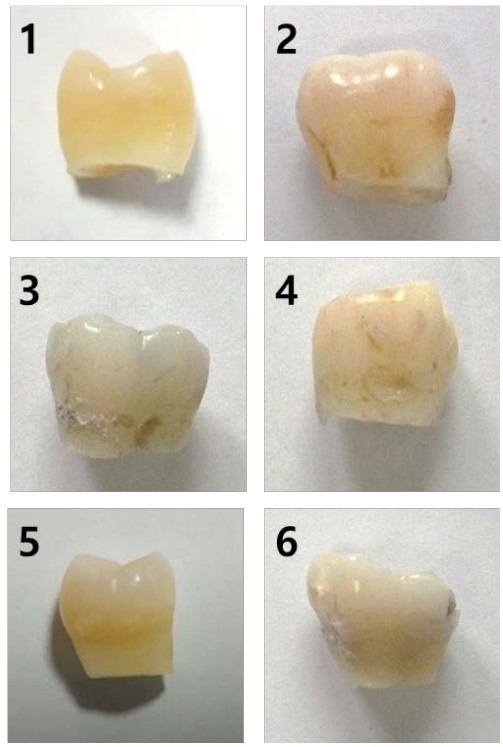

Figure 1.5. Optical characterized data of second molar. Samples that were used to optically be characterized.

1.5 Scope of the dissertation

In this thesis, first objective is to develop a mathematical model to assess the effectiveness of PBM on differentiation of human dental pulp stem cells. Second objective is to define photonic mode of PBM to drag out extremely effectiveness of differentiation. Third objective is to verify the PBM mode *in vivo*.

To do such things, a mathematical model was introduced to derive photonic conditions to get high effectiveness of PBM on differentiation of human dental pulp stem cells. The model has been widely used to attain the photonic signals from biological systems. However, In regard with differentiation of stem cells, it was not connected. For such model, a measurement was performed to get tooth specimen based-on-optimal data of PBM toward *in vitro* in the above. To do this, a system that propagate light energy to cells was developed being capable of modulating continuous wave (CW) or pulsed wave (PW) and pulse frequency, duty cycle and treatment time.

In chapter 2, we introduced delayed luminescence to investigate how pulse frequency PBM with a fixed duty cycle and energy density of 30 % and 38 mJ/cm^2, respectively, promote the induction of hDPSCs into osteogenic differentiation. In analyzing the effectiveness of PBM, mitochondrial mass was employed according to pulse frequencies.

In chapter 3, we verified the effectiveness of PBM on hDPSCs into differentiation of dentinogenesis, varying duty cycle of 0.3 to 60 % with increment of 10 times and pulse frequency *in vitro*. While the applied energy density of 38 mJ/cm^2 was used, here 77 mJ/cm^2 was applied.

In chapter 4, we describes the effects of combination of NIR with blue light on enhancing differentiation of hDPSCs. While blue light is shorter than NIR in wavelength, the photonic energy is a couple of NIR according to the equation of photonic energy ($\sim 1/\lambda$). In this chapter, the blue light was used to excite electrons in molecules higher energy levels and then NIR did to induce mitochondrial activation of promoting differentiation of hDPSCs.

In chapter 5, we verified effects of PBM *in vivo* using a Beagle model. The newly formation of dentin in terms of PBM that showed higher effectiveness of differentiation *in vitro* was assessed after 8 weeks of PBM. This result reflected *in vitro* result on *in vivo*.

Chapter 2

Pulse frequency dependency of photobiomodulation on the bioenergetic functions of human dental pulp stem cells

2.1 Introduction

PBM therapy generally uses light in the red or near-infrared (NIR) region, with wavelengths ranging from 600 to 700 nm and from 780 to 1,100 nm, respectively. The output power varies widely from 1 to 500 mW [35]. PBM has been shown to influence a wide variety of cellular functions, including gene expression, growth and proliferation, survival, and differentiation [64-68]. These functions are primarily mediated by raising the levels of adenosine triphosphate (ATP), which increases the mitochondrial membrane potential, cyclic adenosine monophosphate, calcium (Ca^{2+}), and reactive oxygen species (ROS) and activates transcription factors [18, 19]. Cytochrome c oxidase appears to be the primary photoacceptor and transducer of photosignals in these regions of the light spectrum [69]. The accepted light energy activates the cytochrome c oxidase and triggers a series of biochemical cascades that improve cellular functions [59].

PBM can be classified into two modes by its continuity: continuous wave (CW) and pulsed wave light (PW). Most previous studies have used CW-PBM to aggressively promote the proliferation and differentiation of stem cells[8, 66, 68, 70-82], beginning with dental treatment[80]. CW-PBM typically uses low power density, from 5 mW/cm^2 to 5 W/cm^2 [83], to prevent thermal effects in intracellular molecules. However, PW-PBM is more effective in maintaining an a-thermal environment due to the quenching periods, that is, OFF times. PW-PBM also enables the light to penetrate more deeply into a biological system than CW-PBM because it uses higher peak power while keeping the total energy the same [84]. In addition, PW-PBM can promote light–biological system interactions. Some fundamental frequencies in biological systems, in the range of tens to hundreds Hz, are similar to the pulsing frequencies used in PW-PBM[84].

On the other side, the responsiveness of biological systems to PBM can be identified using delayed luminescence (DL), which is measured in the form of optical photons emitted after the illumination source is switched off. Thus, DL

is a spectral emission from the optical range to NIR, and its intensity is various orders of magnitude [85]. DL demonstrates cellular reduction/oxidation (redox) states in relation to cytochrome c oxidase, which produces ROS in the mitochondrial respiratory chain [53, 55]. Because the cellular redox state appears to differ in the proliferation and differentiation phases of a cell, DL can be used to determine cellular phases [86-88]. The cellular phase is associated with further transient increases in cellular ROS production, which also affects DL [89].

In this study, we used DL to monitor the responses of stem cells to an in-house-fabricated laser device (Fig. 2.1) with a light wavelength of 810 nm and an energy density of 38 mJ/cm^2. The physiological states of hDPSCs were assessed after PBM treatment and compared with DL signals. PW-PBM induced more significant changes in the differentiation of hDPSCs and created longer-lasting DL from the cells than CW-PBM. In addition, specific pulse frequency dependencies appeared. These results suggest that the pattern of PBM, in addition to the light intensity, could be important for biological applications.

2.2 Materials and methods

2.2.1 Cell culture

hDPSCs were isolated from a tooth obtained following Institutional Review Board approval at Seoul National University Hospital (Seoul, South Korea; IRB number 05004). All three patients consented to the use of their teeth for research purposes, and no information about those patients is included in this article. This article does not contain information or images that could lead to the identification of study participants. All methods performed here were in accordance with the relevant regulations. The tooth was dissected aseptically and incubated with 4 ml of 0.25% trypsin-EDTA (Life Technologies) at 37 °C for 30 min. After neutralization with 4 ml of complete medium, solutions were pipetted vigorously to release cells and then passed through a cell strainer (70 mm, Corning). The resulting cells were cultured in complete medium supplemented with 100 mM ascorbic acid (Sigma). hDPSCs were cultured in a 37 °C incubator with 5% CO^2 in complete medium composed of 10% fetal bovine serum (FBS), Dulbecco's modified Eagle's medium, and penicillin (100 U/ml)–streptomycin (100 μg/ml) (all from Gibco, Life Technologies) and supplemented with 100 mM ascorbic acid.

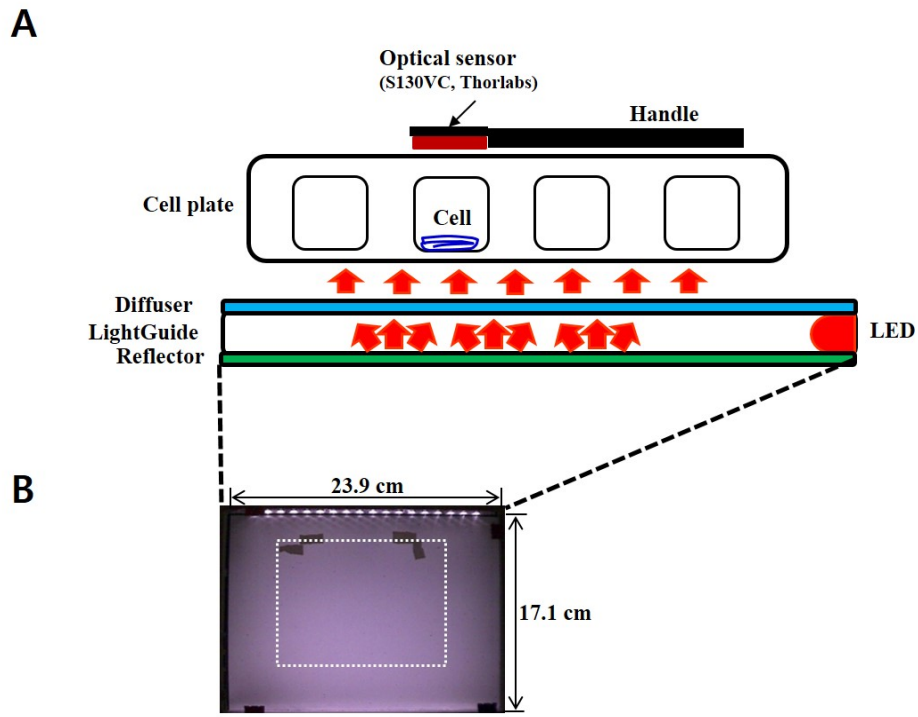

Figure 2.1 (A) Schematics of PBM device and DL detection system. The light from an LED traveled via a reflector, a light-guide, and a diffuser into cells in PBS. DL was measured on top of the cell culture plate during and after PBM. **(B)** A photograph of the PBM system with the homogenous center area marked with white dotted lines.

For differentiation of hDPSCs into an osteogenic linage, 10 mM β-glycerophosphate, 0.05 mM L-ascorbic acid-2-phosphate, and 100 nM dexamethasone were added to the complete medium.

2.2.2 PBM system and treatment

Unlike other light systems, our custom device was fabricated so that light from the LED propagated directly onto cells without a medium, removing the loss of light. It was composed of a diffuser, a light guide, a reflector, and an array of LEDs, as shown in Fig. 2.1. Seventeen LEDs whose wavelength was centered at 810 nm (PV810-3C6W-EDISAA, KAOS, Korea) were positioned at 1-cm intervals at one side the device. Light traveled through a disperser and a reflector, and the light intensity became uniform with a variance of less than 3.9% at the center area (marked with the white dotted square). The system was operated in a continuous wave (CW) mode or in a pulsed wave (PW) mode, with frequencies of 1, 3, 30, 300 Hz and 3 kHz. Constant DC voltage was supplied, and it was switched by an 8-bit micro controller device (UM_MC95FG308_V3.20_EN, Korea). The duty cycle was kept to 30% in all PW-PBM treatment modes. About 18.0 mA was applied to each LED, and the power density was 268 $\mu W/cm^2$. Power density (irradiance, W/cm^2) was measured by a power meter (PM-USB-100, Thorlabs, USA). The exposure time was determined so that the total energy was 38 mJ/cm^2 for all experiments. The light dose was checked before each experiment. For long term exposure for hDPSC differentiation, PBM was conducted every day.

2.2.3 Delayed luminescence spectroscopy

For DL spectroscopy, hDPSCs were first washed twice with DPBS to eliminate any influence of FBS. The light sensor (power range: 500 pW – 0.5 mW, S130VC, Thorlabs, USA), with a resolution of 37 ms per datum, was placed on the PBM system in a CO_2 incubator (MC-20A, Science & Technology Inc., Korea) in darkness for 30 min to remove natural luminescence. The light sensor's area for detection was similar to the diameter of a 24-well plate.

To inhibit the mitochondrial respiratory chain components, it used 100 nM rotenone [90] and 4 μM antimycin-A (AMA) [91] to block the function of complex I and complex III, respectively, in the electron transport chain. hDPSCs were incubated with those solutions for 60 min, and then DL was measured. To test the role of ROS, the cells were treated with NAC for 30 min, and then DL was measured. All the measurements were conducted for 20 min, and all data were subtracted from the cell-free condition. The control (non-illuminated

cells) DL data are not presented because their intensity level (10^{-19} to 10^{-16} W/cm^2) was out of the range of the light sensor, representing spontaneous photon emissions [92] .

2.2.4 Mathematical description of light-induced DL as a probability distribution

The relaxation of a non-equilibrium state into the equilibrium of a complex system can be approximated by a power law [93]. The DL temporal trend for a biological system can be modeled by a hyperbolic function, as given [50]:

$$I(t) = \frac{I_0}{\left(1 + {}^{t}/_{t_0}\right)^{m}} \tag{2.1}$$

where *I(t)* is the emitted intensity that can be obtained from the experimental data, I_0 is the initial value of the emitted intensity, *t* is time, and t_0 is an initial value.

DL intensity, *I(t)*, is associated through the decay probability, *P(t)*, with the degree of excitation, *n(t)*, that attenuates at any time *t* by the expression *I(t)* = - *dn(t)/dt* [93]. This can be evaluated for the value of a dimensionless function obtained from the experimental values of the intensity, *I(t)*, at a time *t*, as follows [93]:

$$P(t) = \left({}^{\frac{dn}{n}}\Big/_{\frac{dt}{t}}\right) = \frac{I(t)t}{n(t)} \tag{2.2}$$

where

$$n(t) = \int_t^{\infty} I(t')dt' \quad n(t) = -\left(\frac{I_0 t_0}{-m+1}\right)\left(1 + \frac{t}{t_0}\right)^{-m+1} \tag{2.3}$$

Using the data from Fig. 2.3, *P(t)* and *n(t)* are obtained.

2.2.5 Cell viability assay

hDPSCs were seeded in a 24-well plate with 2.5 × 10^4 cells/well or in a 96-well plate with 1.0 × 10^4 cells/well. 24 h after seeding, the hDPSCs were

exposed to PW-PBM. Cell viability was assessed 10, 24, 48, and 72 hours after PBM treatment using the WST-1 assay (EZ-cytox, EZ-3000, Korea), as previously described [94]. For these experiments, a plate reader (Tecan, USA) measured the absorbance at 450 nm.

2.2.6 Detection of intracellular ROS

To detect intracellular ROS in hDPSCs after PBM treatment, it used H_2DCFDA (Molecular Probes). hDPSCs were seeded in a 4-well plate with 5 × 10^4 cells/well. 24 h after seeding, the hDPSCs were exposed to PW-PBM. 20 minutes after starting the PBM treatment, the cells were incubated in media containing 10 μM H2DCFDA. After two washes with DPBS, the cells were incubated in complete medium for 30 minutes. Then the cells were trypsinized, and the fluorescence intensity was read via flow cytometry (BD Verse, Germany).

2.2.7 Alkaline phosphatase assay

hDPSCs were seeded in a 96-well plate with 5.0 × 10^4 cells/well in complete medium, and 24 h after seeding, they were treated with PW-PBM in osteogenic differentiation medium. 3, 7, and 14 days after PW-PBM treatment, ALP activity was assessed using the SensoLyte® pNPP Alkaline Phosphatase Assay Kit (AnaSpec, USA) following the manufacturer's instructions.

2.2.8 Electron transmission microscopy

To optimize mitochondrial structural preservation and membrane contrast, cells were fixed with 2% paraformaldehyde and 2.5% glutaraldehyde (Ted Pella, Redding, CA, USA) in 0.15 M sodium cacodylate (pH 7.4) at 37 °C and placed in pre-cooled fixative on ice for 1 h. The cells were post-fixed with 1% osmium tetroxide, 0.8% potassium ferrocyanide, and 3 mM calcium chloride in 0.1 M sodium cacodylate (pH 7.4) for 1 h, washed with ice-cold distilled water, post-stained with 2% uranyl acetate at 4 °C, dehydrated using graded ethanol, and embedded in Durcupan resin (Fluka, St. Louis, MO, USA). Ultrathin (70 nm) sections were post-stained with uranyl acetate and lead salts and observed using a JEOL 1200FX (JEOL, Japan) at 80 kV. Images were digitized at 1,800 dpi using a Nikon Cool scan system (Nikon Instruments Inc., USA), giving an image pixel array of 4,033 × 6,010 and a pixel resolution of 1.77 nm. Mitochondrial lengths were measured with ImageJ.

2.2.9 Mitochondrial bioenergetics

The mitochondrial mass was measured with MitoTracker® Red CMXRos (ThermoFisher Scientific), which binds to cardiolipin in the mitochondrial inner membrane. hDPSCs were seeded onto coverslips in a 4-well plate with 1.0×10^4 cells/well. 24 h after seeding, the hDPSCs were exposed to PW-PBM. 3 days after PBM treatment, the cells were incubated in serum-free medium containing 50 nM MitoTracker for 30 minutes. After washing with Dulbecco's phosphate-buffered saline (DPBS), cells were fixed with 4% PFA and observed with confocal microscopy (LSM-SP8X, Calzeiss, Germany).

To confirm the fluorescence data, the TEM images were analyzed. The mitochondrial volume density, defined as the volume occupied by mitochondria divided by the volume occupied by the cytoplasm, was estimated using stereology as follows. A 112 × 112 square grid (chosen for ease of use) was overlaid on each image in Photoshop (Adobe Systems Inc., USA), and the mitochondria and cytoplasm lying under the intercepts were counted. The relative volume of the mitochondria was expressed as the ratio of intercepts coinciding with this organelle relative to the intercepts coinciding with the cytoplasm.

2.2.10 Statistical analysis

Data were analyzed using Microsoft Excel. Means and standard deviations were calculated. Because many measurement variables in biology fit the normal distribution, we performed an unpaired two-sided student's t test for all data. All the experiments were repeated more than four times, and the standard deviations were plotted in the graph. It was considered results statistically significant when $P < 0.01$ and $P < 0.05$.

2.3 Results

2.3.1 PBM-mediated ROS production, proliferation, and alkaline phosphatase activity

To associate the cellular redox state with PBM, PBM-mediated ROS production was assessed. Increased production of ROS was observed in hDPSCs after treatment with 300-Hz PW-PBM ($P < 0.0095$), whereas no changes were noted after CW-PBM (Fig. 2.2A). Incubation with a ROS scavenger, N-acetyl cysteine (NAC), reduced ROS detection after 300-Hz PW-PBM (Fig. 2.2A). hDPSCs were subjected to CW- and PW-PBM treatment for 3

A

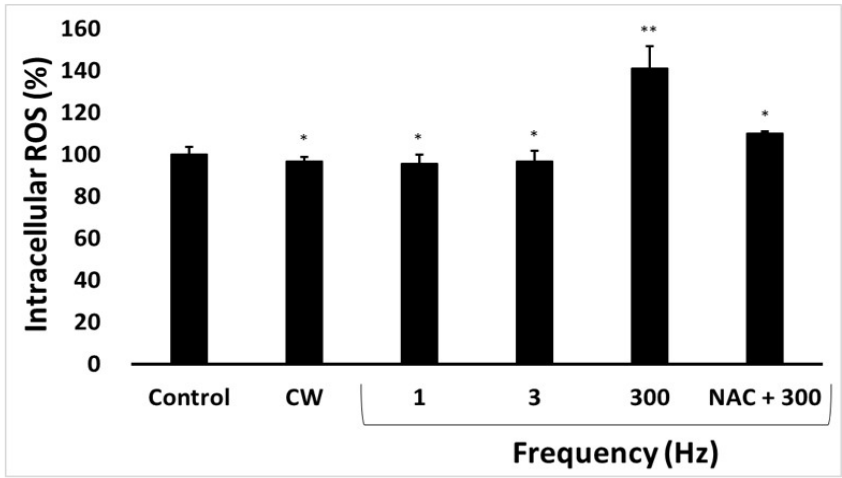
Intracellular ROS (%)
160
140
120
100
80
60
40
20
0
Control
CW
1
3
300
NAC + 300
Frequency (Hz)

B

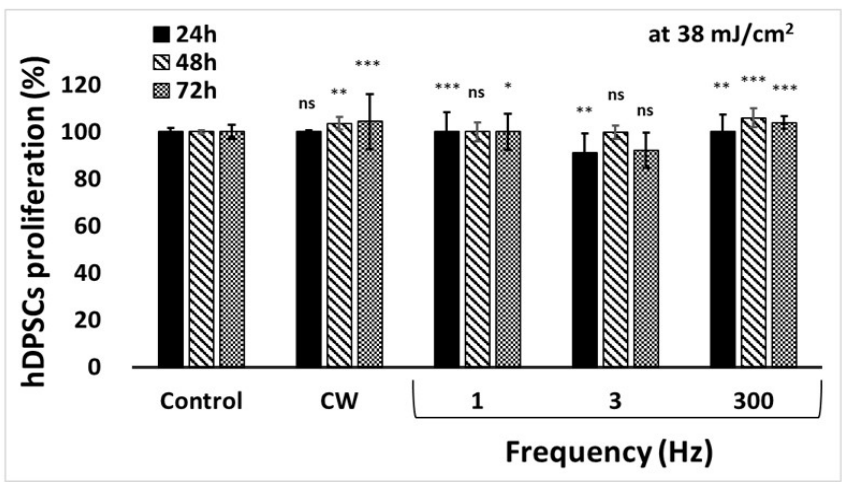
24h
48h
72h
at 38 mJ/cm²
hDPSCs proliferation (%)
120
100
80
60
40
20
0
Control
CW
1
3
300
Frequency (Hz)

C

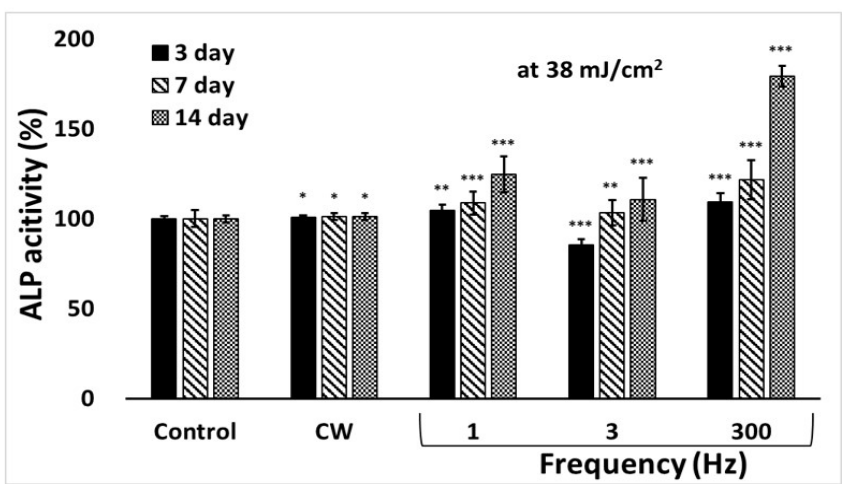
3 day
7 day
14 day
at 38 mJ/cm²
ALP acitivity (%)
200
150
100
50
0
Control
CW
1
3
300
Frequency (Hz)

Figure 2.2 Biological responses of hDPSCs to CW- and PW-PBM with different frequencies. **(A)** Intracellular ROS was measured with H2DCFDA. NAC was used to confirm the fluorescence signals. **(B)** Proliferation of hDPSCs was assessed with WST-1 at the elapsed times of 1, 2, and 3 days. **(C)** Alkaline phosphatase activity was measured at the elapsed times of 3, 7, and 14 days. Statistical significance is marked with *, **, and *** when $P < 0.05$, $P < 0.01$, and $P < 0.001$, respectively.

days to assess their proliferation. hDPSCs subjected to CW-PBM showed a slight increase in proliferation ($P < 0.0009$; Fig. 2.2B), whereas those that received PW-PBM showed either a slight increase or a decrease in the amount of proliferation ($P < 0.0032$ for 3-Hz PBM, $P < 0.00012$ for 300-Hz PBM; Fig. 2.2B). The proliferation of hDPSCs did not reflect the level of PBM-mediated ROS.

The early differentiation of hDPSCs by PBM treatment of 38 mJ/cm^2 was assessed using alkaline phosphatase (ALP) activity after 14 days of treatment. Significantly enhanced ALP activity was observed in the hDPSCs subjected to PW-PBM treatment ($P < 0.001$ for 1 Hz, $P < 0.012$ for 3 Hz, $P < 0.001$ for 300 Hz; Fig. 2.2C), whereas no alteration was observed from CW-PBM on 14 day after PBM treatment. Interestingly, the ALP activity of hDPSCs well reflected the result from 300-Hz PBM-mediated ROS production.

2.3.2 Delayed luminescence

To confirm to the effects of the 810-nm wavelength PBM treatment on the transfer of energy and related chemical responses, it measured DL from the end of light irradiation. Fig. 2.3A shows the patterns of DL in hDPSCs in Dulbecco's phosphate-buffered saline (DPBS) for 5 seconds after CW-PBM or PW-PBM at frequencies of 1, 3, 30, 300, and 3000 Hz. Interestingly, all the frequencies of PW-PBM induced more lagged luminescence than CW-PBM, which showed that some chemical activations result from PW-PBM treatment. Though the total energy transferred to cells was the same, the energy per pulse decreased as the frequency increased. It was found pulse frequency dependencies in the DL patterns; however they were not related to the total energy or energy per pulse. 30- and 300-Hz PBM treatment induced highly lagged DL, and 3-Hz PBM treatment had the least effect on DL.

Considering previous reports [50, 54, 85, 93, 95-97] that showed a relationship between mitochondrial activity and DL, it used rotenone, which inhibits the transfer of electrons from iron-sulfur centers in mitochondrial complex I to ubiquinone, or antimycin-A (AMA), which inhibits the oxidation of ubiquinone in mitochondrial complex III. In both cases, time delays after CW-PBM treatment became slower, but those after PW-PBM treatments were faster than in cells untreated by chemicals (Fig. 2.3B and 2.3C). However, it is clear that the effect of AMA was more significant in reducing DL intensity than DL delays. The pulse frequency dependencies changed differently, indicating the presence of a response protein to PW-PBM. The order of the delay times was kept similar with the addition of rotenone but changed slightly with AMA.

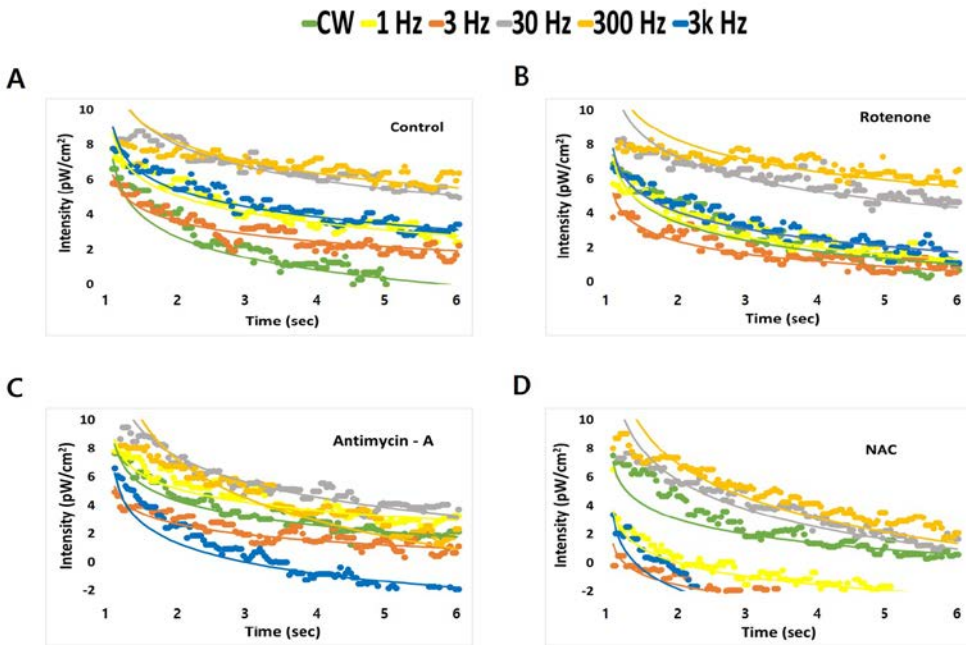

Figure 2.3 DL data from hDPSCs in response to PBM according to pulse frequency. The measured DL in the period between 1s and 6s after PBM was plotted with theoretical fittings. DL was measured when hDPSCs were in PBS with no treatment **(A)**, with pre-treatment in rotenone **(B)**, with pre-treatment in AMA **(C)**, and with pre-treatment in NAC **(D)**.

Because many reports have shown that PBM-induced biological responses are mediated by intracellular ROS [54, 93, 96, 97], we examined the effects of NAC on DL. Fig. 2.3D shows that DL after CW-PBM treatment was almost the same with and without NAC, but delay times after PW-PBM became faster at all frequencies. Especially at 1, 3, and 3000 Hz, the delays dropped abruptly compared with the control levels.

To clearly understand the effects of PBM treatment on DL, we transformed the measured DL intensity, *I(t)*, into the degree of the excitation level, *n(t)*, and the decay probability *P(t)*. The *n(t)* represents how many excited molecules (expected to emit DL) remain, and *P(t)* indicates the decrease rate in *n(t)* over time. The *n(t)* plots show clearly separated values between different frequencies whose *I(t)* curves were difficult to distinguish. Fig. 2.4A shows that the *n(t)* value was highest after 300-Hz PW-PBM and lowest after CW-PBM. The *P(t)* results were the reverse of the *n(t)* results; the value was highest after CW-PBM and lowest after 300-Hz PW-PBM (Fig. 2.4B). When hDPSCs were subjected to rotenone, the *n(t)* became lower and *P(t)* became higher; however, the order among the frequencies remained the same (Fig. 2.4C and 2.4D). When hDPSCs were subjected to AMA, the high *n(t)* values with 30- and 300-Hz PW-PBM became dramatically lower than those with other frequencies (Fig. 2.4E and 2.4F). A similar decrease was observed with NAC (Fig. 2.4G and 2.4H). On the other hand, the probabilities of the control hDPSCs were almost equally distributed with the pulse frequency of PW-PBM.

2.3.3 Morphological changes in mitochondria from PBM treatment

To determine whether PBM treatment triggers an alteration of the intracellular mitochondrial network in hDPSCs, it was assessed the mitochondrial morphology of hDPSCs using MitoTracker® Red CMXRos (ThermoFisher Scientific, USA), which reflects mitochondrial shape. As shown in Fig. 2.5, our control sample contained small, rounded mitochondria. However, hDPSCs exposed to 3-Hz PBM contained elongated, tubular mitochondria. Interestingly, hDPSCs treated with 300-Hz PBM showed much more tubular mitochondrial morphology than hDPSCs exposed to 3-Hz PBM treatment. To confirm those results, it analyzed the alterations in mitochondrial shape using transmission electron microscopy (TEM). Fig. 2.6A shows representative TEM images that reveal that hDPSCs subjected to 3-Hz PBM produced fewer mitochondria. Quantitative analysis showed that the number of mitochondria, normalized to the total area of each image, decreased significantly in hDPSCs exposed to 3-Hz PBM treatment, by 63.69 ± 15.18 % (P

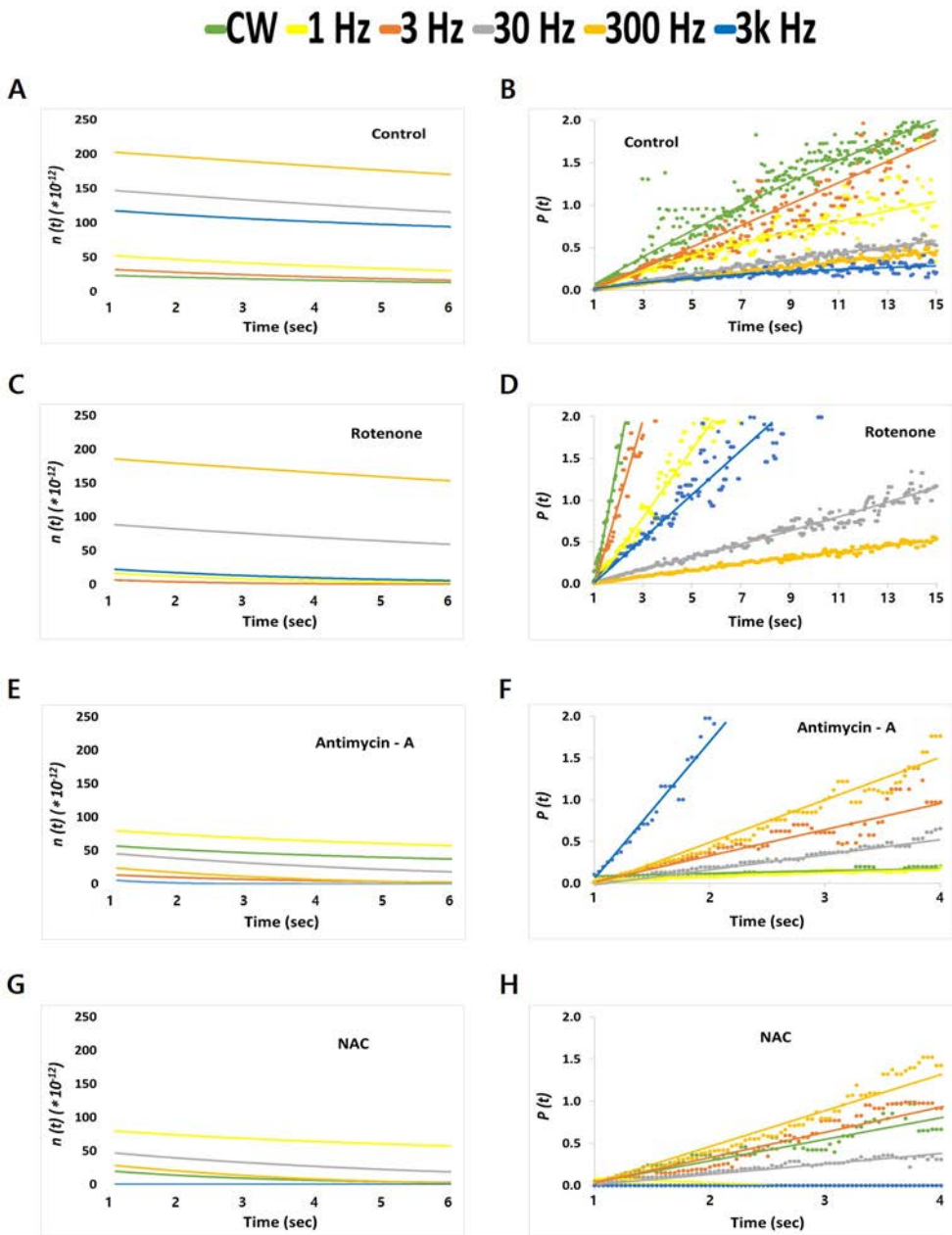

Figure 2.4 The temporal trend of the decay probability *P(t)* **(A, C, E, G)** and the degree of excitation *n(t)* **(B, D, F, H)** from the DL shown in Fig. 2.3. Data were analyzed from the DL measured when hDPSCs were in PBS with no treatment **(A, B)**, with pre-treatment in rotenone **(C, D)**, with pre-treatment in AMA **(E, F)**, and with pre-treatment in NAC **(G, H)**. The time scales of the *P(t)* were changed for clear discrimination.

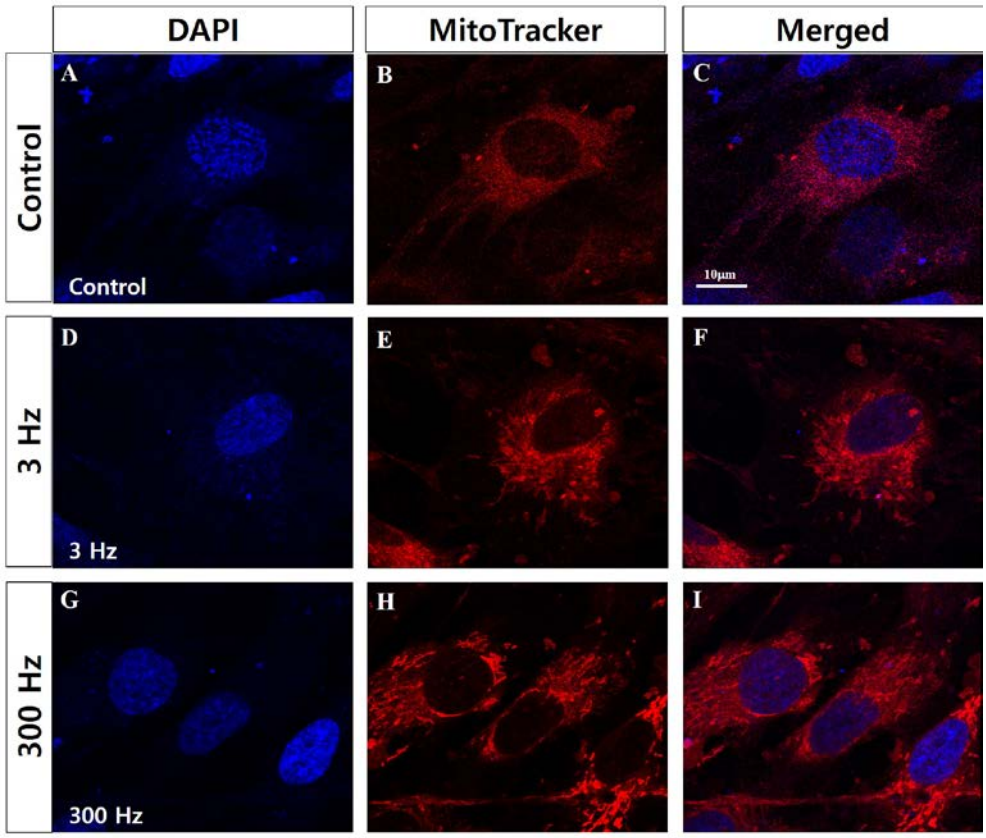

Figure 2.5 Confocal microscopic images of mitochondria in hDPSCs 3 days after PBM treatments. Nuclei were stained with 4',6-diamidino-2-phenylindole (DAPI), and mitochondria were stained with MitoTracker Red. Control hDPSCs **(A–C)**, hDPSCs exposed to 3-Hz PW **(D–F)**, and hDPSCs exposed to 300-Hz PW **(G–I)** were visualized. The scale bar is 10 μm.

< 0.007; Fig. 2.6B). In contrast, PBM treatment of 300 Hz promoted mitochondrial numbers, by 110.6 ± 17.28 % (P < 0.039; Fig. 2.6B), compared to the control. In addition, mitochondrial volume density, defined as the volume occupied by mitochondria divided by the volume of the cytoplasm in percentage terms, decreased in hDPSCs subjected to 3-Hz PBM treatment, by 67.43 ± 6.53 % (P < 0.00027; Fig. 2.6B). In contrast, the hDPSCs that received 300-Hz PBM treatment significantly promoted mitochondrial volume density, by 139.67 ± 9.09 % (P < 0.0024; Fig. 2.6B), compared to the control. In addition, it was found differences in the mitochondrial length of hDPSCs treated with 3- and 300-Hz PBM compared to controls. hDPSCs subjected to 300-Hz PBM treatment showed a mitochondrial length of 109.78 ± 3.17 % (P < 0.05; Fig. 2.6B), compared to controls. Unlike the mitochondrial number and volume density, mitochondrial length increased, compared to controls, in the hDPSCs subjected to 3-Hz PBM treatment. However, it was found no difference in the mitochondrial cristae structure between the controls and hDPSCs subjected to 300-Hz PBM treatment (Fig. 2.6C).

2.4 Discussion

In PBM, pulsed wave light (PW) has been reported to be more effective in some biological systems than continuous wave light (CW) [84]. In particular, PW-PBM more effectively accelerated wound healing, reduced pain, and reduced ischemic stroke, apparently by enhancing ATP synthesis in the mitochondria [84, 98]. It is reported that the effective pulse frequency range for PW-PBM is between 10 and 8,000 Hz [71, 99], with specific effective values for particular cell types. In the case of hDPSCs, no report had considered PW-PBM, even though CW-PBM showed great enhancement in hDPSC differentiation [80]. Therefore, our finding of effective pulse frequencies for hDPSC differentiation, especially in relation to mitochondrial activities, is the first such result. In this study, we considered the relationship between the effectiveness of PBM and mitochondrial activity using DL, the luminescence emitted from living organisms exposed to external light. This lasts from a few seconds to minutes, and the initial intensity exceeds the spontaneous luminescence emitted without exposure to external light. The spontaneous luminescence of living organisms is called biophoton emission and occurs in the ultraviolet (UV) and NIR ranges [89] with a low intensity of 10^{-19} to 10^{-16} W/cm^2 [92]. The endogenous production of excited molecules during oxidative metabolic reactions is known to be a source of biophoton emission [100].

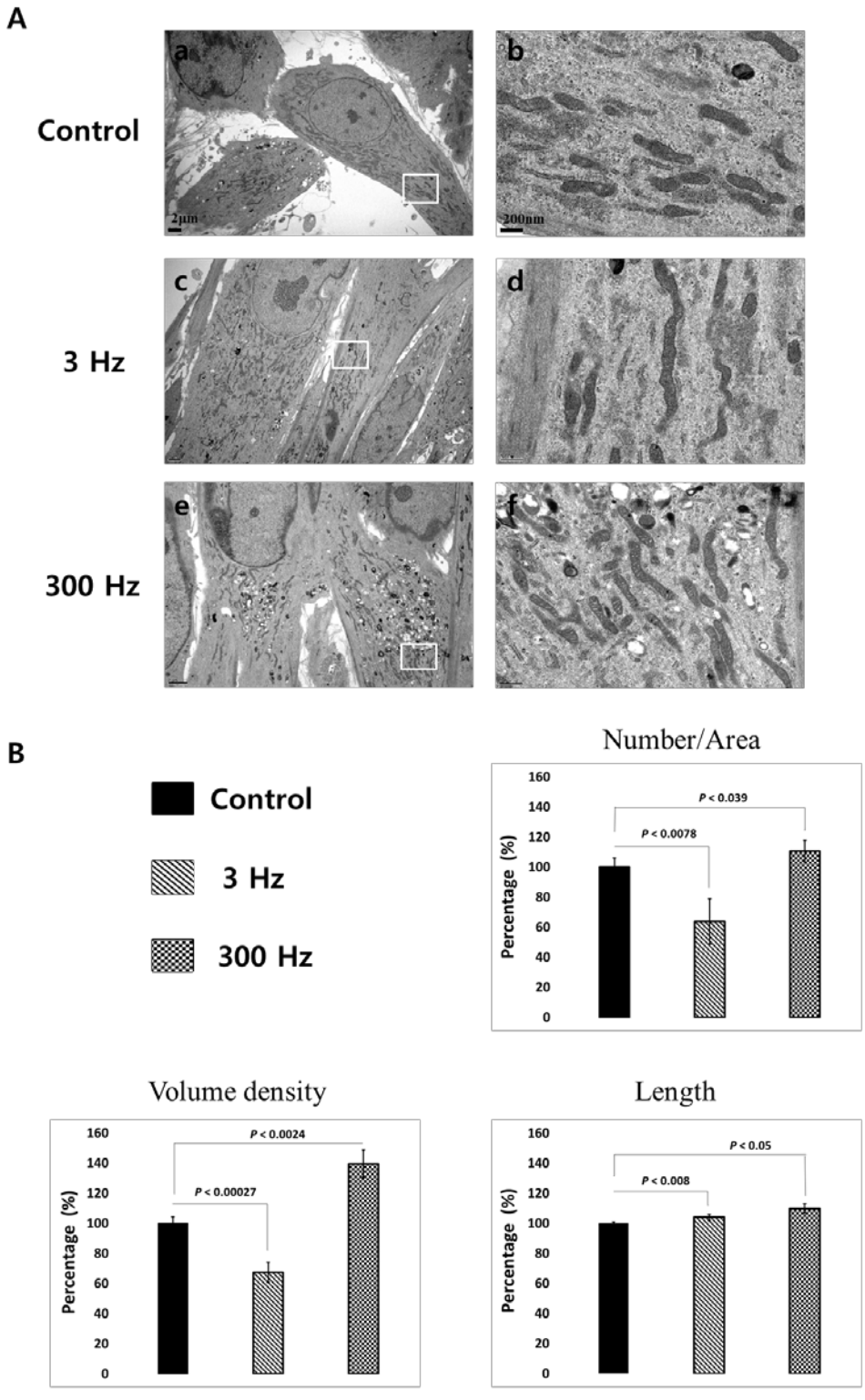
A
Control
3 Hz
300 Hz
a
b
c
d
e
f
2μm
200nm
B
Control
3 Hz
300 Hz
Number/Area
Percentage (%)
P < 0.039
P < 0.0078
Volume density
P < 0.0024
P < 0.00027
Length
P < 0.05
P < 0.008

C

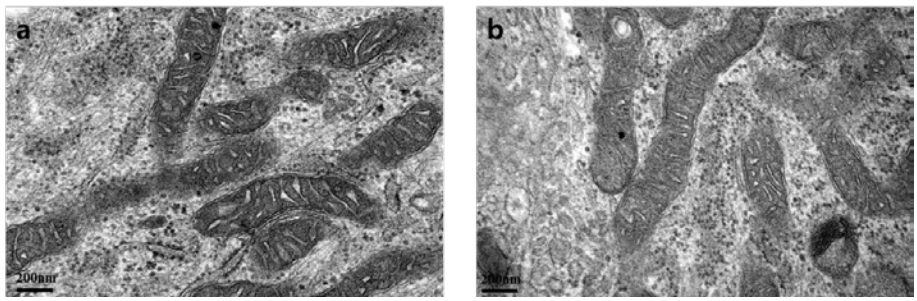

Figure 2.6 (A) Representative TEM images of mitochondria in hDPSCs after 7 days of incubation under osteogenic medium, 7 days after PBM treatment. hDPSCs (control, treated with 3-Hz PW-PBM, and treated with 300-Hz PW-PBM) were compared. The areas marked with white rectangles (a, c, e) were magnified (b, d, f). **(B)** Quantitative analyses of the number of mitochondria per area, mitochondrial volume density per cell, and mitochondrial length. **(C)** Magnified TEM image of mitochondria in control cells (a) and cells subjected to 300-Hz PW-PBM.

Though bothbiophoton emission and DL exist concurrently, we cannot distinguish between the two signals because of the detection limit of our equipment. The detection limit is about 10^{-10} W/cm^2, which is not good enough to detect ultraweak biophoton emissions without light exposure. Therefore, we analyzed our data as representing only DL.

Because of the strong correlation between the properties of DL and the states of biological systems, DL has been regarded as a powerful tool for medical investigations [50, 53-55, 85, 93, 95-97]. However information on the mechanisms for DL in animals is rather scarce, compared to that for plants [101]. Some hypotheses have been suggested. DL could be generated directly from autofluorescence emitters such as flavins [53], from the solitons in hierarchically organized structures such as the cytoskeleton [102], or from collective molecular interactions such as occur in mitochondrial membrane protein complexes [95]. Several papers have reported a close relationship between DL and mitochondria. Baran *et al.* showed that DL originates mainly from mitochondrial complex I, which they probed using complex I targeting agents [96]. They showed that complex I appeared to exhibit cooperative interactions among nicotinamide adenine dinucleotide, flavin mononucleotide, and their binding sites, emitting long-lasting DL with multiscale kinetics, as in plant chloroplasts. In our study, we analyzed DL signals one second after external light exposure, which should eliminate direct autofluorescence, whose lifetime is within a millisecond. Therefore, our DL signals are probably primarily from sequential photochemical reactions in some metastable-state species in mitochondria.

Our experimental data have some different points from those in previous studies. First, a complex III blocking agent (AMA) affected DL signals more than a complex I blocking agent (rotenone). It assume that this difference originated from the different wavelengths of light. Many studies used UV-VIS light, and their target molecules were flavins or nicotinamide adenine dinucleotide (NADH). Because we used NIR light in this study, the target molecules should be different. Cytochrome c and cytochrome c oxidase are known to absorb longer wavelength light, including NIR, which supports the role of complex III in NIR-induced DL [83]. Excited or metastable-state-cytochrome c could bind with complex III forwards or backwards depending on the environmental conditions, as observed in other DL systems. Second, the effects of antioxidants were much bigger than those observed in previous studies. In a previous study, the correlation between DL and ROS/lipofuscin was not particularly significant in UV-induced DL [96]. It is well known that PBM increases ROS production and

that ROS have primary roles in the process of PBM [103]. The ROS might change the chemical environments of mitochondrial complex I or III or be directly bound to them, resulting in longer lasting DL signals following exposure to NIR light. The big reduction in DL seen with the addition of a ROS scavenger supports the relationship between ROS and PBM. Third, the DL we measured followed a single power law, which was confirmed by well fitted linear plots for *P(t)*. In previous studies, DL generally presented multiscale kinetics that should be fitted using combinations of exponential components. Because it was analyzed late period DL, it might have lost information about many quick, complex events. Nevertheless, our late period DL showed that the signal is from a few or a single event, which is meaningful information about PBM-induced changes in cell physiology.

One of the most important findings in this study is that pulsing PBM brings differential biological consequences according to the pulsing frequency. The DL lifetime was longer after PW-PBM irradiation, and the effects of rotenone, AMA, and NAC depended on the pulse frequency. Whereas cells treated with 30–300-Hz PW-PBM had higher and longer-lasting DL in all cases, cells treated with lower or higher frequency PW-PBM showed big changes when AMA and NAC were added. Though the exact molecular reactions to PW-PBM have not been clarified, it have found that certain ranges of pulse frequency have specific biological effects. 30–300-Hz PW-PBM seems to induce highly correlated photochemical reactions that are not easily affected by environmental redox changes. These periodic light stimuli might accelerate or retard some biological processes whose time scales are similar. Three biological processes can be suggested. One is a redox-linked proton pump of cytochrome c oxidase that is triggered by cytochrome c. Electrons from cytochrome c are transferred to the binuclear heme/copper (a_3/Cu_B) oxygen reduction site via a bimetallic Cu_A center at the membrane surface, which takes about a millisecond [104]. Another is the kinetics of ion channels, whose time scale is a few to a hundred milliseconds [105]. Ion concentrations in the mitochondrial membrane are a key factor controlling its functions. The third process is a synchronized whole-cell oscillation through the mitochondrial metabolism triggered by a local release of ROS [106]. It was reported that ROS efflux and antioxidant capacity determined the oscillation.

It should be noted that, among the tested frequencies of PW-PBM, 300-Hz PW had significant effects on hDPSC differentiation, as well as in chemical activations. The intracellular ROS analyzed via H2DCFDA was highest at 300-Hz PW-PBM. A similarly significant enhancement was observed in ALP activity,

which is related to the early and middle stages of hDPSC differentiation into osteogenic lineages. The enhanced ALP activity and DL decreased when NAC was added, which implies that ROS played some role in 300-Hz PW-PBM-induced cellular responses. Our viability test showed that metabolic activities were not triggered by 300-Hz PW-PBM. Thus, this PBM stimulus might trigger cellular differentiation-related pathways rather than proliferation-related ones, which should be further studied.

Meanwhile, some studies report that activated complex I or III in mitochondrial electron transport chain (ETC) stimulates stem cells to differentiate [107, 108]. Complex I or III in the electron transport chain is known to representatively produce superoxide anions. ROS resulting from those superoxide anions contribute to stem cell differentiation, which is different from stem cell type. Myoblasts increased more in complex I than in other complexes when progressing differentiation into muscle, and mouse embryonic stem cells enhanced the activity of complex III to cause other stem cells to differentiate. According to a previous study [83], NIR light changes the mitochondrial metabolism for stem cell differentiation between complex III and complex IV via cytochrome c, resulting in the production of ROS and thereby activating transforming growth factor beta 1 to trigger stem cells to differentiate [80]. In the present study, complex III was activated more than complex I by 300-Hz PW-PBM, as shown by the results of the rotenone- and AMA-blocked decay probability, *P(t)*, in Fig. 2.4. In addition, robust production of ROS was observed following 300-Hz PBM (Fig. 2.2B). This robust activation of complex III by 300-Hz PBM might be associated with the enhanced mitochondrial networks shown in Fig. 2.5 and the increased mitochondrial mass shown in Fig. 2.6. Taken together, we assume that 300-Hz PW-PBM activates ETC in complex III and produces more mitochondrial networks, which influence the differentiation of hDPSCs.

The mitochondrial activation caused by 300-Hz PW-PBM is supported by the changes in mitochondrial morphology and mass. TEM microscopy (Figs. 2.6a-b) demonstrated that 300-Hz PW-PBM induced a significant richness of mitochondrial mass by increasing the number and volume density of mitochondria in the hDPSCs. Though the underlying mechanisms for those changes have not been elucidated, relationships between some physiological observations and mitochondrial morphology and mass have been reported. For example, stem cells increased the production of fusion regulators (Mfn2 and Opa 1) and fission regulators (Fis 1 and Drp1) as differentiation progressed into osteogenesis, which resulted in an increase in mitochondrial mass and

elongation [109]. This observation is consistent with our results that 300-Hz PW-PBM enhanced ALP activity, which accompanied increased mitochondrial mass and length. Another paper reported a negative relationship between mitochondrial elongation and mitochondrial ROS (mtROS) [110]. We demonstrated that the entire cytosolic ROS level was higher after 300-Hz PW-PBM (Fig. 2.2A). Though we did not include this result in this paper, it was found that the level of mtROS was lower under the same conditions. This implies the differential activation of mitochondrial ETCs or the involvement of other mitochondrial redox regulators as a result of PW-PBM. Additionally, it was reported that PBM induced mitochondrial fission and fusion by regulating Ca^{2+} signaling, which has a close relationship with ROS [111]. Future, rigorously designed experiments should determine these cooperating phenomena. Because our microscopic observations were carried out 3 days after PW-PBM, it is difficult to state the exact relationships between our DL measurements and mitochondrial morphological changes. However, our DL screening data predict that 300-Hz PW would have the strongest effect on mitochondrial activation. In addition, we expect that 300-Hz PW-PBM produces some initiating signals that activate mitochondria and hDPSC differentiation. The activation of mitochondrial complex IV could play that initiating role by interacting with cytoplasmic ROS.

2.5 Conclusion

In conclusion, it was found that 300-Hz PW-PBM dominantly prolonged the DL pattern and enhanced ALP activity, which consequently resulted in dentinogenic differentiation of hDPSCs. On the contrary, 3-Hz PW-PBM produced inverse effects on hDPSCs: it decreased the mitochondrial number and volume density, lowered the production of ROS, and produced little effect on DL. In PW-PBM therapy, pulsed waves were originally used only to reduce the thermal damage. However, our results reveal that the repetition frequency is an important factor in biological responses, as are wave frequency and power. These results can be used to enhance the efficiency of PBM treatment in many biological fields, including stem cell engineering.

Chapter 3

Effects of pulsing of light on the dentinogenesis of human dental pulp stem cells *in vitro*

3.1 Introduction

PBM therapy is a therapeutic modality that is increasingly being utilized by clinicians as a treatment paradigm for acute and chronic musculoskeletal injuries, osteoarthritis, inflammation, soft tissue injuries, etc.[112-115]. The red or near-infrared (NIR) light is known to be effective, but UV is known to induce apoptosis when the power density ranges between 5 to 5000 (mW/cm^2) [116]. In addition to the light property itself, it has been reported that the biological effects of PBM depend on how it is applied.

Though many previous studies have used continuous wave (CW) mode due to its easiness to drive, some studies have shown benefits of pulsed wave (PW) [70, 71, 84, 99, 117-122]. First of all, PW reduces the temperature increase in tissues. The quench periods (Off times) permit higher intensity light that deepen the penetration of light into tissue with the same average power[84]. If the target tissue has high scattering properties, PW mode is necessary to deliver sufficient light energy into deep inside the tissue. Since bone-like tissue is one of the highest light scattering tissues, whose center is filled with multipotent stem cells, PW mode should be used to activate internal area of bone-like tissue by PBM. Secondly, PW-PBM has been reported to be more effective in some biological events [122]. These periodic light stimuli may accelerate or retard some biological processes such as the kinetics of ion channels or redox-linked proton pumps whose time scales are in a few to a hundred milliseconds [104]. It is reported that the effective pulse frequency range of PW-PBM is between 10 and 8,000 Hz, and there are specific effective values for different cell types [71, 99].

PBM is specially considered as a prospective tool due to its regulating effects on the proliferation and differentiation of stem cells [7, 43, 77, 123-127]. Human dental pulp derived stem cells (hDPSCs) have attracted attentions in tissue engineering due to their multipotency in differentiation and easy acquisition from wasting teeth [38, 128]. Since PBM does not remain any byproducts, the controllability of hDPSCs by PBM would make them more valuable stem cell sources [36, 80]. Furthermore the functional modulation of

hDPSCs *in situ* by PBM could provide solutions for reducing osteoporosis or bone regeneration. However, there have been few studies on the effects of pulsing or pulsed light on hDPSCs[122, 124]. Herein, we report the effects of pulsing of PBM treatment on the differentiation of hDPSCs. To improve the clinical relevance, we used patient-derived stem cells. The duty cycle and the frequency of PBM treatment were screened based on the hDPSC differentiation. Considering the high scattering of dental tissues, sub-mW order weak PBM was examined. Additionally, the relations of intracellular ROS and mitochondrial activity in PBM induced hDPSC differentiation were examined following previous reports. Many reports showed that cytochrome c oxidase primarily absorbs light in mitochondrial transport chain (ETC), triggering reactive oxygen species (ROS) production, which have been known to be secondary signaling messengers in regulating proliferation and differentiation of stem cell [13, 14, 129, 130]. This basic research provides information that will pave a way for efficient application of PBM for dental stem cell engineering.

3.2 Materials and methods

3.2.1 Fabrication of PBM system and application to cell culture plates

To make a uniform PBM emitting device, we assembled LEDs, a reflector, a light guide, and a diffuser as shown in Fig. 3.1. We used a reflector with diffuser that was used for TV manufacturing. The light intensity was measured using a photodiode (Model: S1227-66BQ) and the intensity variance was calculated by the intensities of three points marked with crosses (x) in Fig. 3.1C. We used LEDs as a light source whose wavelength is centered at 810 nm. The near infrared (NIR) light was confirmed using a spectrometer (Model: PMA-12, Japan). An operating device was designed and fabricated based on an 8-bit-microcontroller (UM_MC95FG308_V3.20_EN, Korea) and coded with C-language for adjusting the waveform, the duty cycle, and treatment time.

Light dose was checked before every experiment with a power meter (PM-USB-100, Thorlabs, USA). The assessed power density (irradiance, W/cm^2) on a site of placing a plate in a continuous wave form was 268 $\mu W/cm^2$ and it was reduced with the duty cycle. For example the power density became 30 % when the duty cycle became 30 %. The pulsed wave was in a square wave form as shown in Fig. 3.1E. For example, 1-Hz-square wave with 30 % duty cycle means that LEDs were ‘on’ for 300 ms and ‘off’ for 700 ms, and 1-Hz-60-%-square wave is that LEDs were ‘on’ for 600 ms and ‘off’ for

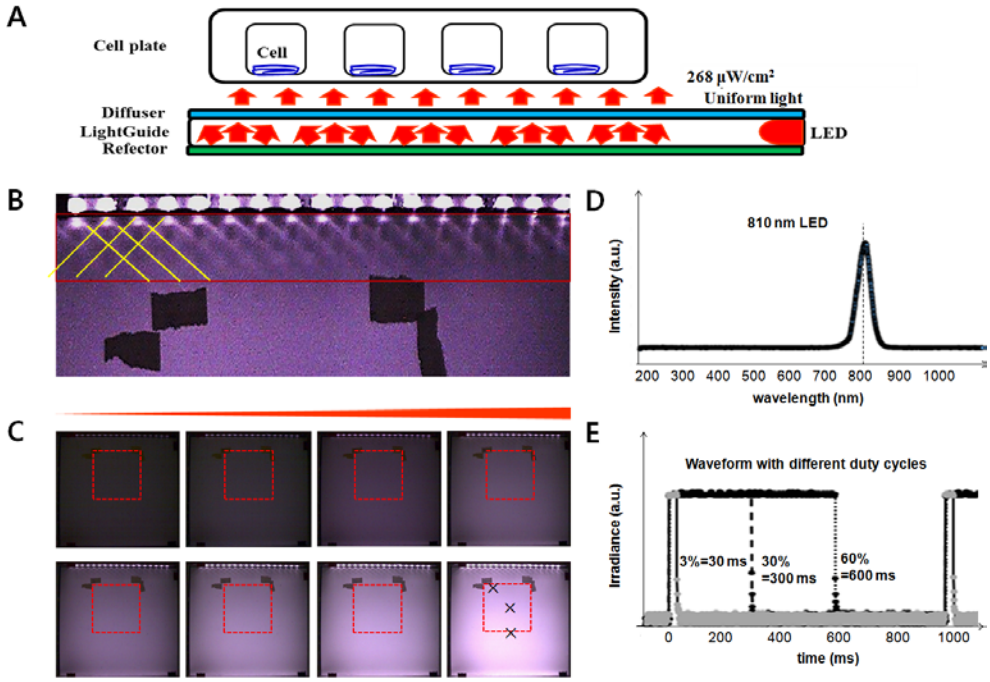

Figure 3.1 An optical device that carries light energy to objects. **A.** A schematic of the device which is composed of LEDs as a light source, and a reflector, a light-guider and a diffuser to make the exposure light uniform. **B.** A photo of the LED source part, from where light travels through a light-guide and becomes uniform at some distance. **C.** Photos of the device with increasing driving voltage. Samples were put within the marked area with dotted rectangle. The variance of light intensity within this area was under 3.9 %. **D.** LEDs irradiated only near infrared 810 nm light. **E.** Applied voltage was modulated in the form of 1 Hz square waves with different duty cycles.

400 ms. Duty cycles and frequencies could be easily controlled with keeping the same peak irradiance. Duty cycles of 0, 0.3, 3, 30, and 60 % and the frequencies of 1, 3, 30, 300, 3000 Hz were used in this experiment. To make the irradiated light energy same (energy fluence 77 mJ/cm^2) in both a continuous wave and pulsed waves, the irradiation time was controlled. For example, the irradiation time was 287 s for a continuous wave and 958s for a pulsed wave. In an experiment to compare the effect of total applied energy, the application time was changed (Fig. 3.2B). In an experiment to determine the most effective duty cycle, we used the same irradiation time though the total energy was different (Fig. 3.2A). All the experimental conditions are summarized in a Table 3.1.

3.2.2 Cell culture

Human molars were obtained from patients. Relevant informed consent was obtained from all participants. Patients consented the use of teeth for research purposes, and no information about patients was included in this article. This article does not contain information or images that could lead to identification of a study participant. The protocol was approved by the Institutional Review Board of Seoul National University Dental Hospital (Seoul, South Korea; IRB number 05004). All experiments were performed in accordance with relevant guidelines and regulations following previously confirmed protocols [131]. Briefly, the tooth specimens were dissected aseptically to disclose a pulp chamber and performed scraping tissues that contain pulp stem cells with a metal scraper. The separated tissues were incubated with 4 ml of 0.25 % trypsin-EDTA (Life Technologies) at 37°C for 30 min, and neutralized with 4 ml of a complete medium which contains α-MEM, 10 % FBS and 1 % penicillin (100 U/ml)-streptomycin (100 μg/ml) supplemented with 100 μM ascorbic acid (all from Gibco, Life Technologies). Then, solutions were pipetted vigorously and passed through a 40-μm cell strainer (Corning) to remove tissue debris. The obtained cells were cultured in a complete medium in a 37 °C incubator with 5 % CO_2, and the colonies were subcultured and expanded to obtain hDPSCs. The hDPSCs in the passage 3-5 were used in this experiment following previous studies. For dentinogenic differentiation of hDPSCs, 10 mM β-glycerophosphate, 0.05 mM L-ascorbic acid-2-phosphate and 100 nM dexamethasone were added. All the chemicals were purchased from Sigma-Aldrich. For PBM treatment, cells were seeded in a 4-well plate with a density of 2.0×10^4 cells/well a day before treatment. For differentiation test (alkaline phosphatase assay and differentiation-related

Table. 3.1 The experimental conditions for this study.

Mode	PW 1Hz				PW30%	CW	PW 30%				
	0.3%	3%	30%	60%	1Hz		1 Hz	3 Hz	30 Hz	300 Hz	3000 Hz
Irradiance ($\mu W/cm^2$)	0.8	8.0	80.4	160.8	80.4	268	80.4				
Time (s)	958	958	958	958	28731	287	958				
Fluence (mJ/cm^2)	0.8	7.7	77	154	2310	77					

molecular assays) the differentiation medium was daily replaced before PBM treatment, and for the other tests the complete medium was daily replaced before PBM treatment. The morphology of cells was observed under inverted microscope (Eclipse Ti, Nikon, Japan).

3.2.3 Measurement of cytoplasmic membrane potential

The cytoplasmic membrane potential (CMP) was assessed soon after PBM treatment by FLIPR (Molecular Devices, CA) according to the manufacturer's protocol. Simply, cells were washed with DPBS one time and FLIPR working solution (FLIPR solution mixed with culture medium by halves) was added. After 30-minute of incubation at room temperature, cells were washed with DPBS, harvested with typsin-EDTA and resuspended in DPBS. The fluorescence of each cell was measured by flow cytometry (BDVerse, BD, Germany) and the mean value of each group was analyzed by the BD FACSuite™ software. The relative intensity of each group to control was expressed as a percent value. The original flow cytometry data is applied in supporting information.

3.2.4 Alkaline phosphatase (ALP) assay

hDPSCs were cultured to be confluence of over about 80 % in culture wells. Then the culture media was replaced with differentiation media, and at the same time, PBM treatment was conducted every day for 3 days or 7 days before alkaline phosphatase (ALP) assay. In order to observe ALP expression in cells, we stained cells with SensoLyte® pNPP Alkaline Phosphatase Assay kit. Briefly, the prepared cells were gently washed twice with 1-X assay buffer. Then, lysis buffer (50 mM Tris HCL and 0.1 % Triton X 100, pH 9.5, Sigma) was added in the cells and the cells were incubated for 10 min at 4 °C. After vibrating the cells for 60 sec, the cell supernatant was transferred into 96-well plate in an amount of 50 μl per well. pNPP substrate of 50 μl was added into each well and mixed the supernatant by gently shaking the plate for 30 sec. The cells were incubated for reaction at 37 °C for 60 min. The absorbance was assessed with a microplate reader (Synergy HT, Biotek) and expressed as a relative value to the control.

3.2.5 WST- 1 assay

For WST-1 assay (CytoSelect™), cells were incubated in complete media with 10 % WST-1 for 1 hr at 37 °C after 24, 48 and 72 hours of PBM treatment. The media was transferred to a new 96-well plate in amount of 100 μl per well

and the absorbance was monitored at 450 nm through a plate reader (Tecan, USA).

3.2.6 Adenine tri-phosphatase (ATP) assay

For ATP evaluation, the cells of 1.0×10^3 cells/well were seeded in a 96-well white plate (3610, Corning). After 6 hours of seeding, the cells were treated by PBM and the media was washed with DPBS before adding CellTiter-Glo® Luminescent Cell Viability Assay (G7572, Promega). The plate was shaken for 5 minutes in medium strength, and the luminescence was measured by a plate reader (Synergy HT, Biotek). The luminescence of each group was expressed relatively to control as a percent value.

3.2.7 Intracellular reactive oxygen species (ROS) and mitochondrial membrane potential (MMP, $\Delta\psi_m$)

After 5-minute of PBM treatment, cells were washed and the ROS probes were added. MitoSOX Red dye (M36008, ThermoFisher Scientific) for superoxide in mitochondria and H_2DCFDA (D399, ThermoFisher Scientific) for intracellular ROS were used. MitoSOX was diluted to 5-μM in HBSS buffer, and cells were incubated in the solution for 10 min at 37°C. After washing with DPBS and trypsinization, the fluorescence per a cell was measured by flow cytometry (BDVerse, BD, Germany). H2DCFDA was diluted to 10 μM in DPBS, and cells were incubated in the solution for 30-min at 37°C. After washing three times with DPBS, cells were incubated for next 30 min, and the fluorescence per a cell was measured by flow cytometry. The relative intensity of each group to the control was expressed as a percent value.

Mitochondrial membrane potential (MMP) was detected by using MitoProbe™ JC-1 assay kit (Thermo fisher Scientific). Cells were incubated in a complete media containing of JC-1 dye (2 μM) for 30 minutes and washed three times with DPBS. After trypsinization, the fluorescence per a cell was measured by flow cytometry. The relative intensity of each group to control was expressed as a percent value.

3.2.8 Real time polymerase chain reaction

After 3 days of daily PBM irradiations in differentiation media, cells were harvested, lysed, and total RNAs were extracted using RNeasy Mini Kit (Qiagen). The total RNAs were converted to cDNAs using reverse transcriptase and random primers (cDNA synthesis kit, Toyobo) according to manufacturer's protocol. The same amount of extracted total RNA taken from each sample was

used in cDNA synthesis. The synthesized cDNAs were used in real time PCR using a CFX96™ Real-Time System (BioRad). The relative gene expression was evaluated by the comparative cycle-threshold method. The relative amount of mRNA expression was normalized by that of RPL13α and expressed as a fold change to control. Primer sequences are as follows: RPL13α (F: 5' CTATGACCAATAGGAAGAGCAACC, R: 5' GCAGAGTATATGACCAGGTGGAA), SOD1 (F: 5' GGCAAAGGTGGAAATGAAGA, R: 5' GGGCCTCAGACTACATCCAA), SOD2 (F: 5' GTTGGCCAAGGGAGATGTTA, R: 5' TAGGGCTGAGGTTTGTCCAG), BAX (F: 5' AACATGGAGCTGCAGAGGAT, R: 5' CAGTTGAAGTTGCCGTCAGA), TGF-β1 (F: 5' ACCTTGGGCACTGTTGAAGT, R: 5' CTCTGGGCTTGTTTCCTCAC).

3.2.9 Western blotting

After 21 days of daily PBM irradiations in differentiation media, the total proteins were isolated using a RIPA lysis buffer (Santa Cruz Biotechnology, Inc., Santa Cruz, CA, USA) supplemented with protease inhibitor mixture according to the manufacturer's instruction. Cell lysates were centrifuged with 13,000 rpm at 4°C, and the sediments were removed. The protein concentrations were determined using a BCA protein assay (Thermo Fisher Scientific, Inc, Rockford, IL, USA). Protein from the cell lysates was mixed with 5× SDS-PAGE loading buffer and boiled for 10 min, prior to electrophoresis by 10 % SDS-PAGE. Following transfer onto methanol-activated polyvinylidene difluoride membranes and blocking, the membranes were incubated overnight at 4°C with polyclonal antibodies for alkaline phosphatase (ALP; Abcam, Cambridge, MA, USA), osteopontin (OPN; Merkmillipore, Billerica, MA, USA), dentin matrix protein 1 (DMP1; Arigo Biolaboratories Corp., Taiwan), osteocalcin (OCN), bone sialoprotein (BSP; Santa Cruz Biotechnology), monoclonal antibodies for beta actin (1:500, Santa Cruz Biotechnology, Inc., Santa Cruz, CA, USA). All antibodies were diluted with phosphate-buffered saline (PBS) solution containing 1 % non-fat dry milk. Following three times washes in TBST (Tris-buffered saline, 0.1 % Tween 20), the membranes were subsequently incubated for 1 hr with horseradish peroxidase-conjugated goat anti-rabbit antibody (Bio-Rad Laboratories, California, USA) or goat anti-mouse antibody (Bio-Rad Laboratories) diluted 1:5,000 in blocking buffer. The membranes were then washed three times with TBST, and signals were detected by pierce ECL system (Thermo Fisher Scientific, Inc.) and exposed to X-ray film. The quantitative densitometric value of each protein was normalized to ß-actin and displayed in histograms.

3.2.10 Statistical analysis

All the experiments were repeated at least 3 times, and the data were expressed as the mean and standard deviation (SD). Statistical significance was evaluated using unpaired Student's t-tests (two-tail, equal SD) with Microsoft Excel. Here, * indicates the p-value is under 0.05, ** under 0.01 and *** under 0.001. We denoted these stars when the value was significantly different from the control value, and p values were marked on the graph when the value was compared with other group.

3.3 Results and Discussion

3.3.1 PBM conditions for effective modulation of hDPSCs activity

Our PBM system was designed to expose cells to light through the bottom of culture dish as shown in Fig. 3.1A. Light from LEDs traveled through the light guide, was reflected by a reflector, diffused through a diffuser, and then reached the cell culture plates. Fig. 3.1B shows that the light traveled through a disperser and a reflector became uniform with the variance under 3.9 %. Samples were put on the area marked with dotted rectangles in Fig. 3.1C. We used a light emitting diode (LED) whose light was centered at 810 nm wavelength (Fig. 3.1D), which was known to activate cells to differentiate [80]. The applied voltage is square waveforms, so the 60 % duty cycle means that LEDs were 'on' for 600 ms and 'off' for 400 ms for 1 Hz waves as shown in Fig. 3.1E.

In order to choose PBM conditions for effective modulation of hDPSC activity on osteogenic differentiation, we firstly screened the change of cytoplasmic membrane potential (CMP). hDPSCs were subjected to 1 Hz square wave PBM with different duty cycles including 0, 0.3, 3, 30, and 60 % for 10 minutes. The total energies were 0.77, 7.7, 77, and 154 mJ/cm^2, respectively. FLIPR fluorescence reduced simultaneously with PBM treatment in all the duty cycles (Fig. 3.2A). When cells become hyper-polarized, the fluorescence of FLIPR dye becomes weaker. The cells were most hyperpolarized at a 30 % duty cycle, even though the energy density was half comparing to 60 %. In order to confirm the effects of power itself, we compared the fluorescence of four groups including control, 77 mJ/cm^2 CW, 77 mJ/cm^2 PW with duty cycle of 30 %, and 2,310 mJ/cm^2 PW with duty cycle of 30 % (Fig. 3.2B). Cells underwent hyperpolarization with both PW-PBMs, however CW-PBM did not induce any changes. In addition, three times higher intensity did not induce higher polarization with same duty cycle. These results imply that the quick responses

of hDPSCs to PBM do not depend on the amount of energy density, but on the discontinuity itself.

Based on the simultaneous changes in CMP, the proliferation and differentiation were also examined in long term. The cell metabolic activity was assessed at elapsed time of 1, 2, and 3 days from PBM treatments. Fig. 3.2C shows the WST-1 assay result from the cells treated with CW-PBM and 1-Hz-30-% duty-cycle-PW-PBM with same 77 mJ/cm^2 energy density. The metabolic activity was significantly enhanced when PW-PBM was applied in comparison with CW-PBM application. Alkaline phosphatase (ALP) activity was examined as an early marker for the osteogenic differentiation at elapsed time of 3 and 7 days from PBM treatments. Fig. 3.2D shows that 1-Hz-30-% duty-cycle-PW-PBM increased the ALP activity significantly at elapsed time of 7 days from PBM treatment with energy density of both 77 mJ/cm^2 and 2,310 mJ/cm^2. The hDPSCs were similarly differentiated, even though the energy density was 3 times different. Together, cellular responses to PW-PBM did not depend upon the applied energy density but on duty cycle.

In addition to the intensity and duty cycle, the frequency of pulse can be influential for biological consequences. To assess the effect of frequency of pulse on hDPSCs, we fixed the duty cycle 30 % and the energy density 77 mJ/cm^2 over all frequencies (0, 1, 3, 30, 300, 3000 Hz). CMP, cellular metabolic activity and ALP activity were assessed. Fig. 3.3A shows that cells have hyperpolarized fashion in all frequencies right after PBM treatment. Fig. 3.3B shows the WST-1 assay result at elapsed time of 24, 48, and 72 hours from PW-PBM treatment. Cellular metabolic activity was increased in most frequencies tested here. Fig. 3.3C shows the analysis of ALP activity at elapsed time of 3 and 7 days from PW-PBM treatment with different frequencies. All cells that were subjected to the PBM revealed high ALP activity, which supports upregulated-osteogenic differentiation. With varying frequency of modulating PBM in a same dose, the metabolic activity of hDPSCs was enhanced most with 300 Hz PW-PBM.

Previous studies showed the relationship between the CMP and the progress of stem cell differentiation [132-135]. Authors found that the hyperpolarized CMP is related to quiescence of cells and the depolarized CMP is generally corresponding to proliferation and cell cycle progression. Cells in S-phase of mitosis have lower CMP difference (depolarized) and cells in cell

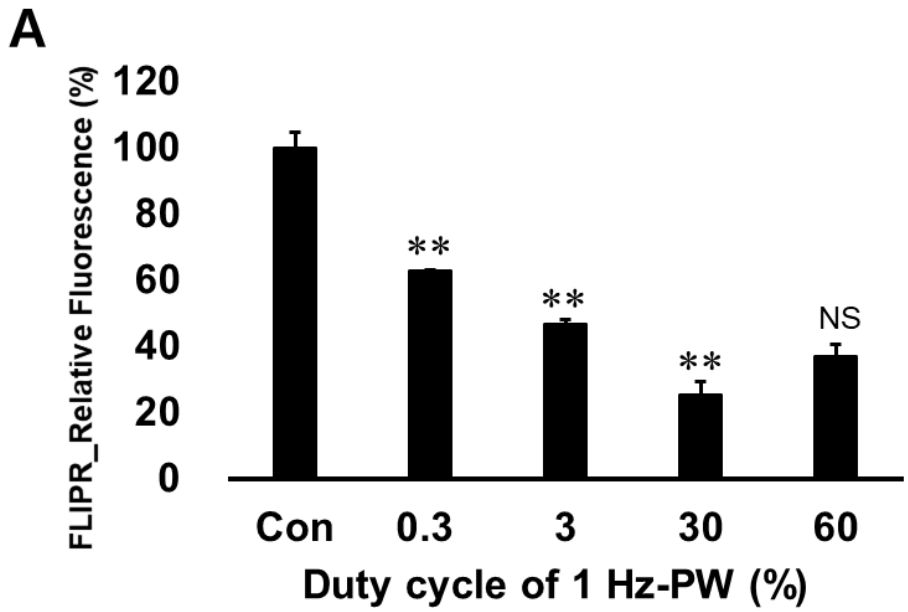
A
FLIPR_Relative Fluorescence (%)
120
100
80
60
40
20
0
**
**
**
NS
Con
0.3
3
30
60
Duty cycle of 1 Hz-PW (%)

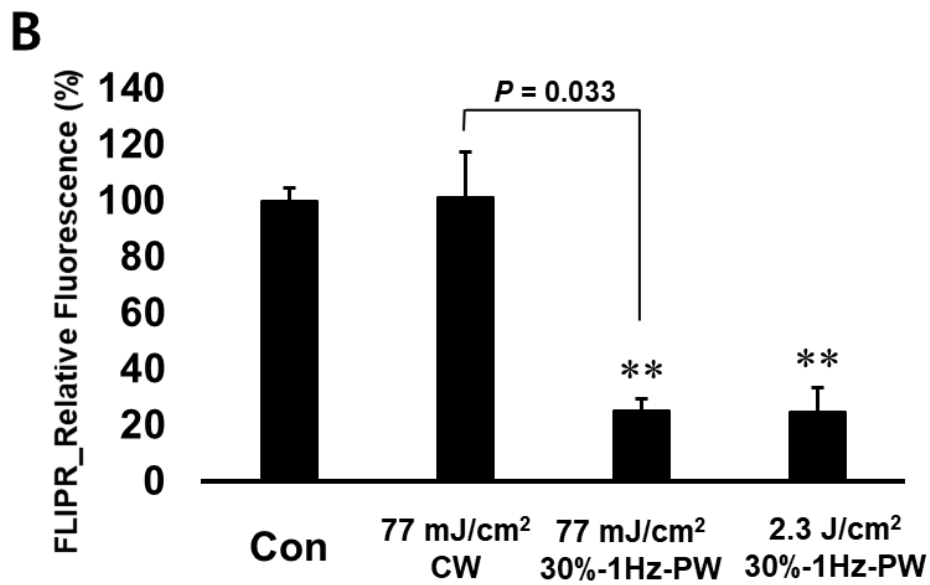
B
FLIPR_Relative Fluorescence (%)
140
120
100
80
60
40
20
0
P = 0.033
**
**
Con
77 mJ/cm2
CW
77 mJ/cm2
30%-1Hz-PW
2.3 J/cm2
30%-1Hz-PW

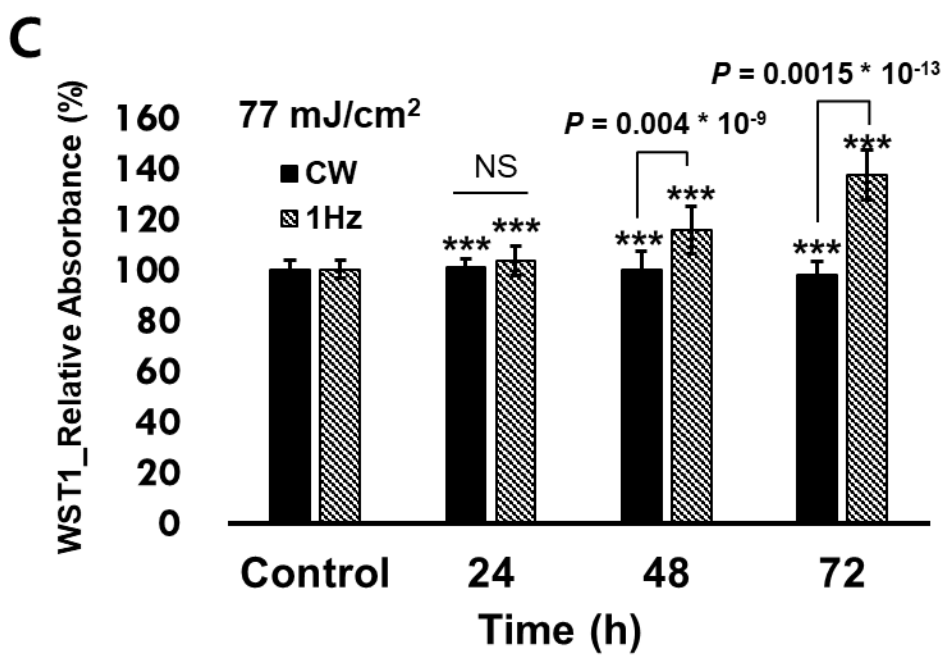
C
WST1_Relative Absorbance (%)
160
140
120
100
80
60
40
20
0
77 mJ/cm2
CW
1Hz
NS
P = 0.004 * 10-9
P = 0.0015 * 10-13
***
Control
24
48
72
Time (h)

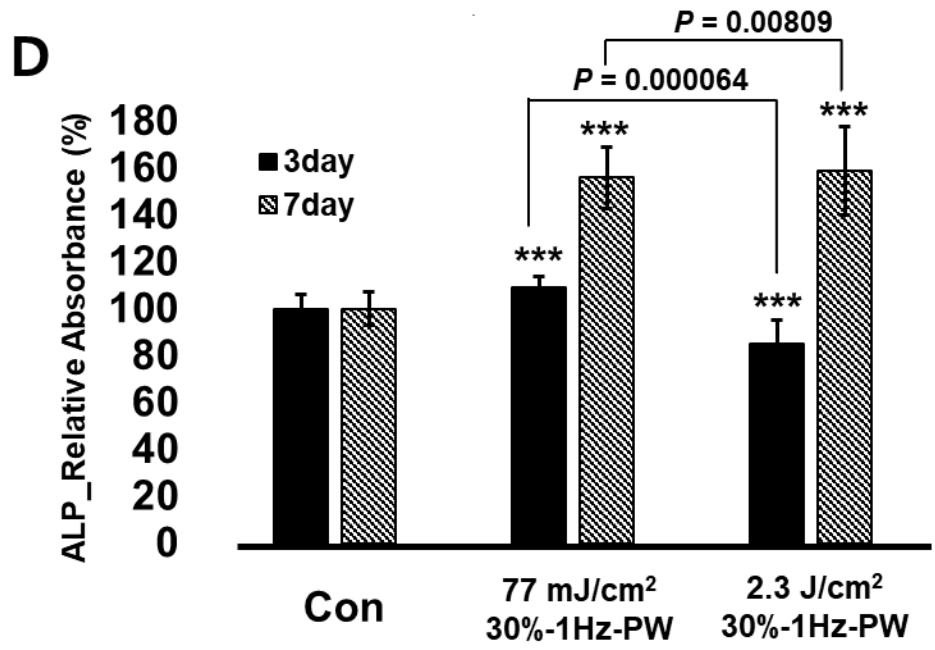
D
ALP_Relative Absorbance (%)
180
160
140
120
100
80
60
40
20
0
3day
7day
P = 0.00809
P = 0.000064
***
Con
77 mJ/cm2
30%-1Hz-PW
2.3 J/cm2
30%-1Hz-PW

Figure 3.2 Effects of power and duty cycle of PBM on hDPSC cytoplasmic membrane potential, metabolic activity and ALP activity. **A.** FLIPR fluorescence intensities of hDPSCs relative to control after 1 Hz PW-PBM treatment with different duty cycles 0.3 to 60 % (n = 3 in each experiment and 3 replicates). **B.** FLIPR fluorescence intensities of hDPSCs relative to control after 77 mJ/cm^2 CW-, 77 mJ/cm^2 PW-, or 2,310 mJ/cm^2 PW-PBM with 30 % duty cycle. The statistical analysis between CW and PW with 77 mJ/cm^2 indicated P expressed 0.033 (n = 3 in each experiment and 3 replicates). **C.** WST-1 assay absorbance relative to control after CW and 1 Hz PBM treatment with 30 % duty cycle. P values between CW and PW (1 Hz) was all under 0.001 (n = 10 in each experiment and 3 replicates). **D.** ALP activity absorbance relative to control after 77 mJ/cm^2 and 2,310 mJ/cm^2 1Hz PW-PBM applied energy density with 30 % duty cycle. P values between 77 mJ/cm^2 and 2.3 J/cm^2 in PW mode was significant (n = 10 in each experiment and 3 replicates).

cycle arrest have higher CMP difference (hyper-polarized). In case of differentiation, CMP increases as differentiation proceeds, since cells must coordinate their exit from the cell cycle with the initiation of their differentiation programs [134]. The relationship between CMP and differentiation was confirmed with chemical reagents which modulated CMP [133]. Our observation of spontaneous increase of CMP and the following increase of ALP activity indicates that molecules related to ion currents through membrane can be targets of PBM inducing cellular physiological responses including stem cell differentiation.

These experiments provide the optimal PW-PBM conditions for efficient hDPSC differentiation. hDPSC differentiation occurred more efficiently in PW stimuli than CW as previously reported with other cells [71, 121]. 30-%-duty cycle was most efficient, and the frequencies between 1 and 3000 Hz with same energy density drove similar responses except 3 Hz. Exceptionally, 3 Hz showed little effects on all the measurements. The peculiar response to 3 Hz PW-PBM should be studied separately. The power up to 2.3 J/cm^2 induced similar hDPSC responses. Therefore, for following experiments, we used PW-PBM with 30 % duty cycle and 77 mJ/cm^2 energy density in the range of 1-3000 Hz frequencies.

3.3.2 Intracellular reactive oxygen species (ROS) and mitochondrial responses

One of the purposes in this study was to search for cellular factors to induce osteogenic differentiation. We estimated the qualitative changes of intracellular ROS after PW-PBM with addition of N-acetyl cysteine (NAC). Fig. 3.3C showed that the addition of NAC during PW-PBM treatment reduced the increase of ALP activity. Since NAC is a well-known ROS scavenger, the enhanced ALP activity might be mediated by intracellular ROS [80]. Among various ROS, mitochondrial $O_2^{\cdot-}$ and cytoplasmic ROS levels were evaluated. Mitochondrial $O_2^{\cdot-}$ is generated as a byproduct of oxidative phosphorylation, and generally accepted as the major intracellular source of ROS. The cytoplasmic ROS includes OH·, NO·, or ROO·, which can be produced from enzymes as well as from mitochondria.

The mitochondrial membrane potential (MMP) is an electrochemical gradient through the mitochondrial inner membrane which is controlled by respiratory complexes I, III, IV and anion channels and drives the synthesis of ATP. The instant increase of MMP and ATP was observed in various cells right after PBM irradiation via enhanced cytochrome c oxidase activity

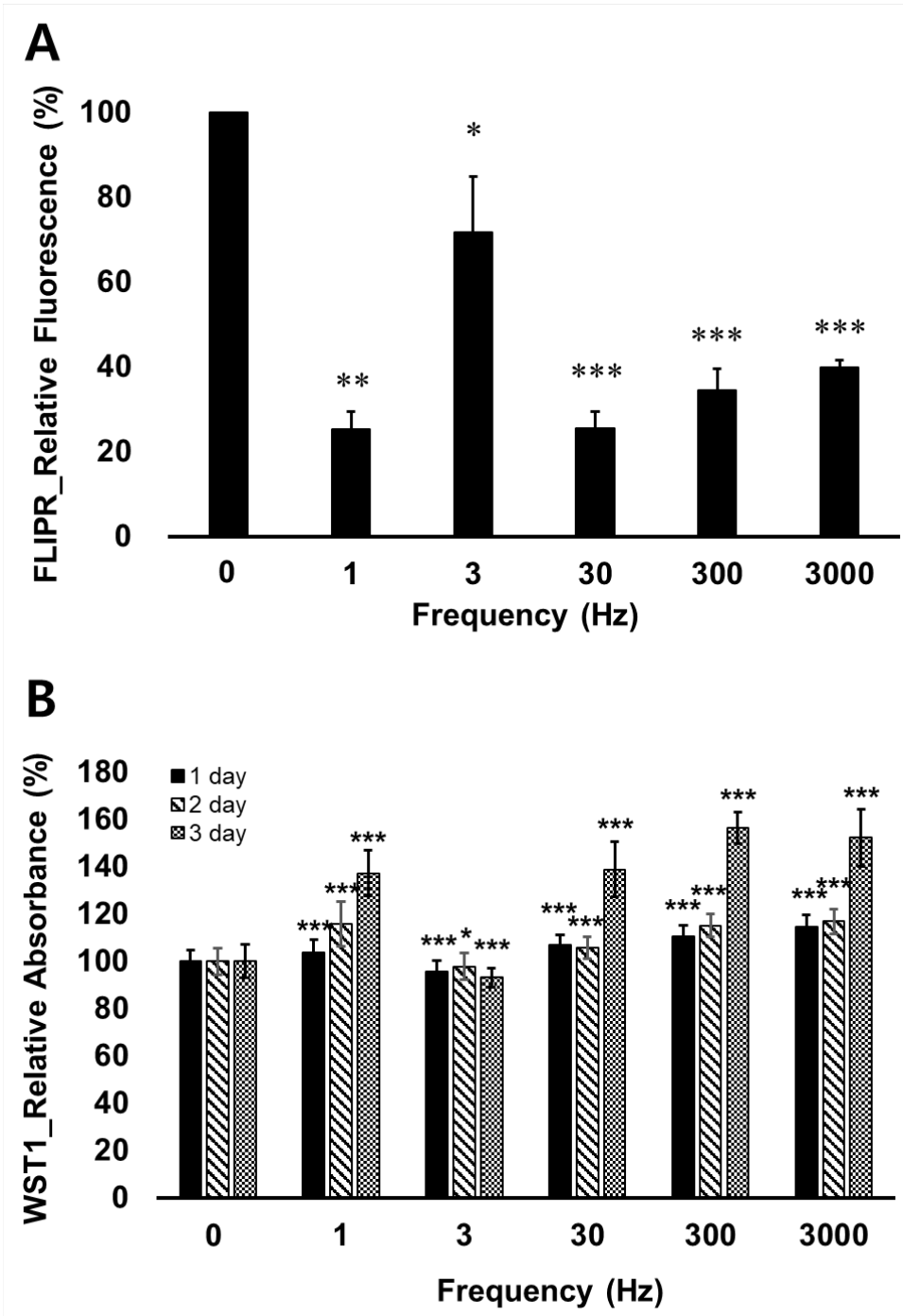
A
FLIPR_Relative Fluorescence (%)
100
80
60
40
20
0
**
*
***
***
***
0
1
3
30
300
3000
Frequency (Hz)
B
WST1_Relative Absorbance (%)
180
160
140
120
100
80
60
40
20
0
1 day
2 day
3 day
0
1
3
30
300
3000
Frequency (Hz)

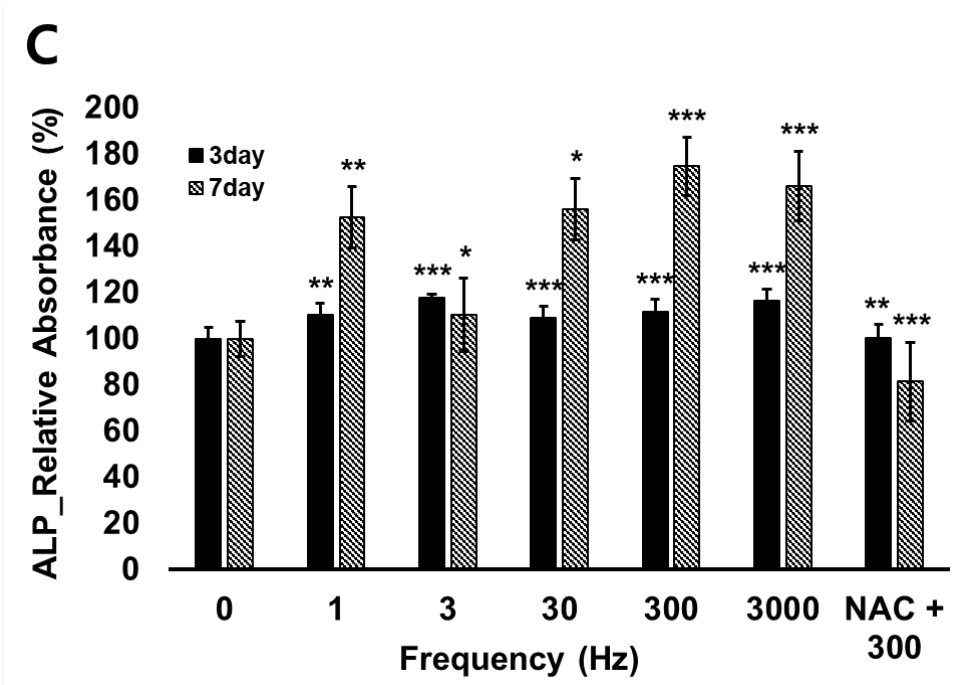

Figure. 3.3 Effects of frequency of PW-PBM on hDPSC cytoplasmic membrane potential, metabolic activity, and ALP activity. **A.** FLIPR fluorescence intensities of hDPSCs relative to control just after 77 mJ/cm^2 PW-PBM in 1, 3, 30, 300, or 3000 Hz with same 30 % duty cycle (n = 3 in each experiment and 3 replicates). **B.** Metabolic activities of hDPSCs relative to control for 3 days after 77 mJ/cm^2 PW-PBM in 1, 30, 300, or 3000 Hz with same 30 % duty cycle (n = 10 in each experiment and 3 replicates). **C.** ALP activity absorbance relative to control for 7 days after 77 mJ/cm^2 PW-PBM in 1, 30, 300, or 3000 Hz with same 30 % duty cycle. NAC was added for the case of 300 Hz PW-PBM (n = 10 in each experiment and 3 replicates).

[13, 18, 129, 135]. Cytochrom C oxidase is well known to absorb specifically NIR light in the range of 810-830 nm [136, 137]. Karu *et. al*. showed cytochrome C oxidase, the terminal enzyme of the mammalian respiratory chain, may play the main role in the initiation of PBM induced signal cascades [13]. MMP is delicately balanced by the concentration of ATP, ROS and Ca^{2+} ions [138]. In normal conditions, increase of MMP is strongly correlated with mitochondrial ATP and ROS generation, which are consistent with our observations.

Fig. 3.4A shows that the formation of cytoplasmic ROS was promoted over all frequencies except for that of 3 Hz. On the contrary, Fig. 3.4B shows that the production of $O_2^{\cdot-}$ in mitochondria was considerably decreased compared with the control over all the frequencies. In order to verify whether the reduction in mitoSox was mediated by the reduction of mitochondrial activity, MMP was evaluated. Fig. 3.4C shows the enhancement of MMP which is generally related to active mitochondrial states. Fig. 3.4D shows the increased amount of the intracellular ATP, which is also related to high activity of mitochondria.

These results showed that PW-PBM enhanced the mitochondrial bioenergetics, reduced mitochondrial superoxide, but at the same time enhanced cytosolic ROS. The ROS are made either in the matrix or in the inter-membrane space of mitochondria and then diffused into cytosol through the mitochondrial membrane. It is known that blocking of respiratory components decreases MMP and increases ROS. The increase of both MMP and ROS, in our experiments, implies that PW-PBM irradiation regulates some other components which initiate a cascade of redox changes and modulation of biochemical reactions. PW-PBM treatment may affect the efflux of $O_2^{\cdot-}$ from mitochondrial inner membrane to cytoplasm. In previous reports, Aon *et. al*. showed that a flash light could induce mitochondrial oscillation accompanying oscillating ROS formation, implicating the balance between ROS generation and their scavenging underlying the mitochondrial network [129]. Otherwise, PW-PBM may specifically activate mitochondrial complex III which enhanced ROS in cytosol easier than complex I which increases the MMP with generating ROS inside inner membrane of mitochondria [139].

3.3.3 Nucleus transcription factors

The increased cytoplasmic ROS has known to regulate nucleus transcription factors which determines cellular fates into proliferation, differentiation, or apoptosis, etc.[140]. The transcription factor nuclear factor kappa B (NF-kB) is one of the main transcription factors in redox signaling,

which induce antioxidant enzymes. Superoxide dismutase (SOD) 1 and 2, superoxide scavengers, are both regulated mainly by NF-kB [141]. SOD1 is located in cytoplasm and SOD2 is located in mitochondria. Both are essential for the survival of aerobic organisms, and their mutations are related to various kinds of diseases. Figs. 3.4E show that both SOD1 and SOD2 are upregulated over all the frequencies, which implies that cellular oxidative stress was increased and defense systems were initiated.

If the amount of ROS is too high, other transcription factors are activated to turn cell fate into cell cycle arrest or apoptosis. Tumor protein P53 is one of the important transcription factors inducing growth arrest in respond to oxidative stresses. Bcl-2-associated X protein (Bax) is one of the proteins transcribed by p53, which induces apoptosis. Fig. 3.4E shows the transcription of Bax genes was reduced following three days of PW-PBM treatment, but transforming growth factor β1 (TGF- β1) was up-regulated. TGF- β1 is a multifunctional peptide whose dysregulation is known to result in apoptosis. In addition, Fig. 3.4F shows the population in each cell cycle after three days of PBM treatment. The populations in G_0/G_1, S and G_2/M were not significantly changed, which indicates that our PW-PBM treatment did not cause excessive levels of ROS to induce cell cycle arrest or apoptosis in hDPSCs [142]. Cells became 100 % confluent after three days of culture regardless PBM treatment. Based on this result, the enhancement of WST-1 measurement may be ascribed to the enhanced metabolic activity of mitochondrial enzyme rather than cell proliferation.

Arany *et al*. showed that non-ionizing PBM treatment activate endogenous TGF-β1 through the increase of ROS[80]. TGF-β1 is known to be a master regulator of hDPSCs into dentinogenic differentiation. In their research, TGF- β1 signals were enhanced with the increase of PBM-treatment time, and the tendency was similar in ALP activities. Interestingly, our real time polymerase chain reaction data showed that the changes in TGF-β1 level according to the PW-PBM frequencies were similar to those in ALP activities. The transcription level was enhanced in most cases except when the frequency was 3 Hz. Though we could not reveal the underlying mechanisms for this frequency dependency, this correlation implies the strong relationship between TGF- β1 signaling and dentinogenic differentiation of hDPSCs.

3.3.4 Dentinogenic differentiation

Our measurements of changes in CMP, ALP activity, and metabolic enzyme activity support the possibility of commitment of hDPSCs into a dentinogenic

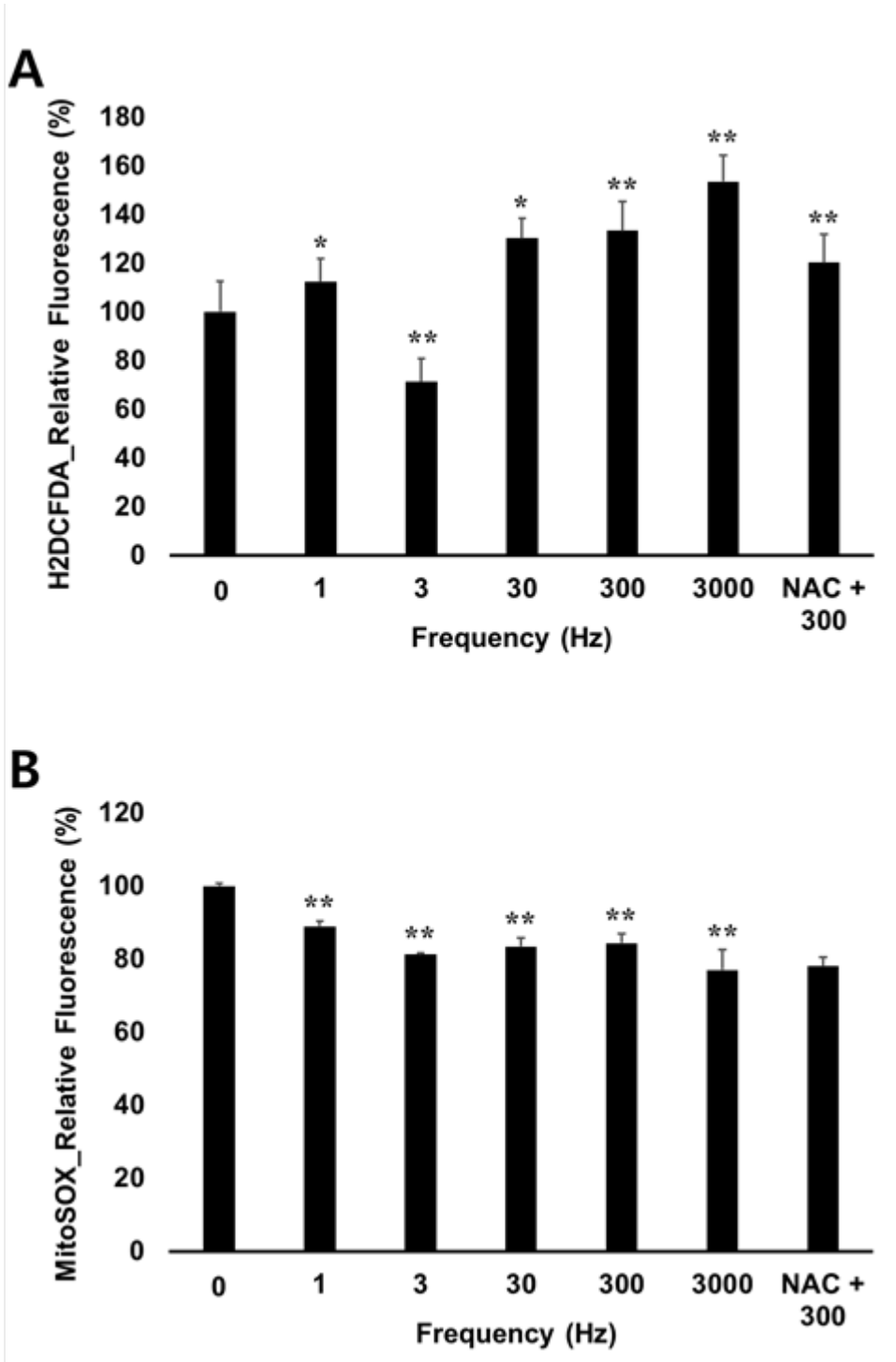
A
H2DCFDA_Relative Fluorescence (%)
180
160
140
120
100
80
60
40
20
0
*
**
*
**
**
**
0
1
3
30
300
3000
NAC + 300
Frequency (Hz)
B
MitoSOX_Relative Fluorescence (%)
120
100
80
60
40
20
0
**
**
**
**
**
0
1
3
30
300
3000
NAC + 300
Frequency (Hz)

C

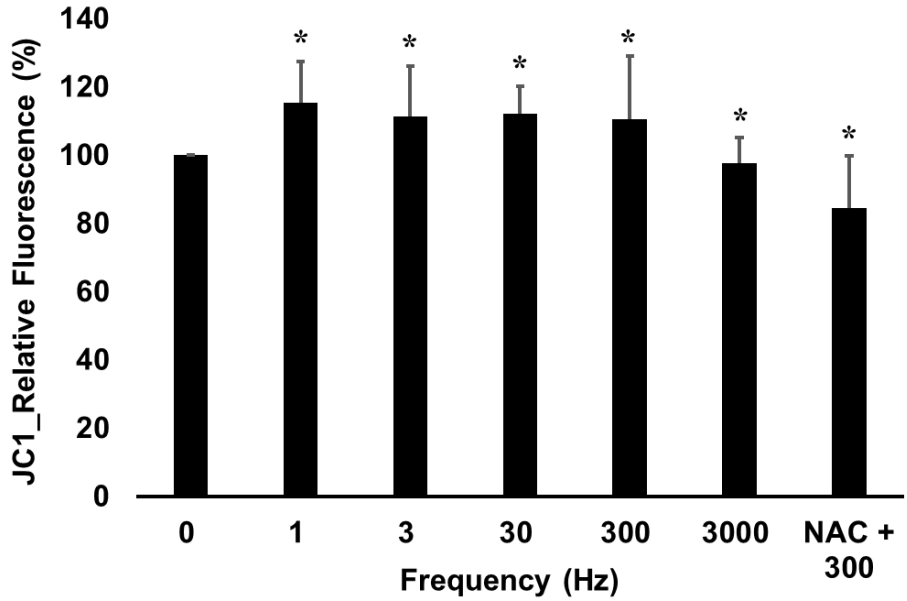
JC1_Relative Fluorescence (%)
140
120
100
80
60
40
20
0
*
*
*
*
*
*
0
1
3
30
300
3000
NAC + 300
Frequency (Hz)

D

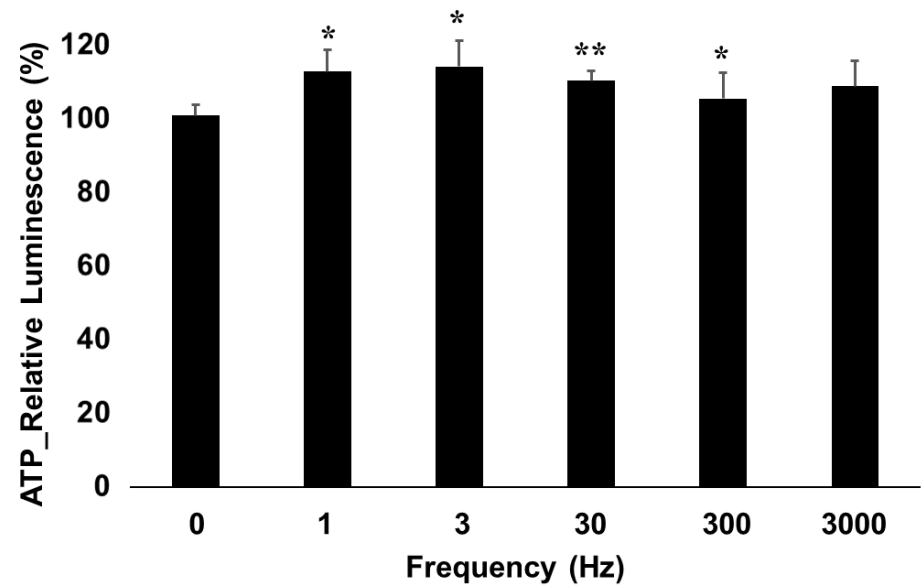
ATP_Relative Luminescence (%)
120
100
80
60
40
20
0
*
*
**
*
0
1
3
30
300
3000
Frequency (Hz)

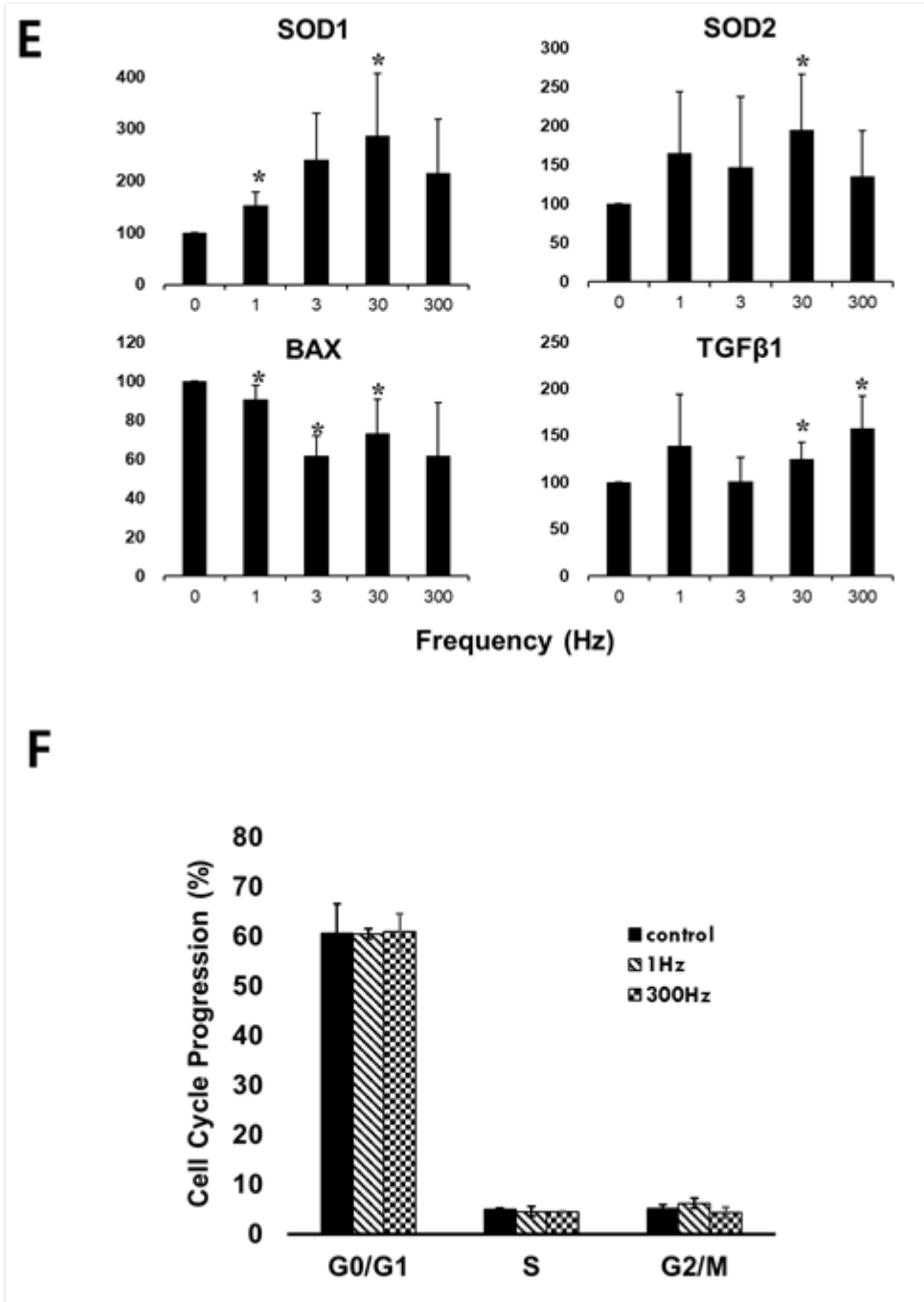
E
SOD1
SOD2
BAX
TGFβ1
Frequency (Hz)
F
Cell Cycle Progression (%)
control
1Hz
300Hz
G0/G1
S
G2/M

Figure. 3.4 Effects of frequency of PW-PBM on intracellular ROS, mitochondrial activity, intracellular ATP of hDPSCs, changes in the nuclear transcriptional levels, and cell cycle cycles. PBM conditions were 1, 3, 30, 300, or 3000 Hz PW-PBM with same 30 % duty cycle and 77 mJ/cm^2 total energy density, and NAC was for the case of 300 Hz PW-PBM. Cells were stained by the following dyes; **A.** H2DCFDA, **B.** MitoSOX, **C.** JC1, and **D.** ATP-luciferase. All the values were expressed as relative intensities to control. Intracellular ROS, mitochondrial membrane potential, and intracellular ATP increased, while mitochondrial superoxide decreased. hDPSCs were treated by PW-PBM of 1, 3, 30, and 300 Hz PW-PBM with 30 % duty cycle daily for 3 days (n = 3 in all each experiment and 3 replicates). **E.** mRNA transcriptional levels for SOD1, SOD2, BAX, and TGF-β1. There was no statistics (n = 3 in each experiment and 3 replicates). **F.** The population ratio in each cell cycle was not changed significantly. Increase of intracellular ROS affects the transcription of redox contolling genes, however it did not induce apoptosis or cell cycle arrest. There was no statistics (n = 3 in each experiment and 3 replicates).

lineage. To verify the induction of dentinogenic differentiation, morphological changes, ALP activity, and protein levels of ALP, dental matrix protein 1 (DMP1), osteopontin (OPN), osteocalcin (OCN), and bone sialoprotein (BSP) were estimated after 21 days of PW-PBM treatment with the frequency of 300 Hz. 300 Hz was chosen because cell's spontaneous responses were significant at that frequency. Figs. 3.5A show bright field images of hDPSCs stained with ALP activity assay kit after 21 days of daily PW-PBM irradiation. The stronger blue color implies the higher activity of ALP. This was confirmed quantitatively by using colorimetric analysis. Fig. 3.5B shows that ALP activity became significantly higher at 21 days of 300-Hz-PW-PBM. Fig. 3.5C shows the protein expression levels of dentinogenic related proteins [80, 143]. The original gel images were added in supporting information. All proteins were upregulated, and the quantification showed statistical significance in Fig. 3.5D. These data confirm that PBM treatment promoted differentiation as well as commitment of hDPSC into a dentinogenic lineage.

In this study, we investigated several cellular responses to PW-PBM which are related to dentinogenic differentiation. Immediately after PBM treatment, CMP increased, MMP decreased, intracellular ROS increased, intracellular ATP increased, and mitochondrial ROS decreased. Three days after PBM treatment, transcription of SOD1, SOD2, TGF-β1 and ALP increased and that of BAX decreased. The long-term cellular differentiation should be ascribed to those initial cellular responses, and their relationships have been studied by many researchers. Sunderlacruz *et.al.* showed that the inhibition of the inhibition of CMP reduced the osteogenic differentiation, and inversely increase of CMP enhanced the differentiation [133]. Pietila, *et al.* showed the strong correlations of MMP with ALP activity and together with Ca deposition [144]. Arany *et al.* showed that the level of ROS is strongly related to dentinogenic differentiation [80]. It is generally known that the low level of ROS contributes to maintain stem and progenitor cell's stemness, while mild level of ROS promotes differentiation, proliferation, migration and survival of the stem cells and progenitor cells [138, 145].

Though our results have similar tendency to those previous works, we found that CMP and intracellular ROS have much higher correlation with ALP activity, a marker for dentinogenic differentiation, than the values related to mitochondrial activity. Mitochondria has been suggested as a main absorber of NIR light which responds immediately [13]. To induce whole cell responses such as proliferation and differentiation, the changes in mitochondria should be transferred to a cell nucleus. In case of PW-PBM with 3 Hz frequency, it

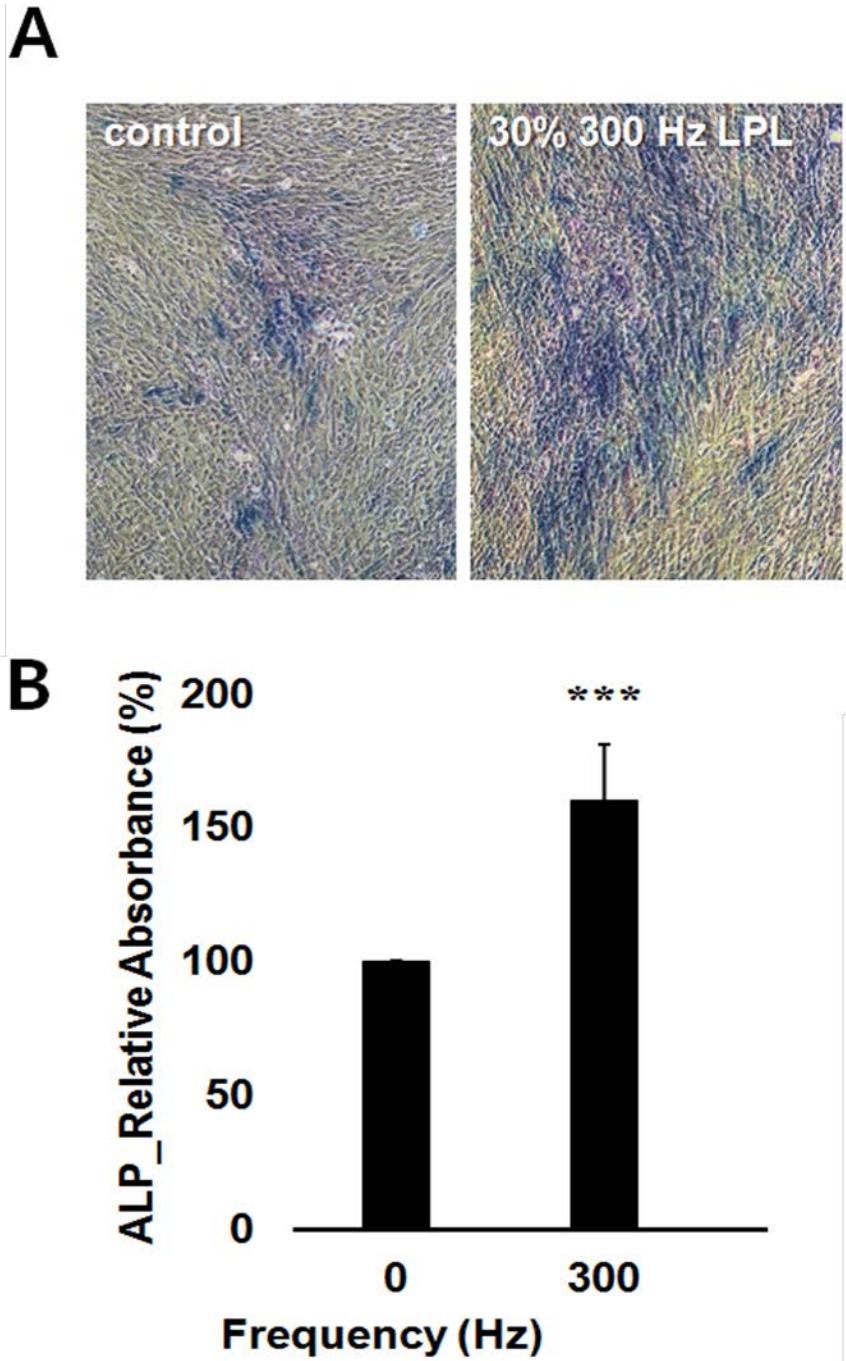
A
control
30% 300 Hz LPL
B
ALP_Relative Absorbance (%)
200
150
100
50
0
***
0
300
Frequency (Hz)

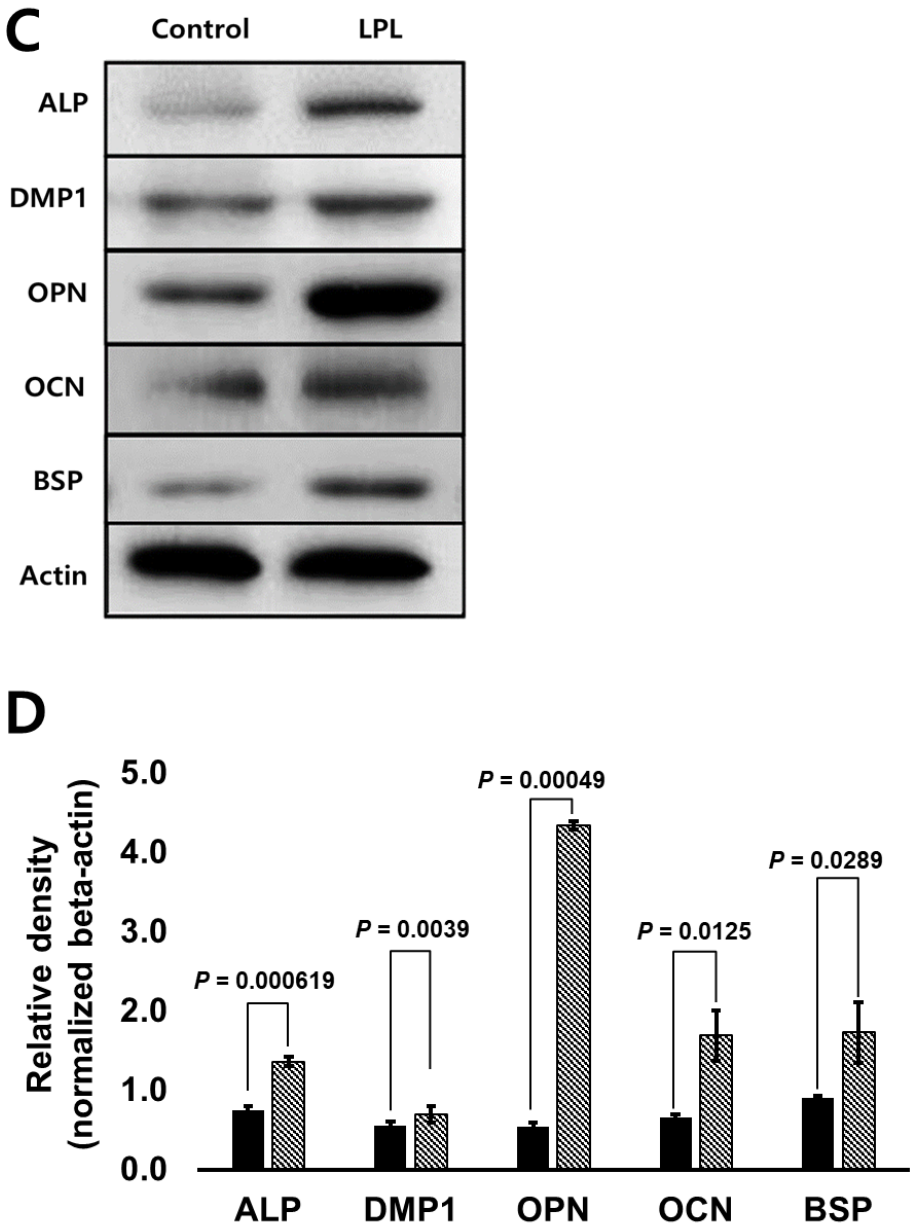

Figure. 3.5 Dentinogenic differentiation of hDPSCs after 21 days of PBM daily treatment. 300 Hz PW-PBM with duty cycles 30 % and 77 mJ/cm^2 total energy density were applied. **A.** Bright field images of hDPSCs stained with ALP staining kit at 21 after 30 %-3Hz-PBM daily irradiation. **B.** ALP activity absorbance relative to control (n = 3 in each experiment and 3 replicates). **C.** Western blots (W.B.) for ALP, DMP1, OPN, OCN, and BSP. **D.** Bar graph showing mean density relative to beta-actin by analyzing Fig.3.5C. The significance between controls and the PBM was all much lower than 0.05 (n = 3 in each experiment and 3 replicates).

induced similar mitochondrial responses but differential whole cell responses in comparison to other frequencies. For example, while most PW-PBM decreased mitochondrial superoxide and increased intracellular ROS, both mitochondrial and intracellular ROS were reduced with only 3Hz-PBM.

3Hz-PBM may activate the decomposition of ROS, inhibit the transfer of ROS through mitochondrial membrane, or modulate the lifetime of ROS itself. Considering the immediate change of CMP and MMP, the ion transfer seems definitively affected by PW-PBM. As suggested in previous studies, NIR light therapy may increases the intracellular ROS through transient mitochondrial activation, which may ultimately alter nuclear gene expression such as TGF-β1 [80]. The pulsing of light may activate or disturb these processes, especially in the mitochondrial signaling to cytoplasm.

3.4 Conclusions

In conclusion, we clearly showed that pulsing of PBM was more efficient in hDPSC differentiation than continuous wave irradiation. In our experiment, CW mode light did not induce significant changes in hDPSC states, which may be ascribed to the weak sub-mW level power of light we used. However, PW mode irradiation of the same power light induced significant changes in CMP and ALP activity. 30 % duty cycle and 300-3000 Hz pulse frequencies showed the highest effects on hDPSC function. Though the mechanism is not clearly known, high production of intracellular ROS and the activation of TGF-β1 signaling pathway should be related to this pulsing mode enhanced hDPSC-dentinogenic differentiation *in vitro*. Those results let us put another step further to understand and utilize PBM therapy in dental medicine.

Chapter 4

Near-infrared irradiation enhance differentiation of human dental pulp stem cells via blue-light-pre-irradiation

4.1 Introduction

Since discovering laser biostimulation of a low-powered ruby laser on growing hair in the mice, PBM has received increasing attention in clinical trials. This PBM has been applied to improve the healing of skin wounds, relieve pain, stiffness, fatigue of rheumatoid arthritis, and neurological disorders, and stimulate the proliferation of mesenchymal and cardiac stem cells[7, 115, 127, 146, 147]. The PBM consists of the application of a low-powered light source; laser or LED[116]. Laser or LED uses of the light in the red or near-infrared (NIR) region, with wavelengths usually in the range of 600 to 700 nm and 780 to 1100 nm. Power density of laser or LED ranges between 5 mW/cm^2 to 5 W/cm^2 [83]. Their output energy density is of a relatively low-density ranging between 0.04 to 50 J/cm^2 not to allow thermal effects[35]. In addition, a blue light also has been used as PBM to promote various kinds of stem cells into proliferation and differentiation[148-150]. The wavelength of blue light usually ranges from 400 to 500 nm with power density of ranging between 0.1 and 126 mW/cm^2. The output power density is ranging from 0.1 to 500 J/cm^2.

Meanwhile, responses of cell or tissue to PBM are performed through the absorption of energy by photoacceptor molecule (chromophores) during light irradiation. In a red- and NIR-ranged PBM, the photoacceptor molecule is thought to be cytochrome c oxidase (CCO)[111]. The CCO play a key role to convert absorbed photon to signals and then stimulate biological processes[151]. The excited cytochrome c oxidase increases the availability of electrons for the reduction of molecular oxygen in its catalytic center, enhancing the mitochondrial membrane potential (MMP) and the levels of adenosine triphosphate (ATP), cyclic adenosine monophosphate (cAMP) and ROS as well[18]. In contrast, porphyrin-containing enzymes and flavoproteins are thought to be photoacceptors linking the mitochondrial respiratory chain in a blue-ranged PBM[152, 153]. The accepted blue light is capable of releasing bioactive nitric oxide (NO) from nitrite and nitrosated proteins. NO plays a key

role in regulating the signals.

Nevertheless, despite such a few information, several studies have reported that blue light disrupts cellular processes: mitosis, mitochondrial function and DNA integrity[154-156]. In addition, it is reported that blue light reduced proliferation in a dose-dependent manner by up to 50%. They may be due to excessive light-induced reactive oxygen species (ROS). In contrast, blue light have been utilized to regulate stem cells (human skin cells or human adipose-derived stem cells) to differentiate[148, 149]. It suggests that mild-intensity blue light is able to help cells to activate metabolism function.

In spite of such advantages of red and NIR-PBM and blue light-PBM to cells, their PBM has not been alternatively utilized to activate more metabolism till now, especially to actively differentiate stem cells into osteogenesis. In the present study, we introduced blue-then-NIR light to maximize osteogenic-differentiation of hDPSCs. There are two kinds of modes in PBM as a way of applying PBM; continuous wave (CW) and pulsed wave (PW). CW has been almost used to PBM for cells or tissues much more than PW. Their effectiveness is controversial among them with targeted pathologies: wound healing, pain, and ischemic stroke[157]. In addition, it is similar in regeneration of nerve and bone. In our previous studies, the PW-effectiveness was much excellent than that of CW when the same energy density was applied. In here, we introduced PW mode than CW. We combined NIR with blue light alternatively in PW mode to enhance effectiveness of differentiate hDPSCs into osteogenesis.

In addition, to screen the pre-effectiveness of PW with blue-then-NIR light, we introduced a delayed luminescence (DL), in which radiate light after exposing light to cells. The DL has been investigated to distinguish between tumor and normal fibroblast or to assess the apoptotic capacity of cells[51, 158]. The origin of the DL is known to be mitochondria and lysosomes that present the chemical-physical properties of cells. Intracellular biomolecules that have been identified to contribute to the DL are nicontinamide adenine dinucleotide (NADH), flavins, protoporphyrin, and cytochrome c oxidase in an electron transport chain system of mitochondria. Among them, NADH emits in the blue light region and cytochrome c oxidase emits in the near infrared (NIR) region in relation to our study. We employed the DL in the present study to whether blue light or NIR or blue-then-NIR light contributes the hDPSCs to differentiate more to pre-investigate.

4.2 Materials and Methods

4.2.1 Cell culture

Human dental pulp stem cells (hDPSCs) were isolated from a tooth obtained following Institutional Review Board approval at Seoul National University Hospital (Seoul, South Korea; IRB number 05004). Patients consented the use of their teeth for research purposes, and no information about patients was included in this article. This article does not contain any information or images that could lead to identification of a study participant. All methods performed here were in accordance with the regulations. The tooth was dissected aseptically, and incubated with 4 ml of 0.25% trypsin-EDTA (Life Technologies) at 37 °C for 30 min. After neutralization with 4 ml of complete medium, solutions were pipetted vigorously to release cells, and then passed through a cell strainer (70 mm, Corning), and the resulting cells were cultured in complete medium supplemented with ascorbic acid (100 mM)(Sigma). hDPSCs were cultured in complete medium composed of 10% FBS, Dulbecco's modified Eagle's medium, penicillin (100 U/ml)–streptomycin (100 μg/ml) (all from Gibco, Life Technologies) supplemented with 100 mM ascorbic acid in a 37 °C incubator with 5% CO_2. For differentiation into osteogenic linage of hDPSCs, the complete medium was added with 10 mM β-glycerophosphate, 0.05 mM L-ascorbic acid-2-phosphate and 100 nM dexamethasone.

4.2.2 Fabrication of PBM system and Light dose

To make a system that serve stimulating hDPSCs with PBM, LED of NIR (810 nm) and blue (405 nm) were employed. A number of NIR and blue LEDs were 40 and 20, respectively. The LEDs of NIR were placed 5 mm in diameter and blue light-LEDs 10 mm. To make lights consistence, a diffuser was put on the top of LEDs. The placement on which was put by a plate with cell kept distance of 200 mm straightly to make incident light to uniform more. A driver of LED device was controlled based on an 8-bit-microcontroller (UM_MC95FG308_V3.20_EN, Korea), which was coded with C-language. The device have the ability to adjust frequency (LED On and Off time; 1 ~ 300 kHz), duty cycle (1 ~ 90%) and treatment time (1 ~ 59 sec, 1 ~ 59 min, 1 ~ 24 h) in the form of square wave. The output power was expressed as energy density (fluence, J/cm^2) The output was taken to 300 Hz-frequency fixing a total energy density at 89 mJ/cm^2. The dosages were planned following: 89 for NIR; 1.2 and 87.8 (BN1); 3.6 and 85.4 (BN2); 12 and 77 (BN3) mJ/cm^2 for blue light and NIR, respectively. Light dose was checked before every experiment with a power

meter (PM-USB-100, Thorlabs, USA). The cells were irradiated daily at the same environment of culturing cells (Fig. 4.1).

4.2.3 Mathematical description of the light-induced DL as a probability distribution

The relaxation of a non-equilibrium state into the equilibrium of a complex system can be approximated by a power law [93]. The DL temporal trend for a biological system can be modeled by a hyperbolic function, as given [50]:

$$I(t) = \frac{I_0}{\left(1 + {}^{t}/_{t_0}\right)^{m}} \tag{4.1}$$

where *I(t)* is the emitted intensity that can be obtained from the experimental data, I_0 is the initial value of the emitted intensity, *t* is time, and t_0 is an initial value.

DL intensity, *I(t)*, is associated through the decay probability, *P(t)*, with the degree of excitation, *n(t)*, that attenuates at any time *t* by the expression *I(t) = - dn(t)/dt* [93]. This can be evaluated for the value of a dimensionless function obtained from the experimental values of the intensity, *I(t)*, at a time *t*, as follows [93]:

$$P(t) = \left({}^{\frac{dn}{n}}\Big/_{\frac{dt}{t}} \right) = \frac{I(t)t}{n(t)} \tag{4.2}$$

where

$$n(t) = \int_t^{\infty} I(t')dt' \quad n(t) = -\left(\frac{I_0 t_0}{-m+1}\right)\left(1 + \frac{t}{t_0}\right)^{-m+1} \tag{4.3}$$

Using the data from Fig. 3.3, *P(t)* and *n(t)* are obtained.

4.2.4 WST-1 measurement

To estimate the proliferation of hDPSCs, 4 * 10^3 cells were seeded into 96-well culture plates. At 24, 48 and 72 hours of LPL treatment, cell culture media was removed from the plate and 110 μL of fresh media with 10% WST-1 (WST

based Cell Viability/Cytotoxicity Assay Kit, EZ-Cytox, Korea) according to the standard protocol of manufacturer was loaded to each well. The plate was then incubated at 37°C for 1 hour. Subsequently, 100 μL of the media was transferred to a new 96-well plate and the plate was measured using a plate reader (Tecan, USA) at 450 nm of wavelength.

4.2.5 Detection of intracellular ROS

For assessment of ROS, H2DCFDA (100mg, D399, ThermoFisher Scientific) was utilized. To avoid the probe acting as photosensitizers themselves, ROS probe was added immediately after the 5-min of LPL treatment, cells were washed with PBS and the ROS probe was added. Then the cells were incubated for 30-min at room temperature. After washed three times with PBS, fresh culture media was added and the cells were incubated for 30 min at room temperature supporting CO_2. The cells were measured by flow cytometry (BDVerse, BD, Germany) for ROS fluorescence and the mean value of each group was analyzed by the BD FACSuite™ software. The relative intensity of each group to control was expressed as a percent value.

4.2.6 Alkaline phosphatase (ALP) assay

For the alkaline phosphatase (ALP) activity assay, hDPSCs were seeded at $1.0*10^4$ cells per well in 96-well plates. The LPL was irradiated daily for 5, 7 and 14 days. On that time, according to the manufacturer's manual (Alkaline Phosphatase Assay Kit, Anaspec, USA), cells were washed twice with 1X assay buffer and lysed in lysis buffer (0.1% Triton X 100, pH 9.5) at 4 ℃ for 10 min under agitation. After vibration in weak, the supernatant of 50 μL per well was collected for alkaline phosphatase assay and transferred into new 96-well plate. pNPP substrate solution of 50 μL was added into each well of the plate and the plate was incubated for 60 min. Then fluorescence of the plate was measured using a plate reader (Tecan, USA) at 405 nm of wavelength.

A.

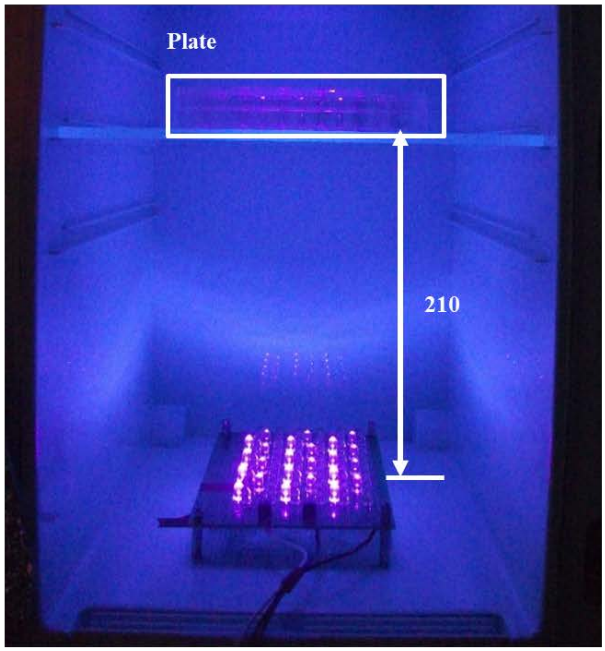

B.

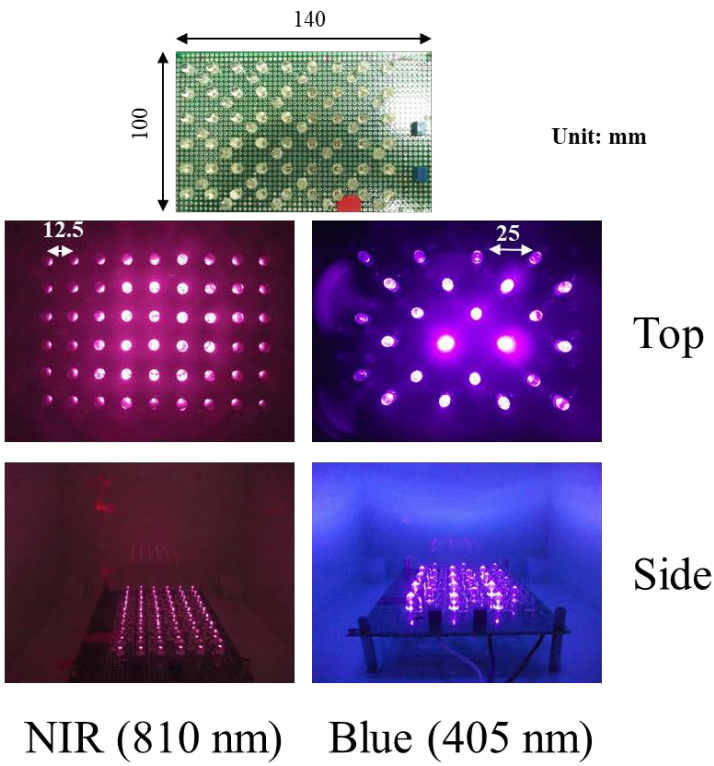

C.

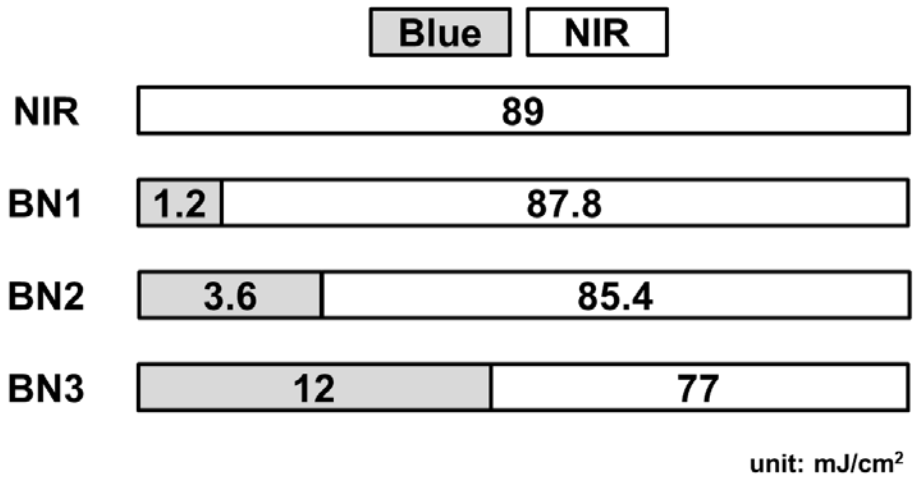

Figure 4.1. PBM system. **(A) (B)** PBM system in incubator. PBM system irradiate NIR light (810 nm) and blue light (405 nm) in separate. LED for NIR light is separated to be 12.5 mm in distance and LED for blue light 25 mm. To aim uniform of lights on the plate, the LED assembly is distant to the plate to be 210 mm. Light from LEDs exposes to cell plate. **(C)** Design for exposing is that NIR is 89, blue and NIR light (BN1) is alternately 1.2 and then 87.8, BN2 is 3.6 and then 84.4, and BN3 is 12 and then 77 mJ/cm^2.

4.2.7 Alizarin Red S staining

For assessing calcium deposition during matrix mineralization, Alizarin Red S staining was used. The cells were seeded at 1.0 * 10^4 cells per well in the 96-well plate. At 14 and 21 days after PBM treatment, the cells were washed twice with PBS and fixed in 4% paraformaldehyde for 10 min. The cells were then washed with deionized water and stained with Alizarin Red S (Sigma-Aldrich, St Louis, Mo, USA) for 10 min at room temperature. And then the dye was removed by deionized water and the stained was taken by stereo type microscopy. For quantification of calcium deposits, dye was extracted using 200 μL of 10% glacial acetic acid at room temperature for 60 min. The amount of calcium deposits was determined using an ELISA plate reader (Tecan, USA) at 490 nm.

4.2.8 Real-time polymerase chain reaction

For real-time polymerase chain reaction (PCR) analysis, hDPSCs were seeded at 5 * 10^4 cells per well in 24-well plate. The hDPSCs were daily irradiated to activate. After 14 days of irradiation, the hDPSCs were harvested and lysed. total RNAs were extracted using RNeasy Mini Kit (Qiagen) and converted to cDNAs using reverse transcriptase and random primers (cDNA synthesis kit, Toyobo) according to manufacturer's protocol. The same amount of extracted total RNA that was taken from each sample was used in cDNA synthesis. The synthesized cDNAs were used in real time PCR using a CFX96TM Real-Time System (BioRad). The relative amount of mRNA expression was normalized by that of RPL13α and expressed as a fold change. The relative gene expression was evaluated by the comparative cycle-threshold method. The expression level of the mRNAs of plasma-treated-cells was normalized by that of control cells. Primer pairs for the following human genes were used: RPL13α (F: 5' CTATGACCAATAGGAAGAGCAACC, R: 5' GCAGAGTATATGACCAGGTGGAA), SOD1 (F: 5' GGCAAAGGTGGAAATGAAGA, R: 5' GGGCCTCAGACTACATCCAA), SOD2 (F: 5' GTTGGCCAAGGGAGATGTTA, R: 5' TAGGGCTGAGGTTTGTCCAG), COL1A (F: 5' GCCGGCAAAGGTAGATGTGA, R: 5' TAGCGGTGGGGTTCGTCGAG), OCN (F: 5' CCCGTCCGAGTTAGATCTCA, R: 5' CAGTGTTGCGCTGTGTGCGG), RUNX2 (F: 5' GATAACCAAGTTAGATTTTA, R: 5' AAGGTTTGACCTTCCGTCAG), ALP (F: 5' TTCGGCTTAGTTAGATCTCA, R: 5' GAGTTCTGCCGAATGTGGAT), TGF-b1(F: 5' GAAGGTTAAGCCAGGGGTCC, R: 5' CAGTTCTGGGGTCCGTCGGG), OPN (F: 5' CTTGGTTAAGCCAGATGTCC, R: 5' AAGGTTTGACCTTTGGCCCT), DSPP (F: 5' GGGGTTCAAGGCCGATCCTA, R: 5' TAGAAATGACCTTCCTCCGG).

4.2.9 Electron transmission microscopy

To optimize mitochondrial structural preservation and membrane contrast, cells were fixed with 2% paraformaldehyde and 2.5% glutaraldehyde (Ted Pella, Redding, CA, USA) in 0.15 M sodium cacodylate (pH 7.4) at 37 °C and placed in pre-cooled fixative on ice for 1 h. The cells were post-fixed with 1% osmium tetroxide, 0.8% potassium ferrocyanide, and 3 mM calcium chloride in 0.1 M sodium cacodylate (pH 7.4) for 1 h, washed with ice-cold distilled water, post-stained with 2% uranyl acetate at 4 °C, dehydrated using graded ethanol, and embedded in Durcupan resin (Fluka, St. Louis, MO, USA). Ultrathin (70 nm) sections were post-stained with uranyl acetate and lead salts and observed using a JEOL 1200FX (JEOL, Japan) at 80 kV. Images were digitized at 1,800 dpi using a Nikon Cool scan system (Nikon Instruments Inc., USA), giving an image pixel array of 4,033 × 6,010 and a pixel resolution of 1.77 nm.

4.2.10 Statistical analysis

All variance values in the text and figure legends are represented as the mean values. Data were analyzed using the two-way ANOVA. Statistical analyses were performed using R console version 3.4.2. Statistically significant differences were defined as $P < 0.05$.

4.3 Results

4.3.1 DL analysis

The DL analysis was conducted for hDPSCs to measure light-induced ultraweak photon emission relaxation dynamics, which links to the functional state of the hDPSCs. The time trends of the experimental data exhibited decay behaviors in Fig. 4.2A, 2D, 2G, and 2J. To make the decay distinct discrimination, we employed the number of excited level (*n(t)*), which means showing the excited state of biological system by PBM. It exhibited that the number of excited level *n(t)* of hDPSCs subjected to blue of 300 Hz (B1) was higher than that of the NIR of 300 Hz (NIR) and less than that of the NIR with blue light of 300 Hz (BN1) in Fig. 4.2B. The other data here were not shown due to their divergence with time. We performed the DL on these convergence data (B1, NIR and BN1) for the various kinds of blockers. The numbers of hDPSCs that were blocked with Antimycin-A were all lowered down almost near zero for blue and NIR including blue-then-NIR light (Fig. 4.2E). The number of Rotenone-blocked hDPSCs subjected to NIR was similar to that of the control but the others were lowered (Fig. 4.2H). The numbers of NAC-treated hDPSCs

all showed low level for the NIR and blue-then-NIR light (Fig. 4.2K). Accordingly, the decay probability *P(t)* of control hDPSCs showed same temporal trend with the number of excited level of control hDPSCs in Fig. 4.2C. Decay probability of the others was followed after their number of excited levels (Fig. 4.2F, 2I and 2L).

4.3.2 Proliferation of hDPSCs

The proliferation of hDPSCs after PBM treatment was measured with WST-1 assay. After irradiation with totally 89 mJ/cm^2, the WST-1 activity was significantly increased in NIR-treated cells (approximately 25 %) and blue-then-NIR-treated cells (BN1-100.5 %; $P < 0.05$, BN2-106.5 %; $P < 0.05$, BN3-114.5 %; $P < 0.05$) compared with the control at 3 days (Fig. 4.3A). Moreover, the proliferation was significantly decreased in the blue-treated cells (B1-98.5 %; ns, B2-92.1 %; $P < 0.05$, B3-94.4%; $P < 0.05$) compared with the control at 3 days of irradiation but might not be sufficient to cause a significant oxidative stress (Fig. 4.3A).

4.3.3 Osteogenic differentiation of hDPSCs

For evaluation of the osteogenic differentiation of hDPSCs, ALP activity and Alizarin Red S staining were utilized. At 7 day after irradiation, hDPSCs that was exposed to the BN1 manner showed a higher ALP activity (702 %; $P < 0.001$) when compared with control and the others. Interestingly, the ALP activities of hDPSCs that was exposed to NIR, blue light and blue-then-NIR light were significantly enhanced (NIR-542 %; $P < 0.001$, BN1-702 %; $P < 0.001$, BN2-548 %; $P < 0.001$, BN3-535 %; $P < 0.001$) on 7 days through on 5 days and then significantly lowered (NIR-188 %; $P < 0.001$, BN1-213 %; $P < 0.001$, BN2-243 %; $P < 0.001$, BN3-192 %; $P < 0.001$) on 14 days after irradiation (Fig. 4.3B). However, all data of ALP activity for hDPSCs that was irradiated caused an increase than the control. Moreover, the PBM promoted the calcium deposition in a dose-rate dependent manner at 14 and 21 day after irradiation (Fig. 4.3C). In order to quantify the calcium deposition, destaining of hDPSCs on ARS staining with destaining solution was performed. The quantification of hDPSCs showed exposure of the NIR manner caused a 28.2 % (ns) increase in deposit calcium at 21 days after irradiation as in Fig. 4.3D, although the others were less than the control (BN1-66.7 %; $P <0.001$, BN2-86.8 %; $P < 0.001$, BN3-69.2 %; ns) at the same day.


NIR
BN1
BN2
BN3
B1
B2
B3

A.

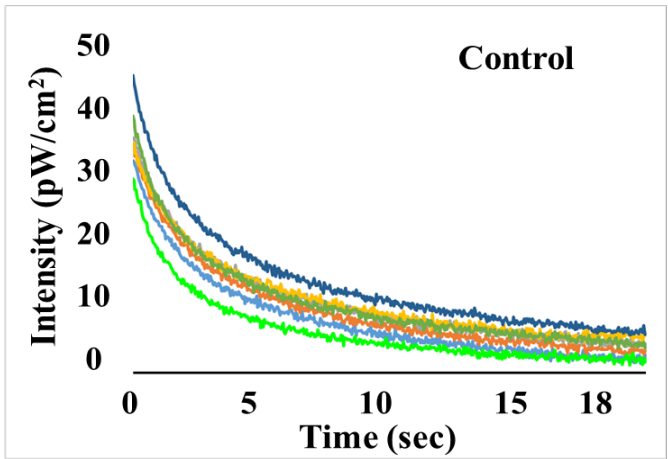
Control
Intensity (pW/cm²)
50
40
30
20
10
0
0
5
10
15
18
Time (sec)

B.

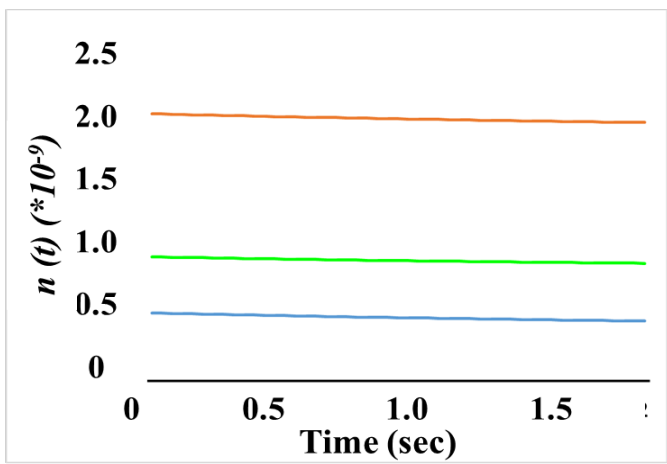
n (t) (*10⁻⁹)
2.5
2.0
1.5
1.0
0.5
0
0
0.5
1.0
1.5
Time (sec)

C.

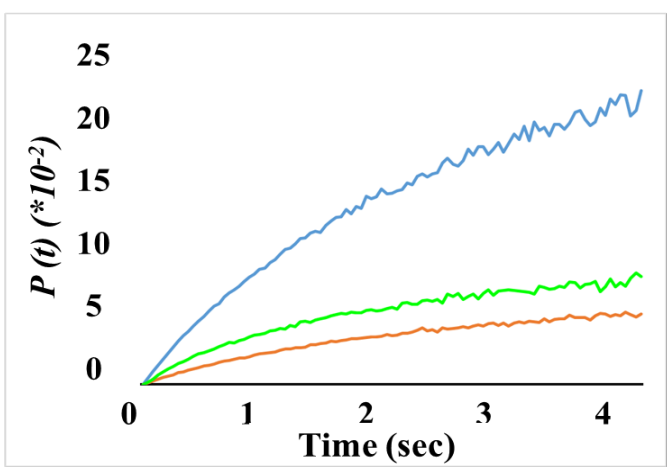
P (t) (*10⁻²)
25
20
15
10
5
0
0
1
2
3
4
Time (sec)


NIR
BN1
BN2
BN3
B1
B2
B3

D.

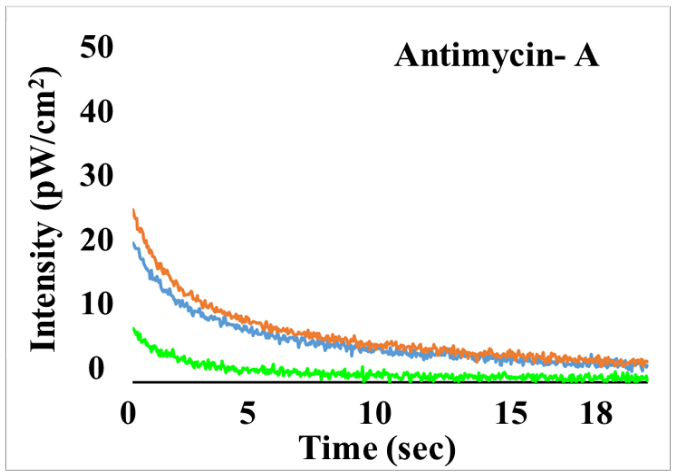
Antimycin- A
Intensity (pW/cm²)
50
40
30
20
10
0
0
5
10
15
18
Time (sec)

E.

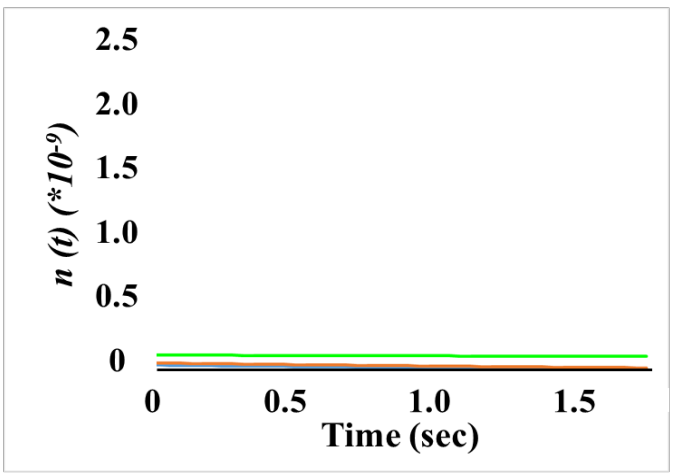
n (t) (*10⁻⁹)
2.5
2.0
1.5
1.0
0.5
0
0
0.5
1.0
1.5
Time (sec)

F.

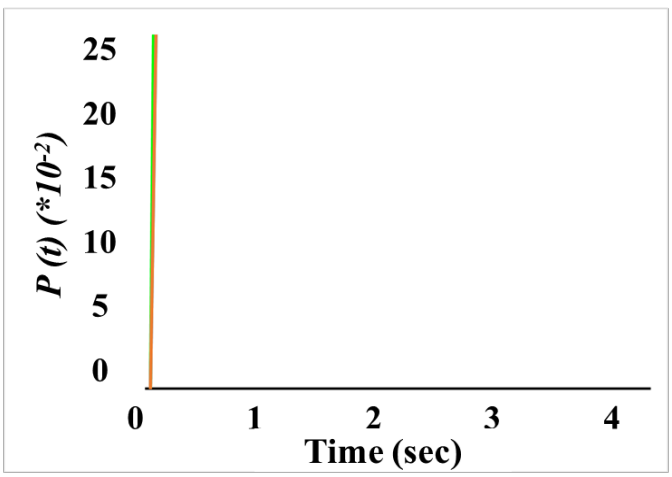
P (t) (*10⁻²)
25
20
15
10
5
0
0
1
2
3
4
Time (sec)


NIR
BN1
BN2
BN3
B1
B2
B3

G.

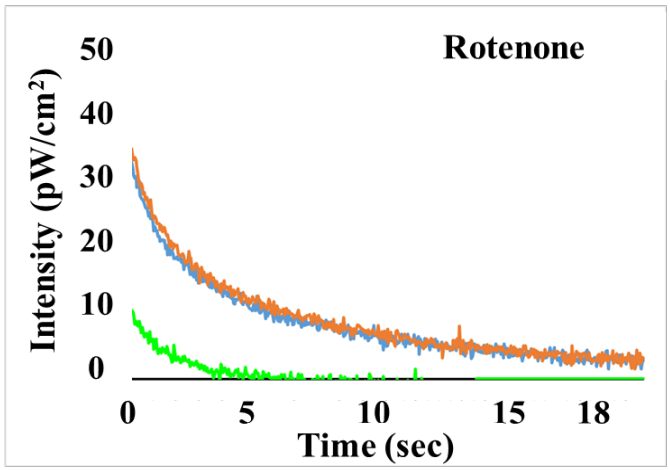
Rotenone
Intensity (pW/cm²)
50
40
30
20
10
0
0
5
10
15
18
Time (sec)

H.

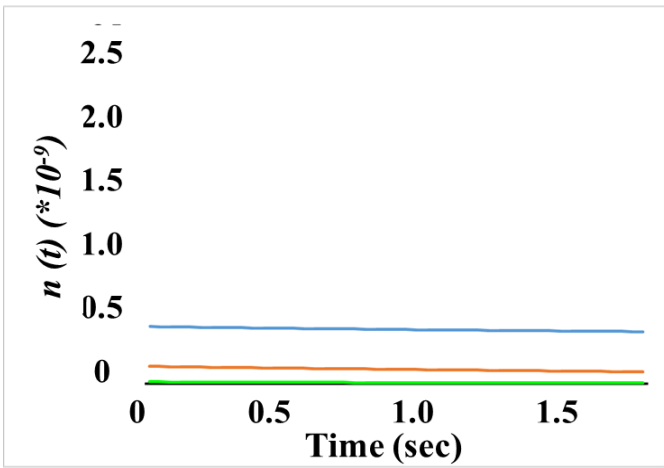
n (t) (*10⁻⁹)
2.5
2.0
1.5
1.0
0.5
0
0
0.5
1.0
1.5
Time (sec)

I.

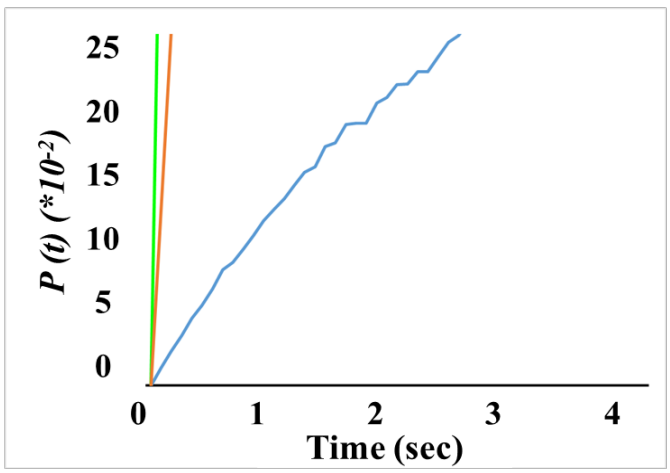
P (t) (*10⁻²)
25
20
15
10
5
0
0
1
2
3
4
Time (sec)


NIR
BN1
BN2
BN3
B1
B2
B3

J.

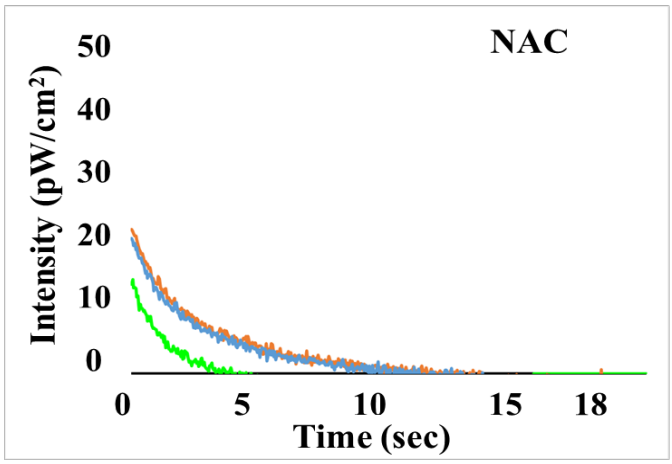
NAC
Intensity (pW/cm²)
50
40
30
20
10
0
0
5
10
15
18
Time (sec)

K.

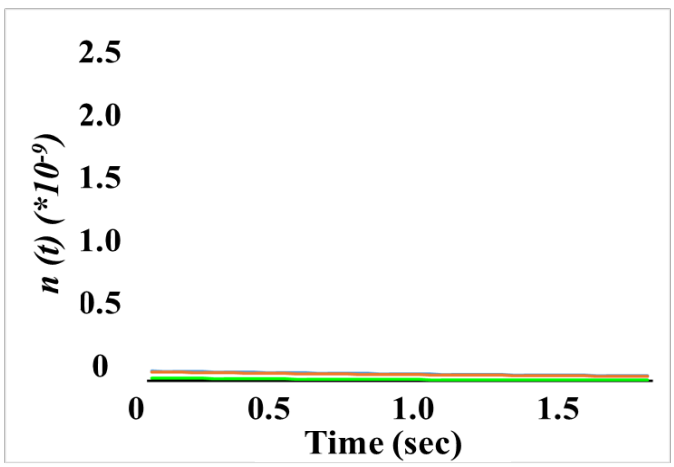
n (t) (*10⁻⁹)
2.5
2.0
1.5
1.0
0.5
0
0
0.5
1.0
1.5
Time (sec)

L.

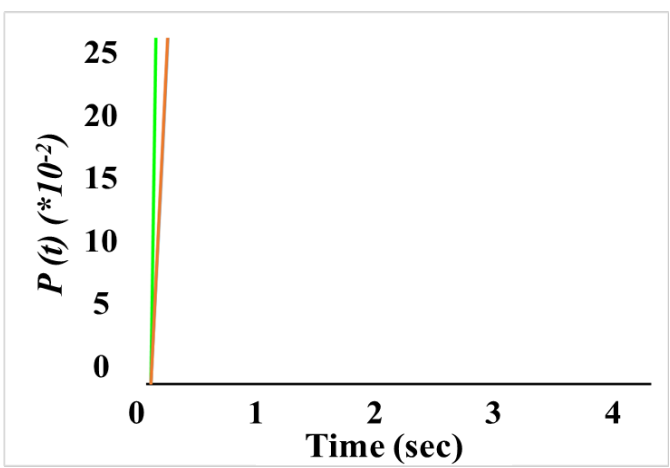
P (t) (*10⁻²)
25
20
15
10
5
0
0
1
2
3
4
Time (sec)

Figure 4.2. DL data from hDPSCs in responses to PBM treatment. The measured DL in the period between 1 s and 18 s after PBM treatment were plotted. DL was measured when hDPSCs were in PBS with no treatment **(A)**, with pre-treatment in antimycin-a **(D)**, with pre-treatment in rotenone **(G)**, and with pre-treatment in NAC **(J)**. The degree of excited level *n(t)* **(B, E, H, K)** and the temporal trend of the decay probability *P(t)* **(C, F, I, L)** from DL. The time scales of the *n(t)* and *P(t)* were changed for clear discrimination.

4.3.4 ROS production and PCR analysis

The ROS production was analyzed for hDPSCs in the NIR-dependent manner. hDPSCs subjected to irradiation showed all significant increase in ROS production (NIR-1.0%, BN1-52 %, BN2-97 %, BN3-101 %) compared to the control. Interestingly, hDPSCs subjected to blue-then-NIR light caused higher production of ROS significantly (Fig. 4.4A). The tendency of ROS production with irradiation manner was similar to the results of ALP activity with its manner (Fig. 4.3B). The RT-PCR analysis was performed for genes of COL1A, OCN, RUNX2, ALP, GTF-b1, SOD2, OPN, and DSPP on 14 days after irradiation. COL1A was activated for NIR, BN1 and BN2 (2.13-fold; $P < 0.05$), OCN for BN3 and BN3, RUNX2 for NIR (1.72-fold; $P < 0.05$), BN2 and BN3, ALP for BN1 (3.1-fold; $P < 0.05$) and BN2, TGF-b1 for NIR (18.7-fold; $P < 0.05$) and BN1, SOD2 for overall, OPN for all manners (NIR-2.7 folds; $P < 0.05$, BN2-1.8 folds; $P < 0.05$, BN3-7.5 folds; $P < 0.01$), DSPP for BN1, BN2 and BN3 (8.7-fold; $P < 0.01$) compared with the control (Fig. 4.4B). ALP expression decreased in the hDPSCs subjected to NIR on 14 days but was not statistically significant, while hDPSCs subjected to blue-then-NIR light produced a few folds of ALP compared to the control. Interestingly, TGF-b1 expression of hDPSCs subjected to NIR and blue-then-NIR light showed over approximately 10-fold, respectively. SOD2 expression of hDPSCs subjected to all manners of PBM showed the little increase compared with the control. OPN and DSPP expression of hDPSCs subjected to BN3 was both higher than these of other manners (Fig. 4.4B).

4.3.5 Morphological changes in mitochondria from PBM treatment

To analyze the alterations in mitochondrial shape by means of PBM treatment, transmission electron microscopy (TEM) was performed (Fig. 4.5). The TEM images revealed that hDPSCs subjected to all experiment conditions were similar to shapes in mitochondria as well as cristae that was developed.

4.4 Discussion

Blue light has a shorter wavelength than NIR. By photon energy equation, $E = hc/\lambda$, which h is Planck constant, c the speed of light in vacuum and λ the photon's wavelength, blue light have a photon energy about twice than the NIR. Thus if blue light expose to hDPScs, blue can cause electrons in the mitochondrial transport chain to easily jump higher levels than the NIR. Blue-then-NIR light may exert cells twice in transporting electrons than using only the NIR and thus make the cells to produce ATP twice, even though using

A.

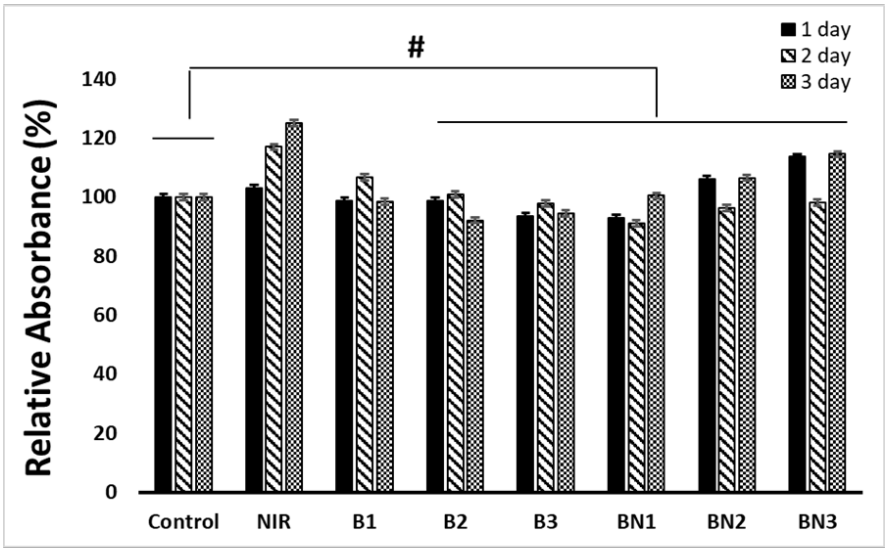
1 day
2 day
3 day
#
Relative Absorbance (%)
140
120
100
80
60
40
20
0
Control
NIR
B1
B2
B3
BN1
BN2
BN3

B.

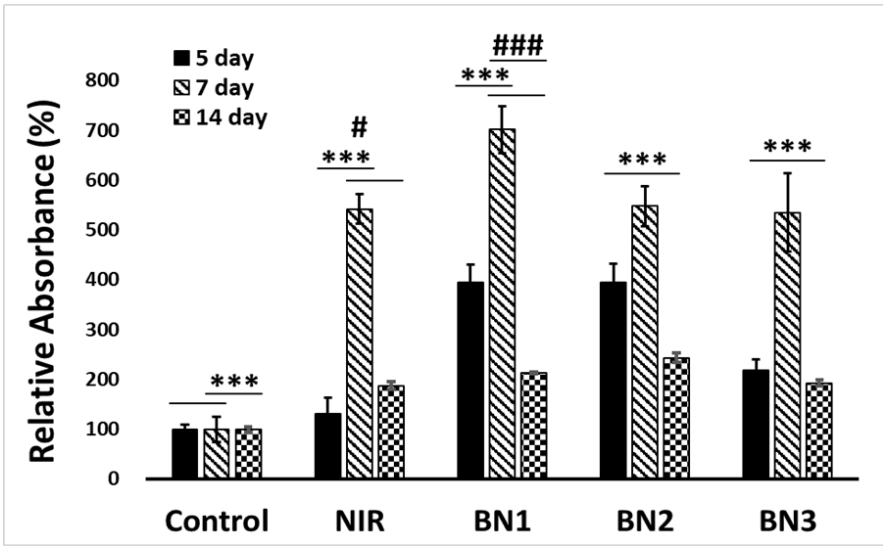
5 day
7 day
14 day
###
***
#
***
***
***
***
Relative Absorbance (%)
800
700
600
500
400
300
200
100
0
Control
NIR
BN1
BN2
BN3

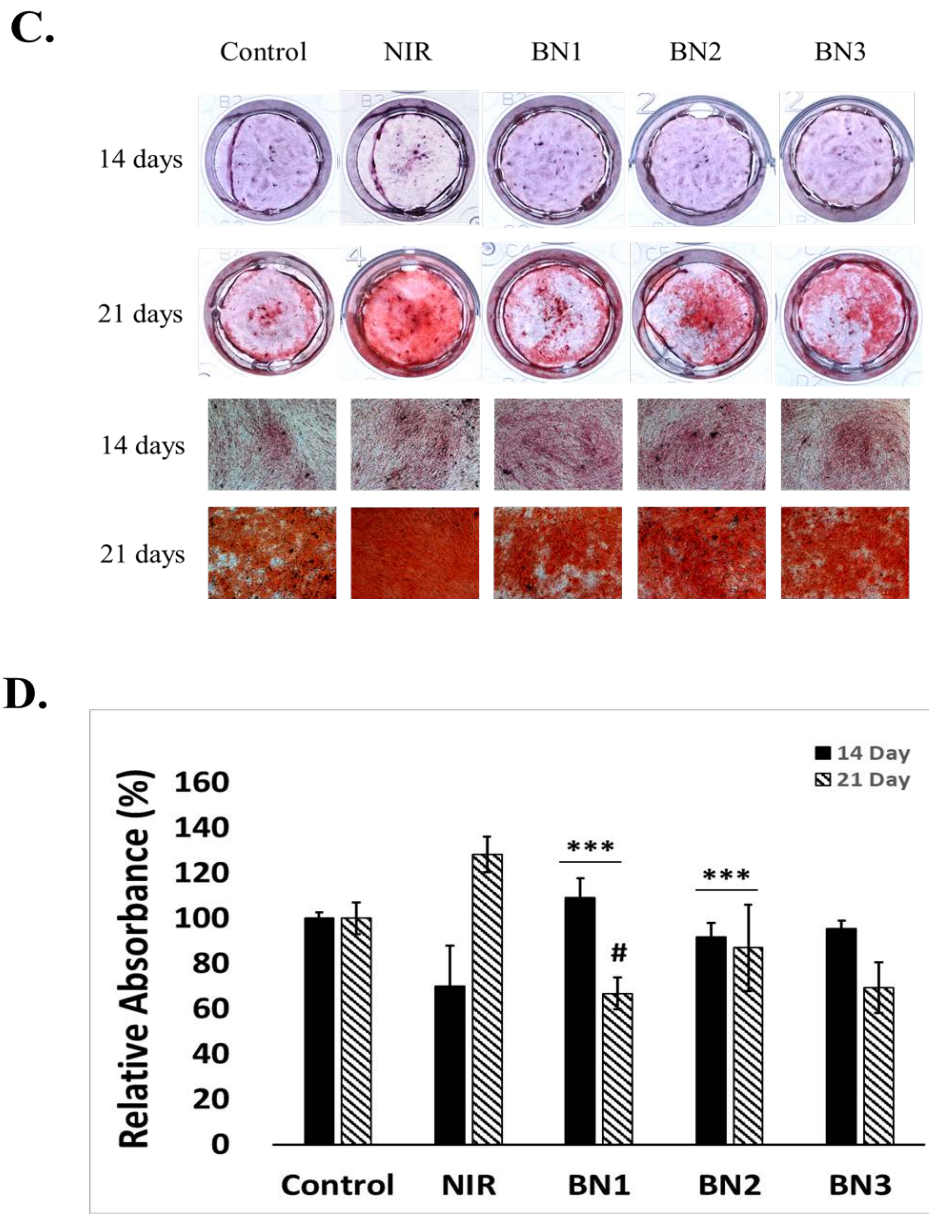

Figure 4.3 Proliferation and differentiation of hDPSCs by means of PBM treatment. **(A)** Proliferation of hDPSCs was assessed by WST-1 for 3 days. (n=6 per group, two-way ANOVA) **(B)** Alkaline phosphatase activity was measured at 3, 7, and 14 days after PBM treatment. (n=6 per group, two-way ANOVA) **(C)** Calcium deposition during matrix mineralization was assessed by Alizarin Red S (ARS) staining at 14 and 21 days after PBM treatment. **(D)** Quantitative analysis of **(C)** ARS staining was performed with destaining solution for ARS (n=6 per group, two-way ANOVA). *** $P < 0.001$ in one group, #$P < 0.05$, ###$P < 0.001$ vs. other group. Data are presented as the mean value.

same power density.

As for blue light it has been made known to disrupt cellular processes such as mitosis, mitochondrial function, or DNA integrity, and that light-induced reactive oxygen species[152, 154-156]. In contrast, a few recent studies on stem cells reported that blue light contribute to modulate stem cells to differentiate specific lineage[148-150]. They suggested that the photoacceptor as a blue light signal transducer might be nitrosated proteins[148] or Flavin[159-163], which is in the beginning of the respiratory chain of mitochondria, to have various kinds of stem cells initiate differentiation into. In addition, NIR has been used to promote proliferation due to more production of ATP and differentiation of stem cells. In proliferation of stem cells, the NIR activates the cytochrome c oxidase and then enhances mitochondrial membrane potential to produce more ATP. In differentiation of stem cells, the NIR causes metabolic switch to shift glycolysis to oxidative phosphorylation and then activates more differentiation[164]. Therefore, blue-then-NIR light can more promote hDPSCs to proliferate and differentiate.

In data of DL, it revealed possible mechanisms of effect of blue-then-NIR light. The ultraweaker delayed luminescence is closely associated with functional state of biological systems[165, 166]. Based on that, some studies showed the possibility to discriminate between normal and tumor conditions [50] and to perform *in vivo* measurements of the mitochondrial oxygen tension[54]. A few studies also showed the ability of the DL to be sensible indicator of alterations induced on functionality of the mitochondrial respiratory chain complex I[93]. In here, the DL dynamics of hDPSCs showed that DL of blue light in cells that was blocked with rotenone produced the significant decrease in, thus meaning the photoacceptor of blue light is Flavin protein. On the other hands, cells that was blocked with Antimycine-A simultaneously showed the significant decrease in, meaning an unknown protein as photoacceptor may be there, even though a photoacceptor in mitrochondrial complex III was cytochrome c oxidase, which is sensitive to range of Red or near infrared (Fig. 4.2). Thus this means blue light is able to excite electrons in a mitochondrial complex I and III to higher levels, simultaneously. NIR exposure after blue light lighting to cells can more make their proteins activate production of ROS and thereafter all ATP.

In the present study, we utilized low level of blue light (rate of blue light to NIR-approximately 1/6.6; power density: NIR 986 and blue light of 149 $\mu W/cm^2$ respectively) to exert the hDPSCs moderately to greatly diminish induction of arrest in cell cycle due to blue light. The proliferation of hDPSCs

A.

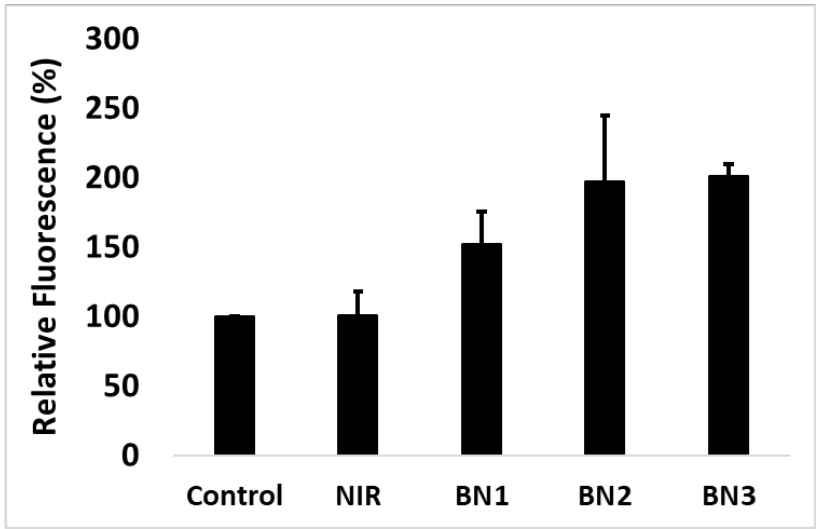
Relative Fluorescence (%)
300
250
200
150
100
50
0
Control
NIR
BN1
BN2
BN3

B.

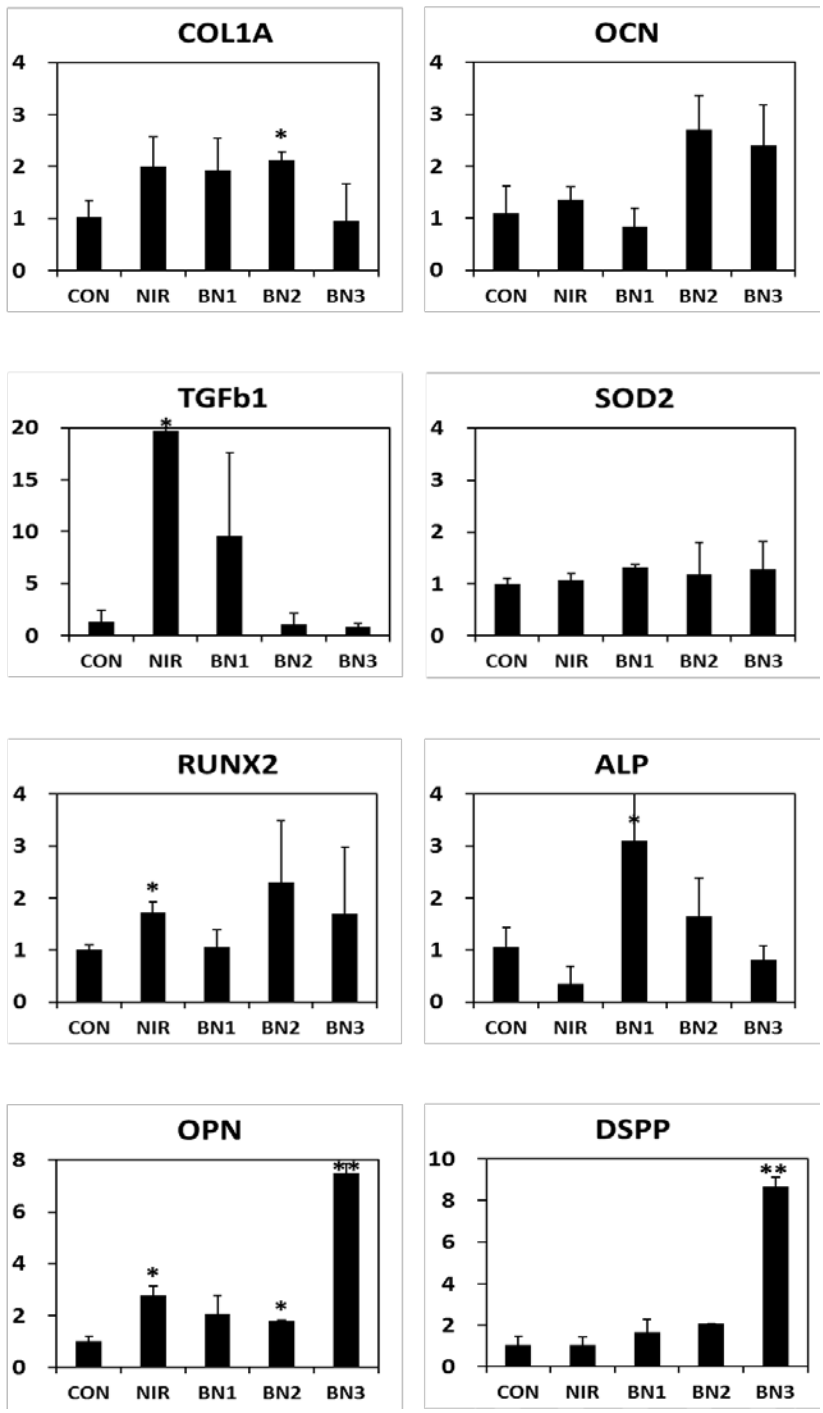

Figure 4.4. Biological responses of hDPSCs to PBM treatment. **(A)** Intracellular ROS was measured with H2DCFDA. NAC was used to confirm the fluorescence signals. **(B)** mRNA transcriptional levels for COL1A, OCN, RUNX2, ALP, TGF-β1, SOD2, OPN, and DSPP (n = 3 in each experiment and 3 replicates).

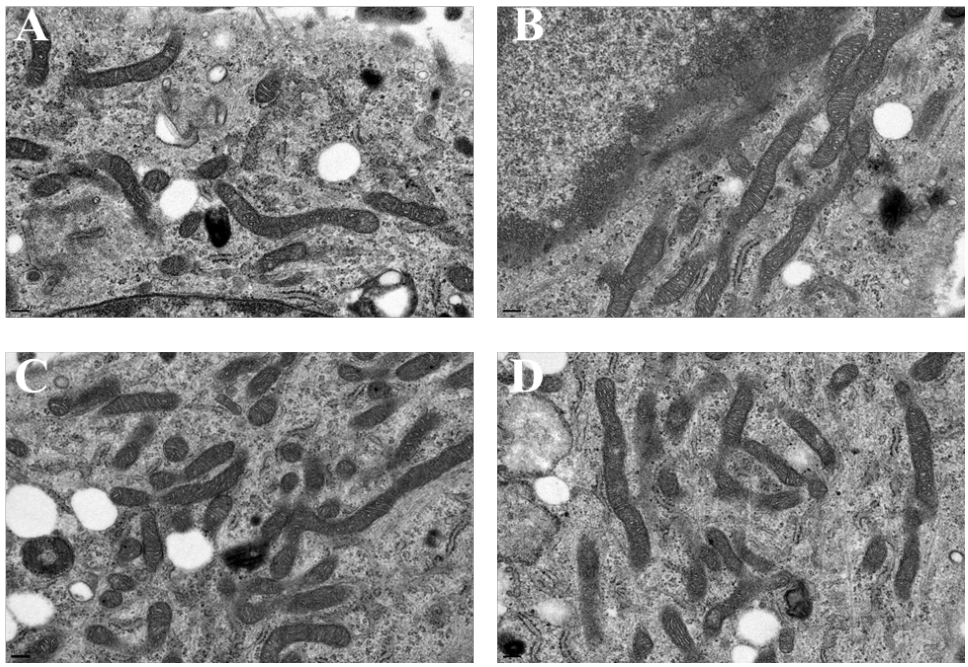

Figure 4.5. Representative TEM images of mitochondria in hDPSCs after 14 days of incubation under osteogenic medium with PBM. **A**. hDPSCs control, **B**. hDPSCs were treated with only NIR, **C**. hDPSCs were subjected with BN1, **D**. hDPSCs were treated with only Blue light. Scale bar is all 0.2 μm.

subjected to blue light showed much less decrease compared to the control in dose dependent manner, suggesting that blue light utilized here was not toxic to cell metabolism.

In blue-then-NIR light, the proliferation was better level compared to the non-irradiated hDPSCs, suggesting that the effects of blue-then-NIR light on hDPSCs might come to appear. But their contribution to the proliferation of hDPSCs was not large. However, blue light gave the effect of exciting NIR more in the ALP activity. hDPSCs exposed to blue-then-NIR light (BN1; blue light-1.2 mJ/cm^2, NIR-87.8 mJ/cm^2) were significantly enhanced than those to only NIR in the ALP activity. This result was in accordance with the ALP expression of PCR that was statistically significant (Fig. 4.4B). In case of applying blue light to be 3.6 and 12 mJ/cm^2, the corresponding ALP activity was similar to that of only NIR. It might be originated from overexpression of ROS to be toxic during lighting blue light longer (Fig. 4.4A). Interestingly, the expression of SOD2, which catalyzes the dismutation of the superoxide radical into either ordinary molecular oxygen or hydrogen peroxide in the mitochondria, was not statistically significant but alike with the control or more than. The difference in two results may be reasoned by which ROS evaluation was from just exposure of light to hDPSCs and PCR analysis was conducted at 14 day after irradiation. In contrast, quantification of forming calcium deposit that was evaluated by ARS staining demonstrated elevation in calcium content in mode of only NIR by nearly 1.2-fold compared to non-irradiated hDPSCs at 21 days but decrease in mode of blue-then-NIR light at the same day. It demonstrates that blue light did not contributed hDPSCs to form calcium deposit.

Interestingly, PCR data demonstrates that only NIR significantly elevated the expression of RUNX2, TGFb1 and OPN gene, while blue-then-NIR light enhanced the expression of COL1A (BN2), ALP (BN1), OPN (BN2 and BN3), and DSPP (BN3) gene. But not all of them were statistically significant. Osteoblast differentiation *in vitro* may be characterized in three stages: (1) cell proliferation, early osteogenic differentiation, (2) matrix maturation, and (3) matrix mineralization[167]. During proliferation, several extracellular matrix proteins may be detected (collagen I, TGF-b, and fibronectin). The matrix maturation may be characterized by maximal expression of ALP. At the beginning of matrix mineralization, genes for proteins (OCN, OPN, and DSPP) are expressed and once mineralization is completed, calcium deposition may be visualized using ARS staining[167]. Here, we discovered that as hDPSCs progress in differentiation, effects of light kinds come to appear. hDPSCs exposed to only NIR and blue-then-NIR light significantly expressed TGFb1

(PCR data) and ALP (ALP activity data) and OPN and DSPP (PCR data), respectively. Given that TGFb1 and ALP are early indicator of differentiation and OPN and DSPP late indicator, it may be pondered that NIR may strongly promote early factors in differentiation and blue light late factors, in spite that NIR was combined with blue light more intensively. According to previous study[80], TGFb1 gene which is activated by NIR triggers hDPSCs to differentiate into osteoblast to form dentin structure.

In present study, blue-then-NIR light less contributed to activate TGFb1 gene. DSPP is the most abundant ECM in dentin and is processed into three major forms: dentin sialoprotein (DSP), dentin glycoprotein (DGP) and dentin phosphoprotein (DPP). Among them, DSP and DPP are chiefly expressed in odontoblasts and dentin[168]. In PCR data, overexpression of DSPP than the control suggests that shorter NIR with longer blue light (BN3) may promote formation of dentin with which it activates hDPSCs to differentiate into odontoblasts. RUNX-2 is now recognized as one of the most important osteogenic differentiation transcription factor. In the present study, hDPSCs was similarly responsed to both only NIR and blue-then-NIR light in the expression of RUNX-2. SOD2 is pivotal in reactive oxygen species (ROS) release during oxidative stress in mitochondria. In present study, the expression of SOD2 in the hDPSCs was mild over NIR and blue-then-NIR light. It suggests that NIR and blue-then-NIR light does not produce a burst of ROS to be harmful to metabolism in mitochondria. In addition, the mitochondrial shapes in analysis of TEM reflects on such things, that is, blue light did not exert on hDPSCs harmfully.

4.5 Conclusion

In conclusion, the DL yields turned out that blue-then-NIR light make the functional state of hDPSCs excite to higher level than that of only NIR. In addition, the yields revealed that a photoreceptor of blue light may be in complex III in mitochondrial electron transport chain system. The effect of blue-then-NIR on differentiation of hDPSCs into osteogenesis showed that the ALP activity of blue-then-NIR light was higher than that of only NIR, as shown in DL yields. However, ARS results exhibited blue-then-NIR light was decreased in calcium deposition than that of only NIR after 21 days of irradiation. Results of PCR showed that TGF-b1 was highly activated by NIR and DSPP as an important factor for forming dentin was highly promoted by blue-then-NIR light. Those results can be utilized to enhance effectiveness of hDPSCs to differentiate clinically.

Chapter 5

Generation of dentin upon beagle's tooth by means of photobiomodulation

5.1 Introduction

Teeth are complex organs containing two separate specialized hard tissues, dentin and enamel, which form an integrated attachment complex with bone via a specialized ligament. Embryologically, teeth are ectodermal organs that form from sequential reciprocal interactions between oral epithelial cells (ectoderm) and cranial neural crest derived mesenchymal cells. The epithelial cells give rise to enamel forming ameloblasts, and the mesenchymal cells form all other differentiated cells. Teeth continue developing postnatally; the outer covering of enamel gradually becomes harder, and root formation, which is essential for tooth function, only starts to occur as part of tooth eruption in children.

After grown-up, the teeth is maintained by tooth's proper function and metabolism and repeatedly repaired and restored. Some stem cells can be used for tooth repair, restoration and regeneration and, significantly, non-dental uses, such a developing stem cell-based therapies for major life-threatening diseases. For dentin formation, dental pulp stem cells is used and for cementum formation, periodontal ligament stem cells used. In particular, dentin is a relatively inert tissue. During primary dintinogenesis growth factors and bioactive molecules are secreted by odontoblasts and are incorporated within the dentin extracellular matrix[169]. These molecules are bound to protein precursors or binding proteins and sequestered in a protected state within dentin[170-172]. In here, an important but often overlooked advantage of teeth as a source of stem cells is that postnatal root formation (a rich source of dental stem cells) is a developmental process, and thus cells involved in root formation are more embryonic-like than other sources of dental stem cells. The humble tooth clearly has a very important role to play in future developments in regenerative medicine.

In spite of such this, the studies in dental regeneration has been faced a number of obstacles in clinical trials. Although many animal models have been developed, it can not still overcome in practicing dentists. We noticed dentin as an alternative materials. Following tissue injury, a complex series of events,

involving various intra- and extracellular signaling, are initiated with the aim of promoting tissue repair. Bioactive molecules released from dentin have the potential to initiate the cellular events, which may lead to regeneration of pulp and dentine[173]. Hence, this study aimed to assess dentin formation following exposure of near infrared (NIR) to a whole tooth. NIR light has been employed to stimulate or induce biological event; proliferation and differentiation[72, 73, 84, 123-125, 174]. As known to be lower scattering and absorbing by water molecules, NIR light from either light emission diode (LED) or laser propagates into whole tooth and is able to stimulate periodontal ligament (PDL) and dental pulp stem cells (hDPSCs) as most important cells in regeneration. In addition, we also identify the regeneration of PDL with NIR light to determine whether NIR light promote chemotaxis and growth of odontoblasts.

5.2 Materials and Methods

5.2.1 Animal

The research was conducted as an *in vivo* experimental study. The research protocol was approved by the Animal Research Ethics Committee with permit number of SNU-120427-2-2. Male beagle (n = 1), weighing 12 kg was used in this study. The animal were housed in collective cage under standard conditions of temperature (22 ± 2 °C), relative humidity (55 ± 10%), and light/dark cycle (12 / 12 h). The animal was fed with crushed commercial dog food and water. For this study, the targeted tissue was divided into two groups. One group was both right upper and lower jaw for controls including premolars (P1-4). Another group was both left upper and lower jaw for PBM including premolars (P1-4).

5.2.2 Photobiomodulation

In this study, an 9-LED array that was composed of 810 nm LEDs (MTE2081-OH5, Marktech Optoelectronics, USA) with half intensity beam angle of ± 7 degree was used to irradiate the teeth of beagle. The array was operated in a pulsed wave (PW) mode with frequency of 300 Hz of duty cycle 30 % and was switched by 8-bit micro controller device (UM_MC95FG308_V3.20_EN, Korea). Power density of 1.91 mW/cm^2 which was measured by a power meter (PM-SUB-100, Thorlabs, USA), was applied for 42 sec to be energy density of 80 mJ/cm^2. The light intensity was checked before every experiment and the LED-array was held perpendicular to the

Figure 5.1 The LED system of PBM and exposure to teeth of beagle

mucosa, directly contacting the tissue surface to irradiate daily for induction of formation of neo-dentin throughout the 8-week (Fig. 5.1).

5.2.3 Histological procedure

After 8-week of irradiation, the animal was euthanized with a lethal dose of sodium-penthotal. Mandibular blocks were retrieved and stored in a 5 % formaldehyde solution (pH 7). The upper jaw and lower jaw were separately dissected from them and immediately immersed in a solution of 4 % formaldehyde to be fixed for 2-week. The fixed specimens were decalcified with rapid decalifier (Shandon TBD-1™, Thermo Scientific, USA) for 8 days by means of shaker with 10 RMP. The samples were dehydrated in ethyl alcohol of gradually increasing concentrations from 70 to 100 %. After paraffin embedding, the samples were serially sectioned to be a thickness of 6 μm and stained with hematoxylin-eosin (H&E). The sections were counterstained with primary polyclonal antibody to DMP1 (Takara Bio Inc., Otsu, Shiga, Japan) to identify vascularity in odontoblast layer in pulp chamber.

5.2.4 Micro-CT tomography

The dissected mandibular blocks were scanned using a SkyScan micro CT scanner (SkyScan 1172 X-ray Microtomograph, Antwerp, Belgium). The scanner was composed with a X-ray tube (80-kV/125 μA) and a precision object manipulator for moving the sample. The scanner was equipped with a twelve-bit digital cooled CCD camera with fiber optics (pixel size 11.2–11.6 μm, object to source 105.95 mm, camera to source 217.9 mm). An aluminium filter with 0.5- mm-thickness was utilized. As previous study[175], the mandibular blocks was mounted in a 7-mm-diameter plastic container on the scanning platform and the transmission X-ray image was set for 180 degrees of rotation with 0.4° rotational steps. The work of scanning was required 60 min to be completed for one specimen. Each raw data set was then reconstructed into images using SkyScan's cluster reconstruction software (NRecon/NRecon Server). One preliminary image was scanned in the automatic setting and another with histogram adjustment as appropriate for complete processing; this process optimizes the contrast over the density range of the interest, i.e. root and the root canal. Cross-sections were then reconstructed using a modified Feldkamp cone-beam algorithm (NRecon, Version 1.5.1.4; 11.6 μm average pixel size, image size: 900 × 900 pixel).

5.2.5 Scanning electron microscopy (SEM)

For taking an analysis of SEM, the decalcified samples were dehydrated sequentially with increasing concentrations of ethanol 930, 50, 80, and 100 %), coated with gold, and visualized at an accelerating voltage using a scanning electron microscope (Zeiss, Munich, Germany).

5.2.6 Statistical analysis

The means and standard deviations of each parameter were calculated for two groups. Differences between the groups were analyzed using student's t test that was performed using Microsoft Excel.

5.3 Results

5.3.1 Development of dentin tissue was verified by Micro-CT tomography

We investigated whether PBM could develop a resident dentin into more additional one. In this animal model, the premolars (P1, P2, P3, P4) were centrally observed by micro-CT analysis in the lower and upper jaw (right side as controls and left side as PBM) at 8 weeks after PBM. The PBM-resulting tooth successfully promoted more production of dentin to be averagely increase of 15.5 and 4.2 % for the upper and the lower jaw compared with the controls (right side jaw), respectively (Fig. 5.2). Each tooth revealed 13.3, 17.1, 11.3, and 20.0 % increase for P1, P2, P3, and P4 of upper jaw, respectively, while 3.6, 6.0, 0.0, and 7.0 % increase for lower jaw, respectively. The increment of dentin of upper jaw by means of PBM was more greatly than that of lower jaw (Fig. 5.2).

5.3.2 Histological analysis of teeth

We next performed the H&E staining for tooth to identify the promotion of dentin by PBM. To do this, we representatively sectioned P1 of both lower and upper jaw as A, B and C cut in Fig. 5.2A. The resulting analysis revealed that both the controls and the PBMs throughout all cuts were histologically similar, that is, they have all composites of consisting pulp chamber: dentin, predentin, odontoblast, and pulp stem cells. Nevertheless, as the result of analysis of micro-CT, we was not able to find out a difference in production of dentin for the control and the PBMs (Fig. 5.3).

5.3.3 Structural analysis by SEM

In order to identify whether the dentin resulting from mineralization of

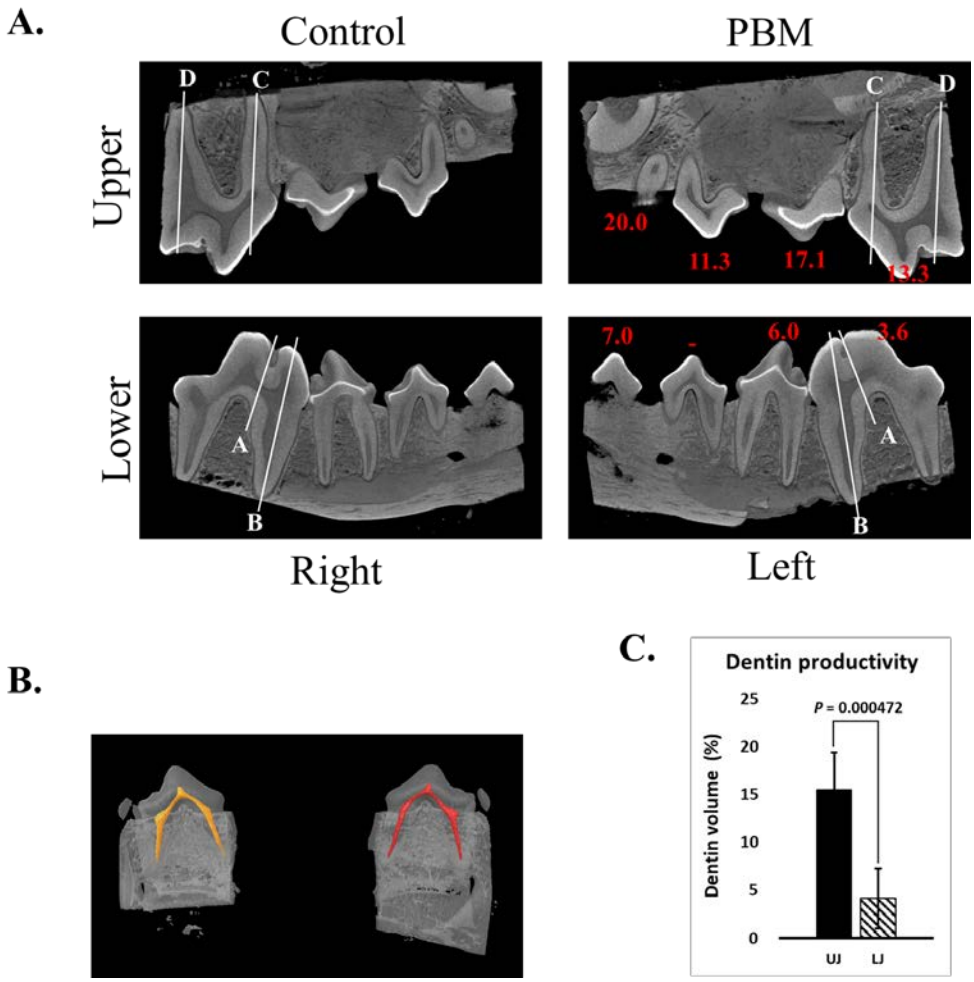

Figure 5.2 Micro-CT images. **(A)** Upper and lower jaw of beagle's teeth. Right sides were used as control and left side for PBM. NIR daily exposed the teeth to be energy density of 80 mJ/cm^2 for 8-week. Changes of the volume of pulp cavity indicating as dentin formation were measured through analysis of micro-CT images to be 13.3 (P1), 17.1 (P2) , 11.3 (P3), and 20.0 % (P4) for upper jaw and 3.6, 6.0, 0.0, and 7.0 % for lower jaw. Average of dentin formation for upper jaw was 15.5 %, while 4.5 % for lower jaw **(C). (B)** It shows a representative analyzing volume of dentin formation for premolar number 2 (P2).

odontoblast that was differentiated from pulp stem cells by means of PBM was produced more compared with the controls, we performed the analysis of SEM for C-cut of first premolar (Fig. 5.2A). The SEM images revealed that both the control and the tooth by PBM had distinctive layers of dentin, odontoblast, cell-free zone, and cell-rich zone. Higher magnification observations revealed that a layer of odontoblast cells subjected to PBM were lined against the predentin-like tissue, while the control did not, even though that had odontoblast layer (Fig. 5.4). The odontoblasts by PBM were most likely to be seen coming out from dentin's tubules, while the control did not see any cells although there was a layer of odontoblast (Fig. 5.4d,e).

5.3.4 Developed periodontal ligament by PBM

To investigate the development of periodontal ligament with PBM, we examined histological analysis by H&E for D-cuts of the control and the tooth by PBM (Fig. 5.2A). We was able to observe more the dense ligament of the tooth by PBM than the control over three parts region (Fig. 5.5).

5.3.5 Vasculature by PBM

Vasculature is important in promoting dentinogenesis of odontoblast. To identify, immunohistochemistry was performed with DMP1, in which was made known to stain the tubular epithelium of the distal tubule [176]. The tubular epitheilium was stained moderately other than peripheral tissue. Compared to the control, it was observed that vasculature was developed for PBM-irradiated sample in the site of layer of odontoblast (Fig. 5.6).

5.4 Discussion

There are two modes for PBM: continuous wave (CW) and pulsed wave (PW). PW mode is a modality that alternatively turns on LED or laser in time, while CW mode constantly turns on ones. In view of effectiveness, PW has been known to be more effective on biological systems than CW[84, 177]. It is generation of less heating that PW has quench time following the pulsed on times, thus PW is able to use high power of light instantly. The biological systems may also have some fundamental frequency that exists in the range of tens to hundreds of Hz[84]. We investigated previously the effects of PBM on proliferation and differentiation of dental pulp stem cells (hDPSCs) *in vitro* [177]. We examined PW over 1, 3, 30, 300 and 3000 Hz for hDPSCs in

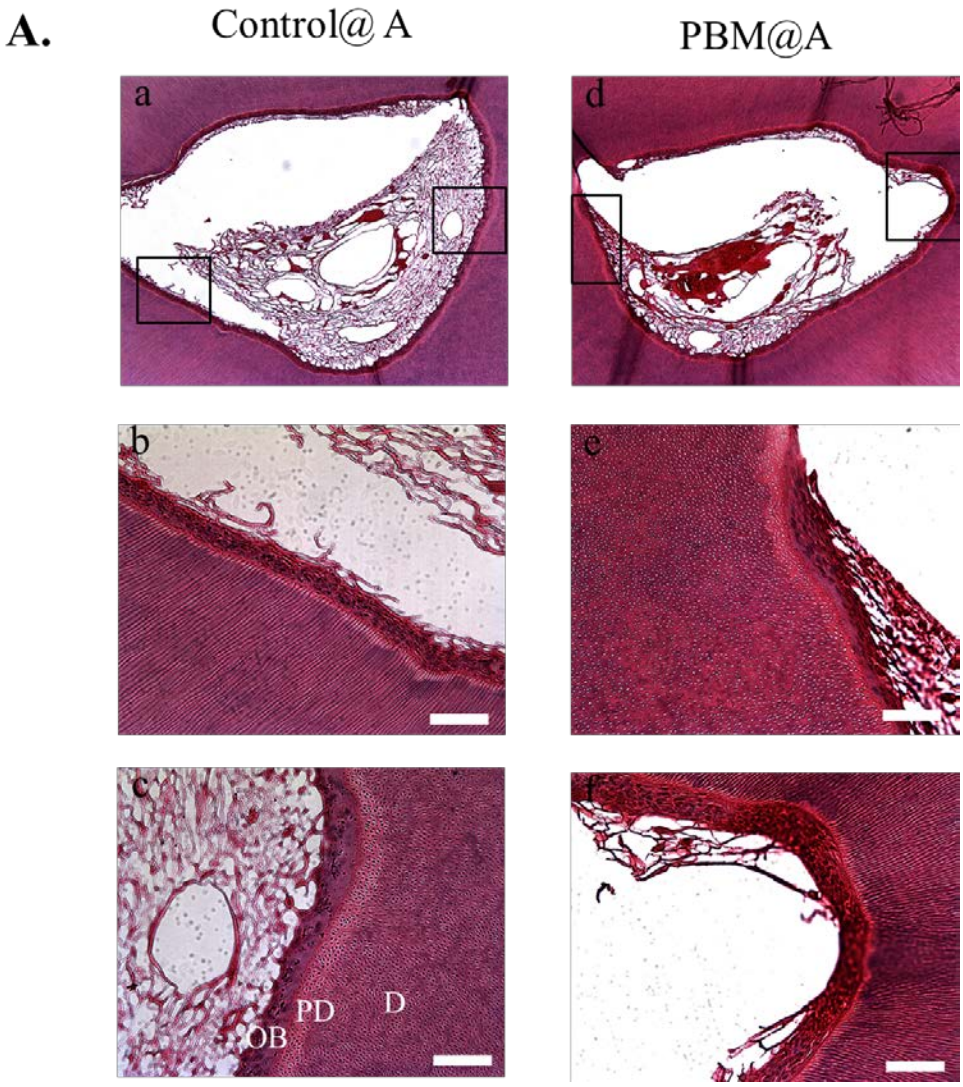
A.
Control@ A
PBM@A
a
d
b
e
c
PD
D
OB
f

B.

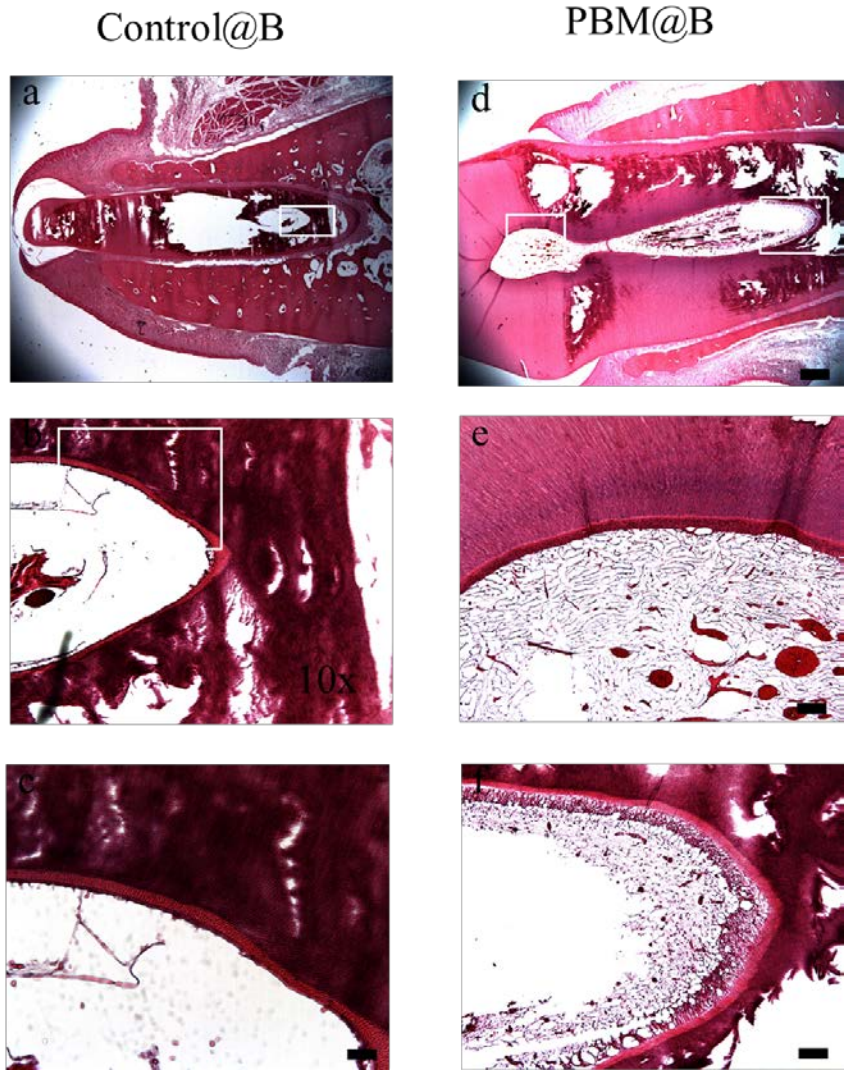

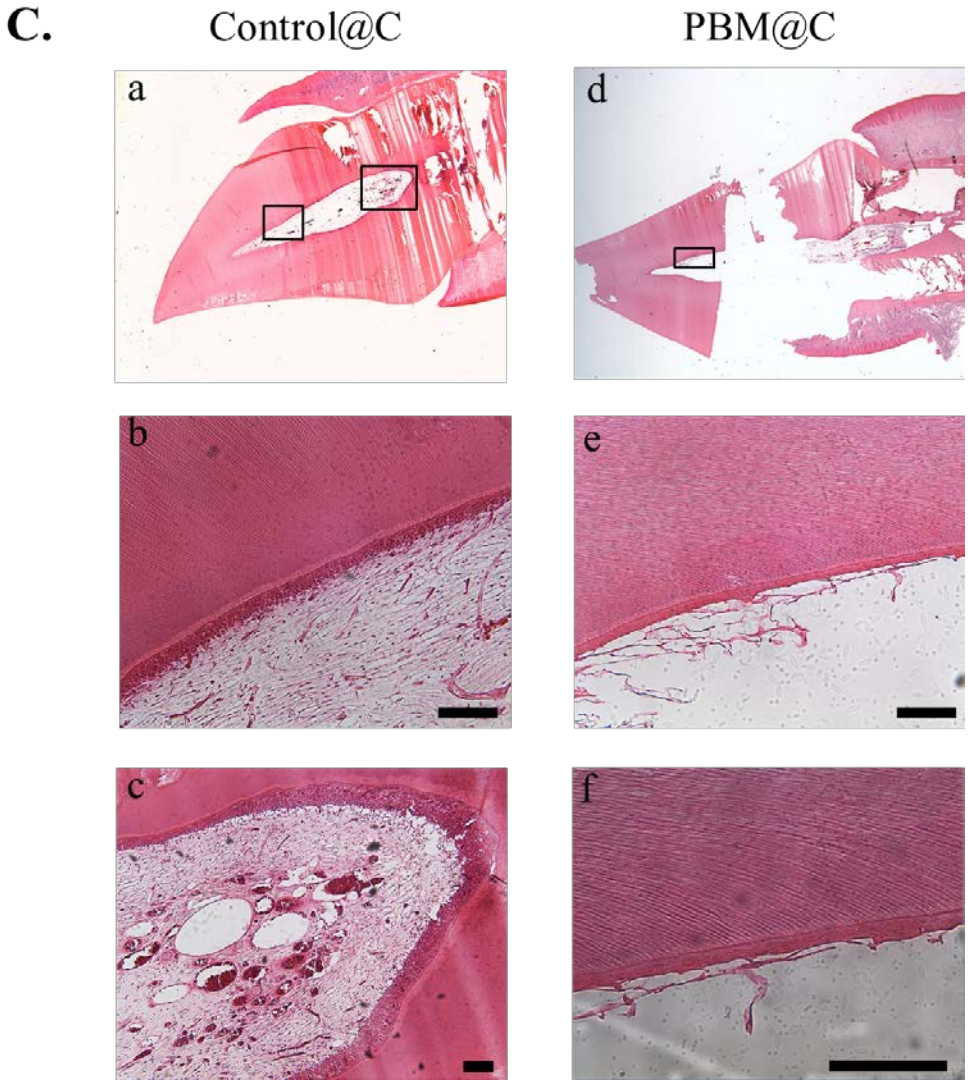

Figure 5.3 H & E images for **A-, B-** and **C-**cut of teeth in Fig. 5.2A. The layer of dentin, predentin and odontoblast was observed over all samples. Scale bar is 50 μm in all images.

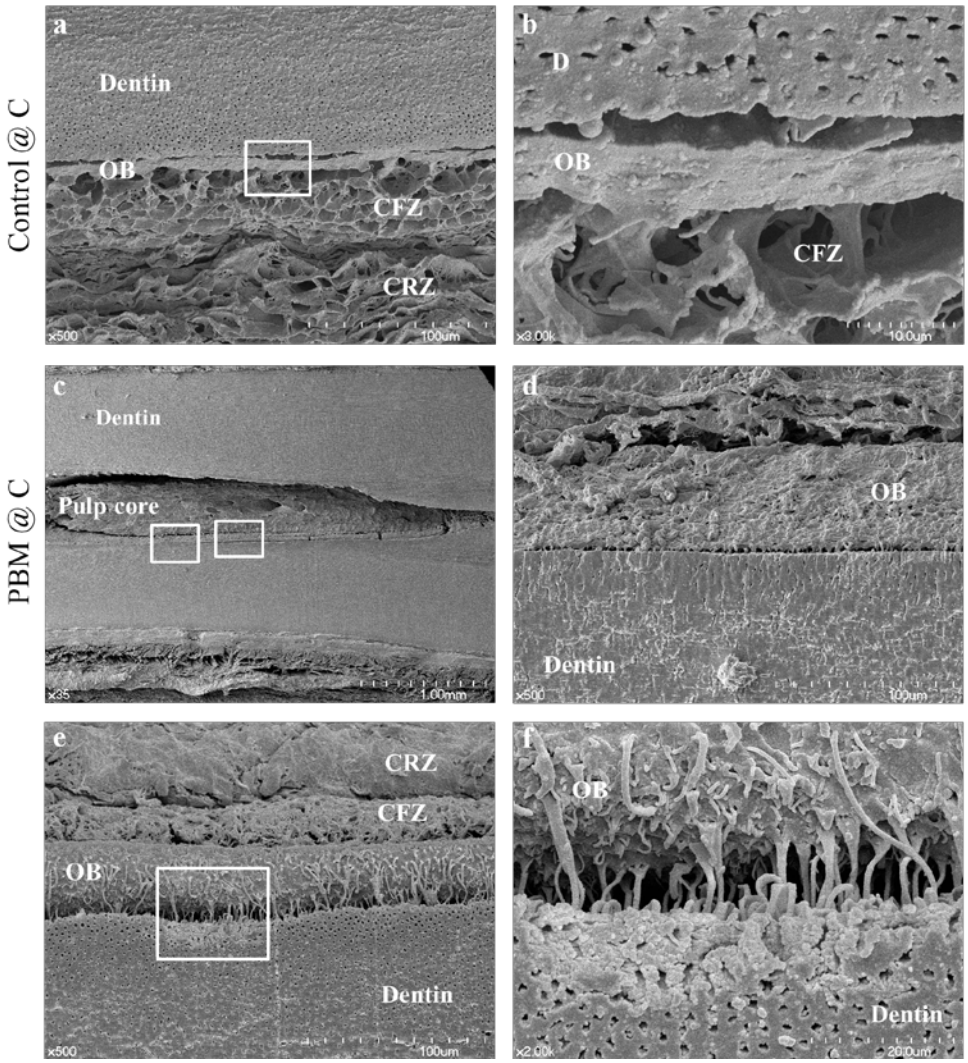

Figure 5.4 SEM images. These images got from C-cut as shown in Fig. 5.2A. **(a)** and **(b)** control. **(c) ~ (f)** were teeth subjected to PBM. Activated odontoblasts capable of generating new tubular dentin were observed **(f)** while even though odontoblast-like layer was there **(b).** Scale size is 10, 1, 100, 10, 10, and 2 μm for **(a)** to **(f).**

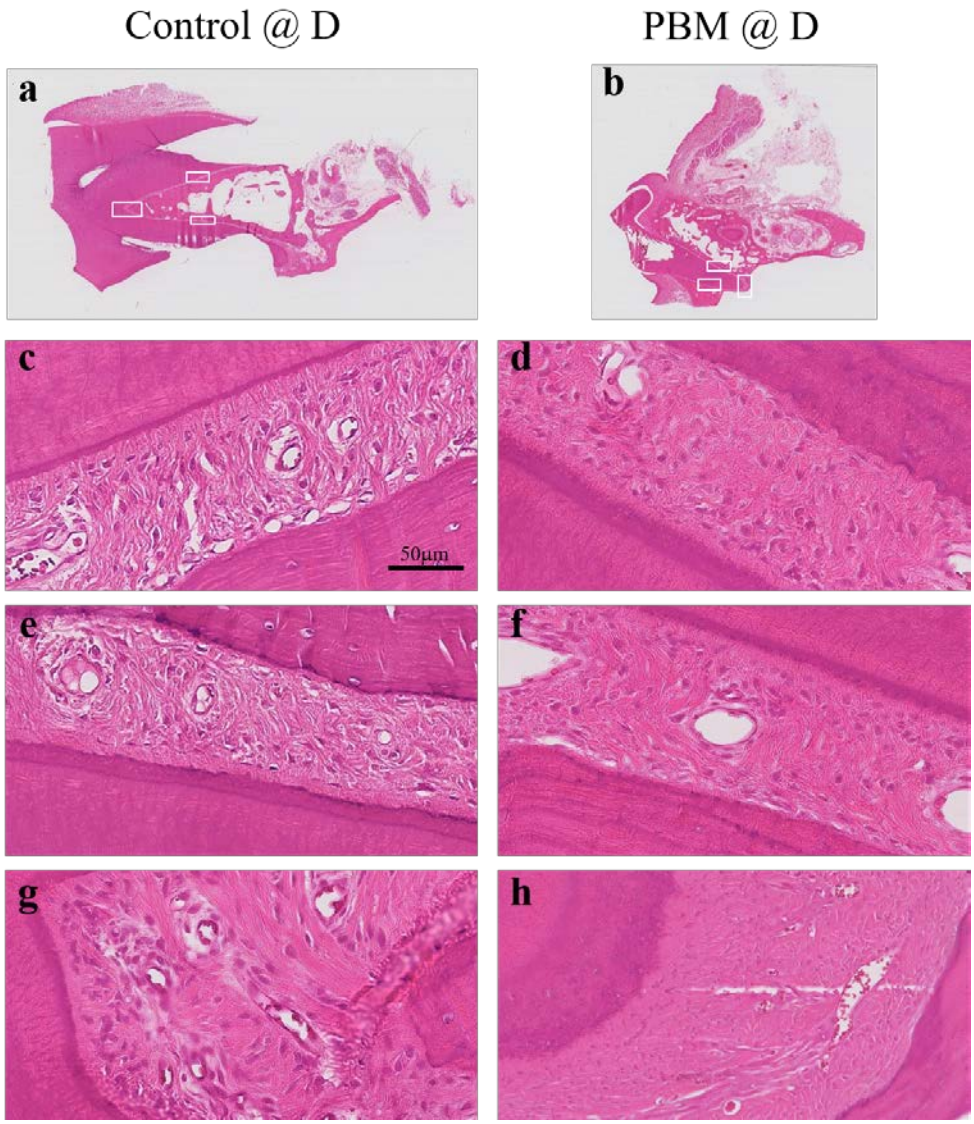

Figure 5.5. H & E images for PDL layer from D-cut in Fig. 5.2A. Their magnificent was performed to be 40 X.

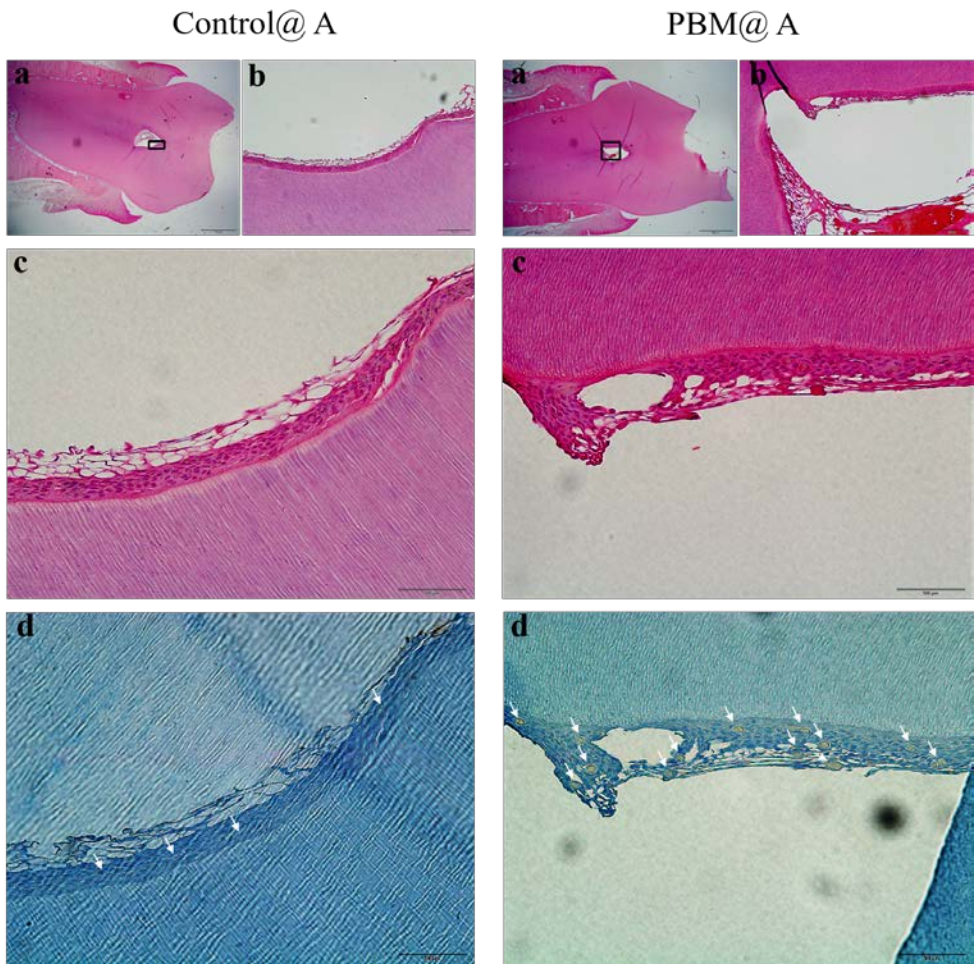

Figure 5.6. Vasculature images that were assessed by immunohistochemistry of DMP1 from A-cut in Fig. 5.2A. Arrows indicate the tubular epithelium of the distal tubule. Scale bar for **c** and **d** of control and PBM samples is 500 μm.

proliferating and differentiating, including CW experiment, keeping energy density constant.

PW has been more effective on proliferation and differentiation than CW. Among PWs, it was, in particular, 300 Hz-PW that produced highest induction of osteogenesis *in vitro* from hDPSCs supplemented with ascorbic acid and dexamethasone. The effectiveness of 300 Hz-PW was in accordance with results of production of cytosolic reactive oxygen species (ROS) by PBM. The ROS has been known to trigger the transforming growth factor beta 1 (TGF-b1) in dental tissue and following stimulation of TGF-b1 to hDPSCs make hDPSCs toward dentinogenic dfiferentaition[80]. Origin of the ROS is reported to be produced in complex I and complex III in the mitochondrial electron transport chain system which produce adenosine triphosphate (ATP). Both complex I and III produce same kind of superoxide (O_2^-) anion from electrons leaked at those complexes. Various kinds of ROSs result from this superoxide anion. Even though we exactly do not know about the mechanisms of higher harvest of 300 Hz-PW on differentiation, migration rate of electrons in the mitochondrial transport chain to react with oxides may be considered to synchronize with period time of 300 Hz. This result was identified from the delayed luminescence (DL), which is the prolonged ultra-weaker emission of optical photons from a biological sample and present mitochondrial behaviors to incident light. The DL has been utilized to investigate apoptotic progress and distinguish between normal and cancer cells. The DL is dependent on light wavelength to be applied to cells. We found out the DL was also dependent on period of turning on and off light source (so-called pulse frequency), appearing higher level of exciting for 300 Hz-PW herein.

Hence, we applied 300-Hz-PW-PBM to beagle's teeth to verify whether production of dentin tissue is promoted by PBM *in vivo*. In general, PBM is examined with damaged spot of a tooth including separated control. Before starting examination, samples are tomographed by a micro-CT to compare after completion. We applied PBM for normal dental tissue without any damages and took the control that was in the absence of PBM. Not knowing an initial volume of pulp chamber, we got started the examination, taking the controls on right side of beagle's jaw (upper and lower jaw) and the PBMs on the opposite side. After completing the examination, the results revealed that the volume of pulp chamber for the samples of premolar subjected to 300-Hz-PW was increased to be about 15 % and 4.2 % among upper jaws and lower ones, respectively, compared to the controls (right sides). Without initial data, because we set samples without PBM as controls after 8 weeks of examination,

it is able to be controversial that compares among upper jaws and lower jaws. Nevertheless, it is important for the results of PBM. First, it is only this result for the development of dentin tissue by means of PBM, in particular, 300-Hz-PW. Maintenance of dental pulp function is critical for the homeostasis of teeth; loss of dental pulp is often followed by tooth fracture and/or periapical disease and, finally, loss of teeth. When dental pulp is infected, it is difficult for the immune system to eradicate the infection, due to lack of blood supply to the pulp. Partially removing the infected pulp, termed partial pulpectomy, has proved to be ineffective, as infecting organisms may be left behind[178, 179]. Thus infection of adult pulp by trauma or caries often necessitates root canal therapy, in which the entire pulp is removed and the pulp cavity disinfected and filled with an artificial material. In the present study, it presented a possible alternative for overcoming lack of blood supply to the pulp. It is due to that the dentin formation may reflect on active blood supply to the pulp differentiating toward odontoblast and then the following active odontoblast forming dentin tissue. Increase in vascularity with PBM also provide an evidence of such thing. On the other hands, dentin is regared as a bioactive extracellular matrix, which contain dentin sialophosphoprotein (DSPP) and TGF-beta as an important signaling molecules[180, 181]. The tissue may be activated by NIR light and release such materials to trigger or promote pulp stem cells to differentiate into odontoblast.

Second, 300-Hz-PBM can make other tissues including periodontal ligament (PDL) active to be healthy. NIR light that was used in our study travels into pulp cavity through enamel and dentin tissue and simultaneously PDL. Such an integrated complex all get influence on irradiated light. In particular, PDL tissue that is put outer complex get stronger light than the others. There is many of vascularity in the PDL and pulp cavity. Thus the light can make them active to form new vasculature. In our study, we observed that the 300-Hz-PBM promoted PDL to be much more compared to the control. PDL plays key roles of absorbing external mechanical force and brace the tooth to be set. Thus the more PDL forms, the healthier the tooth become. Taken together, our findings show that odontoblast activation/dentin formation/increase vascularity can be accomplished with a 300-Hz-PBM mediated approach[182]. This study is the first step toward reaching the goal of regenerating functional pulp/dentin that is very similar to its natural conterparts. To achieve this goal, future investigations must include the use of a damaged dentin model, being with data as control from micro-CT to be captured before starting examination. Besides gaining vascularity, the analysis

of the regenerated pulp/dentin tissue requires extensive immunohistochemistry.

5.5 Conclusion

In conclusion, the PBM promoted increase of 15.5 % in formation of dentin in a Beagle's tooth by analysis of micro-CT, compared to the controls. The Results of PBM *in vitro* might be reflected on *in vivo*. It may be by PBM that odontoblast was activated, in which shown in analysis of SEM. H&E verifies that periodontal ligament (PDL) was made dense by PBM. PBM may be utilized to make dentin or PDL healthy.

Chapter 6

Summary

Delayed luminescence (DL) is a spectral emission from the optical range to NIR radiated after the illumination source is switched off. DL can demonstrate cellular reduction/oxidation states in relation to cytochrome c oxidase, which produces reactive oxygen species (ROS) in the mitochondrial respiratory chain. DL can determine cellular phase in the proliferation and differentiation due to that the cellular redox state differ in their phases. In this study, DL showed that 300-Hz pulsed wave photobiomodulation (PW-PBM) dominantly had a prolonged DL pattern among PW-PBMs and a higher degree of the excitation level and a lower temporal trend of the decay probability as well. The resulting mitochondrial activity showed increases in the mitochondrial number, volume density and length, accompanying the production of ROS and the enhanced alkaline phosphatase (ALP) activity.

Moreover, in order to verify the 300-Hz-PW-PBM in another ways, a diverse assess was performed. In analysis of cytoplasmic membrane potential (CMP), ALP activity and ROS production, 30 % duty cycle and 300-3000 Hz pulse frequencies showed the significant effects on osteogenic differentiation of hDPSC. The PW-PBM elevated the activation of TGF-β1 signaling pathway enhancing hDPSC-dentinogenic differentiation *in vitro* as well. In the fashion of blue-then-NIR light, it make more hDPSCs into osteogenesis than that of only NIR in assaying the ALP activity. Results of polymerase chain reaction (PCR) showed that transforming growth factor-beta-1 (TGF-b1) was highly activated by NIR and dentin sialophosphoprotein (DSPP) as an important factor for forming dentin was highly promoted by blue-then-NIR light.

In a beagle test for formation of dentin *in vivo*, PBM promoted increase of 15.5 % in analysis of micro-CT, compared to the controls. Odontoblast was identified to be activated, accompanying periodontal ligament (PDL) that was made dense by PBM, in which showed in assess of SEM and H&E. Those results may be utilized to enhance effectiveness of hDPSCs to differentiate into osteogenesis.

Reference

[1] P. Mojzes, L. Chinsky, P.Y. Turpin, Interaction of Electronically Excited Copper(Ii) Porphyrin with Oligonucleotides and Polynucleotides - Exciplex Building Process by Photoinitiated Axial Ligation of Porphyrin to Thymine and Uracil Residues, J Phys Chem-Us, 97 (1993) 4841-4847.

[2] S.G. Kruglik, P. Mojzes, Y. Mizutani, T. Kitagawa, P.Y. Turpin, Time-resolved resonance raman study of the exciplex formed between excited Cu-porphyrin and DNA, J Phys Chem B, 105 (2001) 5018-5031.

[3] R.R. Anderson, J.A. Parrish, The optics of human skin, J Invest Dermatol, 77 (1981) 13-19.

[4] J.R. Zijp, J.J. Bosch, Theoretical model for the scattering of light by dentin and comparison with measurements, Appl Opt, 32 (1993) 411-415.

[5] K. Kwon, T. Son, K.J. Lee, B. Jung, Enhancement of light propagation depth in skin: cross-validation of mathematical modeling methods, Lasers in medical science, 24 (2009) 605-615.

[6] B.J. Quirk, M. Torbey, E. Buchmann, S. Verma, H.T. Whelan, Near-infrared photobiomodulation in an animal model of traumatic brain injury: improvements at the behavioral and biochemical levels, Photomedicine and laser surgery, 30 (2012) 523-529.

[7] H. Tuby, L. Maltz, U. Oron, Low-level laser irradiation (LLLI) promotes proliferation of mesenchymal and cardiac stem cells in culture, Lasers in surgery and medicine, 39 (2007) 373-378.

[8] F.F. Sperandio, A. Simoes, L. Correa, A.C. Aranha, F.S. Giudice, M.R. Hamblin, S.C. Sousa, Low-level laser irradiation promotes the proliferation and maturation of keratinocytes during epithelial wound repair, Journal of biophotonics, 8 (2015) 795-803.

[9] T.N. Demidova-Rice, E.V. Salomatina, A.N. Yaroslavsky, I.M. Herman, M.R. Hamblin, Low-level light stimulates excisional wound healing in mice, Lasers in surgery and medicine, 39 (2007) 706-715.

[10] K.D. Desmet, D.A. Paz, J.J. Corry, J.T. Eells, M.T. Wong-Riley, M.M. Henry, E.V. Buchmann, M.P. Connelly, J.V. Dovi, H.L. Liang, D.S. Henshel, R.L. Yeager, D.S. Millsap, J. Lim, L.J. Gould, R. Das, M. Jett, B.D. Hodgson, D. Margolis, H.T. Whelan, Clinical and experimental applications of NIR-LED photobiomodulation, Photomedicine and laser surgery, 24 (2006) 121-128.

[11] P.R. Arany, R.S. Nayak, S. Hallikerimath, A.M. Limaye, A.D. Kale, P. Kondaiah, Activation of latent TGF-beta1 by low-power laser *in vitro* correlates with

increased TGF-beta1 levels in laser-enhanced oral wound healing, Wound Repair Regen, 15 (2007) 866-874.
[12] P.A. Jenkins, J.D. Carroll, How to report low-level laser therapy (LLLT)/photomedicine dose and beam parameters in clinical and laboratory studies, Photomedicine and laser surgery, 29 (2011) 785-787.
[13] T.I. Karu, Mitochondrial signaling in mammalian cells activated by red and near-IR radiation, Photochemistry and photobiology, 84 (2008) 1091-1099.
[14] J.T. Eells, M.T. Wong-Riley, J. VerHoeve, M. Henry, E.V. Buchman, M.P. Kane, L.J. Gould, R. Das, M. Jett, B.D. Hodgson, D. Margolis, H.T. Whelan, Mitochondrial signal transduction in accelerated wound and retinal healing by near-infrared light therapy, Mitochondrion, 4 (2004) 559-567.
[15] M.W. Cleeter, J.M. Cooper, V.M. Darley-Usmar, S. Moncada, A.H. Schapira, Reversible inhibition of cytochrome c oxidase, the terminal enzyme of the mitochondrial respiratory chain, by nitric oxide. Implications for neurodegenerative diseases, FEBS letters, 345 (1994) 50-54.
[16] F. Antunes, A. Boveris, E. Cadenas, On the mechanism and biology of cytochrome oxidase inhibition by nitric oxide, Proceedings of the National Academy of Sciences of the United States of America, 101 (2004) 16774-16779.
[17] A. Galkin, A. Higgs, S. Moncada, Nitric oxide and hypoxia, Essays in biochemistry, 43 (2007) 29-42.
[18] S. Wu, F. Zhou, Y. Wei, W.R. Chen, Q. Chen, D. Xing, Cancer phototherapy via selective photoinactivation of respiratory chain oxidase to trigger a fatal superoxide anion burst, Antioxid Redox Signal, 20 (2014) 733-746.
[19] R.O. Poyton, K.A. Ball, Therapeutic photobiomodulation: nitric oxide and a novel function of mitochondrial cytochrome c oxidase, Discov Med, 11 (2011) 154-159.
[20] N. Lane, Cell biology: power games, Nature, 443 (2006) 901-903.
[21] S. Shiva, M.T. Gladwin, Shining a light on tissue NO stores: near infrared release of NO from nitrite and nitrosylated hemes, J Mol Cell Cardiol, 46 (2009) 1-3.
[22] T.D. Magrini, N.V. dos Santos, M.P. Milazzotto, G. Cerchiaro, H. da Silva Martinho, Low-level laser therapy on MCF-7 cells: a micro-Fourier transform infrared spectroscopy study, J Biomed Opt, 17 (2012) 101516.
[23] G.R. Dubyak, Signal transduction by P2-purinergic receptors for extracellular ATP, Am J Respir Cell Mol Biol, 4 (1991) 295-300.
[24] H. Karmouty-Quintana, Y. Xia, M.R. Blackburn, Adenosine signaling during

acute and chronic disease states, J Mol Med (Berl), 91 (2013) 173-181.
[25] J.Y. Wu, C.H. Chen, C.Z. Wang, M.L. Ho, M.L. Yeh, Y.H. Wang, Low-power laser irradiation suppresses inflammatory response of human adipose-derived stem cells by modulating intracellular cyclic AMP level and NF-kappaB activity, PloS one, 8 (2013) e54067.
[26] A.C. Chen, P.R. Arany, Y.Y. Huang, E.M. Tomkinson, S.K. Sharma, G.B. Kharkwal, T. Saleem, D. Mooney, F.E. Yull, T.S. Blackwell, M.R. Hamblin, Low-level laser therapy activates NF-kB via generation of reactive oxygen species in mouse embryonic fibroblasts, PloS one, 6 (2011) e22453.
[27] A. Bindoli, M.P. Rigobello, Principles in redox signaling: from chemistry to functional significance, Antioxid Redox Signal, 18 (2013) 1557-1593.
[28] H.J. Forman, F. Ursini, M. Maiorino, An overview of mechanisms of redox signaling, J Mol Cell Cardiol, 73 (2014) 2-9.
[29] T.I. Karu, L.V. Pyatibrat, N.I. Afanasyeva, Cellular effects of low power laser therapy can be mediated by nitric oxide, Lasers in surgery and medicine, 36 (2005) 307-314.
[30] W.C. Tsai, C.C. Hsu, J.H. Pang, M.S. Lin, Y.H. Chen, F.C. Liang, Low-level laser irradiation stimulates tenocyte migration with up-regulation of dynamin II expression, PloS one, 7 (2012) e38235.
[31] H. Abrahamse, Regenerative medicine, stem cells, and low-level laser therapy: future directives, Photomedicine and laser surgery, 30 (2012) 681-682.
[32] K.H. Min, J.H. Byun, C.Y. Heo, E.H. Kim, H.Y. Choi, C.S. Pak, Effect of Low-Level Laser Therapy on Human Adipose-Derived Stem Cells: *In Vitro* and In Vivo Studies, Aesthetic Plast Surg, 39 (2015) 778-782.
[33] X. Liao, G.H. Xie, H.W. Liu, B. Cheng, S.H. Li, S. Xie, L.L. Xiao, X.B. Fu, Helium-neon laser irradiation promotes the proliferation and migration of human epidermal stem cells in vitro: proposed mechanism for enhanced wound re-epithelialization, Photomedicine and laser surgery, 32 (2014) 219-225.
[34] D.M. Soares, F. Ginani, A.G. Henriques, C.A. Barboza, Effects of laser therapy on the proliferation of human periodontal ligament stem cells, Lasers in medical science, 30 (2015) 1171-1174.
[35] Y.Y. Huang, A.C. Chen, J.D. Carroll, M.R. Hamblin, Biphasic dose response in low level light therapy, Dose Response, 7 (2009) 358-383.
[36] J.D. Carroll, M.R. Milward, P.R. Cooper, M. Hadis, W.M. Palin, Developments in low level light therapy (LLLT) for dentistry, Dental materials : official publication of the Academy of Dental Materials, 30 (2014) 465-475.

[37] S. Gronthos, M. Mankani, J. Brahim, P.G. Robey, S. Shi, Postnatal human dental pulp stem cells (DPSCs) in vitro and in vivo, Proceedings of the National Academy of Sciences of the United States of America, 97 (2000) 13625-13630.

[38] M. Miura, S. Gronthos, M. Zhao, B. Lu, L.W. Fisher, P.G. Robey, S. Shi, SHED: stem cells from human exfoliated deciduous teeth, Proceedings of the National Academy of Sciences of the United States of America, 100 (2003) 5807-5812.

[39] W. Sonoyama, Y. Liu, D. Fang, T. Yamaza, B.M. Seo, C. Zhang, H. Liu, S. Gronthos, C.Y. Wang, S. Wang, S. Shi, Mesenchymal stem cell-mediated functional tooth regeneration in swine, PloS one, 1 (2006) e79.

[40] Y. Makino, H. Yamaza, K. Akiyama, L. Ma, Y. Hoshino, K. Nonaka, Y. Terada, T. Kukita, S. Shi, T. Yamaza, Immune therapeutic potential of stem cells from human supernumerary teeth, Journal of dental research, 92 (2013) 609-615.

[41] L. Ma, R. Aijima, Y. Hoshino, H. Yamaza, E. Tomoda, Y. Tanaka, S. Sonoda, G. Song, W. Zhao, K. Nonaka, S. Shi, T. Yamaza, Transplantation of mesenchymal stem cells ameliorates secondary osteoporosis through interleukin-17-impaired functions of recipient bone marrow mesenchymal stem cells in MRL/lpr mice, Stem cell research & therapy, 6 (2015) 104.

[42] M.M. Kanafi, Y.B. Rajeshwari, S. Gupta, N. Dadheech, P.D. Nair, P.K. Gupta, R.R. Bhonde, Transplantation of islet-like cell clusters derived from human dental pulp stem cells restores normoglycemia in diabetic mice, Cytotherapy, 15 (2013) 1228-1236.

[43] P. Eduardo Fde, D.F. Bueno, P.M. de Freitas, M.M. Marques, M.R. Passos-Bueno, P. Eduardo Cde, M. Zatz, Stem cell proliferation under low intensity laser irradiation: a preliminary study, Lasers in surgery and medicine, 40 (2008) 433-438.

[44] I.M. Zaccara, F. Ginani, H.G. Mota-Filho, A.C. Henriques, C.A. Barboza, Effect of low-level laser irradiation on proliferation and viability of human dental pulp stem cells, Lasers in medical science, 30 (2015) 2259-2264.

[45] L.O. Pereira, J.P. Longo, R.B. Azevedo, Laser irradiation did not increase the proliferation or the differentiation of stem cells from normal and inflamed dental pulp, Arch Oral Biol, 57 (2012) 1079-1085.

[46] A. Ballini, F. Mastrangelo, G. Gastaldi, L. Tettamanti, N. Bukvic, S. Cantore, T. Cocco, R. Saini, A. Desiate, E. Gherlone, S. Scacco, Osteogenic differentiation and gene expression of dental pulp stem cells under low-

level laser irradiation: a good promise for tissue engineering, J Biol Regul Homeost Agents, 29 (2015) 813-822.

[47] M.J. Holder, M.R. Milward, W.M. Palin, M.A. Hadis, P.R. Cooper, Effects of red light-emitting diode irradiation on dental pulp cells, Journal of dental research, 91 (2012) 961-966.

[48] S. Matsui, Y. Tsujimoto, K. Matsushima, Stimulatory effects of hydroxyl radical generation by Ga-Al-As laser irradiation on mineralization ability of human dental pulp cells, Biological & pharmaceutical bulletin, 30 (2007) 27-31.

[49] M. Wohlgenannt, X.M. Jiang, Z.V. Vardeny, R.A. Janssen, Conjugation-length dependence of spin-dependent exciton formation rates in pi-conjugated oligomers and polymers, Phys Rev Lett, 88 (2002) 197401.

[50] F. Musumeci, L.A. Applegate, G. Privitera, A. Scordino, S. Tudisco, H.J. Niggli, Spectral analysis of laser-induced ultraweak delayed luminescence in cultured normal and tumor human cells: temperature dependence, Journal of photochemistry and photobiology. B, Biology, 79 (2005) 93-99.

[51] F. Musumeci, G. Privitera, A. Scordino, S. Tudisco, C. Lo Presti, L.A. Applegate, H.J. Niggli, Discrimination between normal and cancer cells by using spectral analysis of delayed luminescence., Appl Phys Lett, 86 (2005).

[52] P. Chen, L. Zhang, F. Zhang, J.T. Liu, H. Bai, G.Q. Tang, L. Lin, Spectral discrimination between normal and leukemic human sera using delayed luminescence, Biomed Opt Express, 3 (2012) 1787-1792.

[53] E.G. Mik, J. Stap, M. Sinaasappel, J.F. Beek, J.A. Aten, T.G. van Leeuwen, C. Ince, Mitochondrial PO2 measured by delayed fluorescence of endogenous protoporphyrin IX, Nat Methods, 3 (2006) 939-945.

[54] E.G. Mik, T. Johannes, C.J. Zuurbier, A. Heinen, J.H. Houben-Weerts, G.M. Balestra, J. Stap, J.F. Beek, C. Ince, In vivo mitochondrial oxygen tension measured by a delayed fluorescence lifetime technique, Biophys J, 95 (2008) 3977-3990.

[55] F.A. Harms, W.M.I. de Boon, G.M. Balestra, S.I.A. Bodmer, T. Johannes, R.J. Stolker, E.G. Mik, Oxygen-dependent delayed fluorescence measured in skin after topical application of 5-aminolevulinic acid, Journal of biophotonics, 4 (2011) 731-739.

[56] G.H. Schatz, A.R. Holzwarth, Mechanisms of chlorophyll fluorescence revisited: Prompt or delayed emission from photosystem II with closed reaction centers?, Photosynth Res, 10 (1986) 309-318.

[57] E.G. Mik, T. Johannes, C.J. Zuurbier, A. Heinen, J.H.P.M. Houben-Weerts, G.M.

Balestra, J. Stap, J.F. Beek, C. Ince, In vivo mitochondrial oxygen tension measured by a delayed fluorescence lifetime technique, Biophys J, 95 (2008) 3977-3990.

[58] S. Desagher, J.C. Martinou, Mitochondria as the central control point of apoptosis, Trends Cell Biol, 10 (2000) 369-377.

[59] T. Karu, Primary and secondary mechanisms of action of visible to near-IR radiation on cells, Journal of photochemistry and photobiology. B, Biology, 49 (1999) 1-17.

[60] M.D. Maloney, J.J. Goater, R. Parsons, H. Ito, R.J. O'Keefe, P.T. Rubery, M.H. Drissi, E.M. Schwarz, Safety and efficacy of ultraviolet-a light-activated gene transduction for gene therapy of articular cartilage defects, J Bone Joint Surg Am, 88 (2006) 753-761.

[61] T.I. Karu, L.V. Pyatibrat, T.P. Ryabykh, Melatonin modulates the action of near infrared radiation on cell adhesion, J Pineal Res, 34 (2003) 167-172.

[62] R. Duan, T.C. Liu, Y. Li, H. Guo, L.B. Yao, Signal transduction pathways involved in low intensity He-Ne laser-induced respiratory burst in bovine neutrophils: a potential mechanism of low intensity laser biostimulation, Lasers in surgery and medicine, 29 (2001) 174-178.

[63] X. Shen, W. Mei, X. Xu, Activation of neutrophils by a chemically separated but optically coupled neutrophil population undergoing respiratory burst, Experientia, 50 (1994) 963-968.

[64] Y. Wollman, S. Rochkind, In vitro cellular processes sprouting in cortex microexplants of adult rat brains induced by low power laser irradiation, Neurol Res, 20 (1998) 470-472.

[65] H.L. Liang, H.T. Whelan, J.T. Eells, H. Meng, E. Buchmann, A. Lerch-Gaggl, M. Wong-Riley, Photobiomodulation partially rescues visual cortical neurons from cyanide-induced apoptosis, Neuroscience, 139 (2006) 639-649.

[66] Y. Wollman, S. Rochkind, R. Simantov, Low power laser irradiation enhances migration and neurite sprouting of cultured rat embryonal brain cells, Neurol Res, 18 (1996) 467-470.

[67] Y. Zhang, S. Song, C.C. Fong, C.H. Tsang, Z. Yang, M. Yang, cDNA microarray analysis of gene expression profiles in human fibroblast cells irradiated with red light, J Invest Dermatol, 120 (2003) 849-857.

[68] G. Shefer, T.A. Partridge, L. Heslop, J.G. Gross, U. Oron, O. Halevy, Low-energy laser irradiation promotes the survival and cell cycle entry of skeletal muscle satellite cells, J Cell Sci, 115 (2002) 1461-1469.

[69] T.I. Karu, Multiple roles of cytochrome c oxidase in mammalian cells under action of red and IR-A radiation, IUBMB Life, 62 (2010) 607-610.

[70] Y.S. Chen, S.F. Hsu, C.W. Chiu, J.G. Lin, C.T. Chen, C.H. Yao, Effect of low-power pulsed laser on peripheral nerve regeneration in rats, Microsurgery, 25 (2005) 83-89.

[71] B.S. Sushko, P. Lymans'kyi Iu, S.O. Huliar, [Action of the red and infrared electromagnetic waves of light-emitting diodes on the behavioral manifestation of somatic pain], Fiziol Zh, 53 (2007) 51-60.

[72] B. Mvula, T. Mathope, T. Moore, H. Abrahamse, The effect of low level laser irradiation on adult human adipose derived stem cells, Lasers in medical science, 23 (2008) 277-282.

[73] D. Yang, W. Yi, E. Wang, M. Wang, Effects of light-emitting diode irradiation on the osteogenesis of human umbilical cord mesenchymal stem cells in vitro, Scientific reports, 6 (2016) 37370.

[74] S. Hallen, P. Brzezinski, Light-induced structural changes in cytochrome c oxidase: implication for the mechanism of electron and proton gating, Biochim Biophys Acta, 1184 (1994) 207-218.

[75] Y. Ozawa, N. Shimizu, Y. Abiko, Low-energy diode laser irradiation reduced plasminogen activator activity in human periodontal ligament cells, Lasers in surgery and medicine, 21 (1997) 456-463.

[76] V. Paakkonen, J. Vuoristo, T. Salo, L. Tjaderhane, Effects of TGF-beta 1 on interleukin profile of human dental pulp and odontoblasts, Cytokine, 40 (2007) 44-51.

[77] J.Y. Wu, Y.H. Wang, G.J. Wang, M.L. Ho, C.Z. Wang, M.L. Yeh, C.H. Chen, Low-power GaAlAs laser irradiation promotes the proliferation and osteogenic differentiation of stem cells via IGF1 and BMP2, PloS one, 7 (2012) e44027.

[78] Y.Y. Huang, K. Nagata, C.E. Tedford, T. McCarthy, M.R. Hamblin, Low-level laser therapy (LLLT) reduces oxidative stress in primary cortical neurons in vitro, Journal of biophotonics, 6 (2013) 829-838.

[79] J.A. Salmos-Brito, R.F. de Menezes, C.E. Teixeira, R.K. Gonzaga, B.H. Rodrigues, R. Braz, R.V. Bessa-Nogueira, M.E. Gerbi, Evaluation of low-level laser therapy in patients with acute and chronic temporomandibular disorders, Lasers in medical science, 28 (2013) 57-64.

[80] P.R. Arany, A. Cho, T.D. Hunt, G. Sidhu, K. Shin, E. Hahm, G.X. Huang, J. Weaver, A.C. Chen, B.L. Padwa, M.R. Hamblin, M.H. Barcellos-Hoff, A.B. Kulkarni, J.M. D, Photoactivation of endogenous latent transforming growth factor-beta1 directs dental stem cell differentiation for regeneration, Science translational medicine, 6 (2014) 238ra269.

[81] M.E. Chaves, A.R. Araujo, A.C. Piancastelli, M. Pinotti, Effects of low-power

light therapy on wound healing: LASER x LED, An Bras Dermatol, 89 (2014) 616-623.
[82] A.N. Emelyanov, V.V. Kiryanova, Photomodulation of proliferation and differentiation of stem cells by the visible and infrared light, Photomedicine and laser surgery, 33 (2015) 164-174.
[83] L.F. de Freitas, M.R. Hamblin, Proposed Mechanisms of Photobiomodulation or Low-Level Light Therapy, IEEE J Sel Top Quantum Electron, 22 (2016).
[84] J.T. Hashmi, Y.Y. Huang, S.K. Sharma, D.B. Kurup, L. De Taboada, J.D. Carroll, M.R. Hamblin, Effect of pulsing in low-level light therapy, Lasers in surgery and medicine, 42 (2010) 450-466.
[85] A. Scordino, A. Campisi, R. Grasso, R. Bonfanti, M. Gulino, L. Iauk, R. Parenti, F. Musumeci, Delayed luminescence to monitor programmed cell death induced by berberine on thyroid cancer cells, J Biomed Opt, 19 (2014) 117005.
[86] T. Kamiya, M. Courtney, M.O. Laukkanen, Redox-Activated Signal Transduction Pathways Mediating Cellular Functions in Inflammation, Differentiation, Degeneration, Transformation, and Death, Oxid Med Cell Longev, 2016 (2016) 8479718.
[87] R.H. Burdon, Superoxide and hydrogen peroxide in relation to mammalian cell proliferation, Free Radic Biol Med, 18 (1995) 775-794.
[88] J. Tafur, P.J. Mills, Low-intensity light therapy: exploring the role of redox mechanisms, Photomedicine and laser surgery, 26 (2008) 323-328.
[89] J. Tafur, E.P. Van Wijk, R. Van Wijk, P.J. Mills, Biophoton detection and low-intensity light therapy: a potential clinical partnership, Photomedicine and laser surgery, 28 (2010) 23-30.
[90] N. Li, K. Ragheb, G. Lawler, J. Sturgis, B. Rajwa, J.A. Melendez, J.P. Robinson, Mitochondrial complex I inhibitor rotenone induces apoptosis through enhancing mitochondrial reactive oxygen species production, J Biol Chem, 278 (2003) 8516-8525.
[91] Y.H. Han, S.H. Kim, S.Z. Kim, W.H. Park, Antimycin A as a mitochondria damage agent induces an S phase arrest of the cell cycle in HeLa cells, Life Sci, 83 (2008) 346-355.
[92] B. Devaraj, M. Usa, H. Inaba, Biophotons: Ultraweak light emission from living systems, Curr Opin Solid St M, 2 (1997) 188-193.
[93] A. Scordino, I. Baran, M. Gulino, C. Ganea, R. Grasso, J.H. Niggli, F. Musumeci, Ultra-weak delayed luminescence in cancer research: a review of the results by the ARETUSA equipment, Journal of photochemistry and

photobiology. B, Biology, 139 (2014) 76-84.
[94] C. Zhang, M. Soori, F.L. Miles, R.A. Sikes, D.D. Carson, L.W. Chung, M.C. Farach-Carson, Paracrine factors produced by bone marrow stromal cells induce apoptosis and neuroendocrine differentiation in prostate cancer cells, Prostate, 71 (2011) 157-167.
[95] I. Baran, C. Ganea, S. Privitera, A. Scordino, V. Barresi, F. Musumeci, M.M. Mocanu, D.F. Condorelli, I. Ursu, R. Grasso, M. Gulino, A. Garaiman, N. Omusso, G.A.P. Cirrone, G. Cuttone, Detailed Analysis of Apoptosis and Delayed Luminescence of Human Leukemia Jurkat T Cells after Proton Irradiation and Treatments with Oxidant Agents and Flavonoids, Oxidative Medicine and Cellular Longevity, DOI Artn 498914
10.1155/2012/498914(2012).
[96] I. Baran, D. Ionescu, S. Privitera, A. Scordino, M.M. Mocanu, F. Musumeci, R. Grasso, M. Gulino, A. Iftime, I.T. Tofolean, A. Garaiman, A. Goicea, R. Irimia, A. Dimancea, C. Ganea, Mitochondrial respiratory complex I probed by delayed luminescence spectroscopy, J Biomed Opt, 18 (2013) 127006.
[97] S.N. Letuta, S.N. Pashkevich, A.T. Ishemgulov, Y.D. Lantukh, E.K. Alidzhanov, S.S. Sokabaeva, V.V. Bryukhanov, Delayed luminescence of erythrosine in biological tissue and photodynamic therapy dosimetry, Journal of photochemistry and photobiology. B, Biology, 163 (2016) 232-236.
[98] P.A. Lapchak, L. De Taboada, Transcranial near infrared laser treatment (NILT) increases cortical adenosine-5'-triphosphate (ATP) content following embolic strokes in rabbits, Brain Res, 1306 (2010) 100-105.
[99] P.A. Lapchak, K.F. Salgado, C.H. Chao, J.A. Zivin, Transcranial near-infrared light therapy improves motor function following embolic strokes in rabbits: an extended therapeutic window study using continuous and pulse frequency delivery modes, Neuroscience, 148 (2007) 907-914.
[100] B. Halliwell, Free radicals, reactive oxygen species and human disease: a critical evaluation with special reference to atherosclerosis, Br J Exp Pathol, 70 (1989) 737-757.
[101] D.J. Suggett, O. Prášil, M.A. Borowitzka, SpringerLink (Online service), Chlorophyll a Fluorescence in Aquatic Sciences: Methods and Applications, Developments in Applied Phycology 4, Springer Science+Business Media B.V.,, Dordrecht, 2010, pp. 1 online resource.
[102] L. Brizhik, F. Musumeci, A. Scordino, M. Tedesco, A. Triglia, Nonlinear dependence of the delayed luminescence yield on the intensity of irradiation in the framework of a correlated soliton model, Phys Rev E Stat Nonlin Soft Matter Phys, 67 (2003) 021902.

[103] G. Pal, A. Dutta, K. Mitra, M.S. Grace, T.B. Romanczyk, X. Wu, K. Chakrabarti, J. Anders, E. Gorman, R.W. Waynant, D.B. Tata, Effect of low intensity laser interaction with human skin fibroblast cells using fiber-optic nano-probes, Journal of photochemistry and photobiology. B, Biology, 86 (2007) 252-261.

[104] I. Belevich, D.A. Bloch, N. Belevich, M. Wikstrom, M.I. Verkhovsky, Exploring the proton pump mechanism of cytochrome c oxidase in real time, Proceedings of the National Academy of Sciences of the United States of America, 104 (2007) 2685-2690.

[105] G. Gilboa, R. Chen, N. Brenner, History-dependent multiple-time-scale dynamics in a single-neuron model, J Neurosci, 25 (2005) 6479-6489.

[106] M.A. Aon, S. Cortassa, E. Marban, B. O'Rourke, Synchronized whole cell oscillations in mitochondrial metabolism triggered by a local release of reactive oxygen species in cardiac myocytes, J Biol Chem, 278 (2003) 44735-44744.

[107] S. Lee, E. Tak, J. Lee, M.A. Rashid, M.P. Murphy, J. Ha, S.S. Kim, Mitochondrial H2O2 generated from electron transport chain complex I stimulates muscle differentiation, Cell Res, 21 (2011) 817-834.

[108] S.L. Pereira, M. Graos, A.S. Rodrigues, S.I. Anjo, R.A. Carvalho, P.J. Oliveira, E. Arenas, J. Ramalho-Santos, Inhibition of mitochondrial complex III blocks neuronal differentiation and maintains embryonic stem cell pluripotency, PloS one, 8 (2013) e82095.

[109] M.F. Forni, J. Peloggia, K. Trudeau, O. Shirihai, A.J. Kowaltowski, Murine Mesenchymal Stem Cell Commitment to Differentiation Is Regulated by Mitochondrial Dynamics, Stem cells, 34 (2016) 743-755.

[110] T. Ahmad, K. Aggarwal, B. Pattnaik, S. Mukherjee, T. Sethi, B.K. Tiwari, M. Kumar, A. Micheal, U. Mabalirajan, B. Ghosh, S. Sinha Roy, A. Agrawal, Computational classification of mitochondrial shapes reflects stress and redox state, Cell Death Dis, 4 (2013) e461.

[111] S. Passarella, T. Karu, Absorption of monochromatic and narrow band radiation in the visible and near IR by both mitochondrial and non-mitochondrial photoacceptors results in photobiomodulation, Journal of photochemistry and photobiology. B, Biology, 140 (2014) 344-358.

[112] M.J. Conlan, J.W. Rapley, C.M. Cobb, Biostimulation of wound healing by low-energy laser irradiation. A review, J Clin Periodontol, 23 (1996) 492-496.

[113] L. Lilge, K. Tierney, E. Nussbaum, Low-level laser therapy for wound healing: feasibility of wound dressing transillumination, J Clin Laser Med

Surg, 18 (2000) 235-240.
[114] R.T. Chow, L. Barnsley, Systematic review of the literature of low-level laser therapy (LLLT) in the management of neck pain, Lasers in surgery and medicine, 37 (2005) 46-52.
[115] J.C. Rojas, F. Gonzalez-Lima, Low-level light therapy of the eye and brain, Eye Brain, 3 (2011) 49-67.
[116] H. Chung, T. Dai, S.K. Sharma, Y.Y. Huang, J.D. Carroll, M.R. Hamblin, The nuts and bolts of low-level laser (light) therapy, Ann Biomed Eng, 40 (2012) 516-533.
[117] S.O. el Sayed, M. Dyson, Effect of laser pulse repetition rate and pulse duration on mast cell number and degranulation, Lasers in surgery and medicine, 19 (1996) 433-437.
[118] V. Schubert, Effects of phototherapy on pressure ulcer healing in elderly patients after a falling trauma. A prospective, randomized, controlled study, Photodermatol Photoimmunol Photomed, 17 (2001) 32-38.
[119] T.I. Karu, L.V. Pyatibrat, S.F. Kolyakov, N.I. Afanasyeva, Absorption measurements of a cell monolayer relevant to phototherapy: reduction of cytochrome c oxidase under near IR radiation, Journal of photochemistry and photobiology. B, Biology, 81 (2005) 98-106.
[120] D.M. Walsh, G.D. Baxter, J.M. Allen, Lack of effect of pulsed low-intensity infrared (820 nm) laser irradiation on nerve conduction in the human superficial radial nerve, Lasers in surgery and medicine, 26 (2000) 485-490.
[121] Y. Ueda, N. Shimizu, Effects of pulse frequency of low-level laser therapy (LLLT) on bone nodule formation in rat calvarial cells, J Clin Laser Med Surg, 21 (2003) 271-277.
[122] P. Brondon, I. Stadler, R.J. Lanzafame, Pulsing influences photoradiation outcomes in cell culture, Lasers in surgery and medicine, 41 (2009) 222-226.
[123] A. Stein, D. Benayahu, L. Maltz, U. Oron, Low-level laser irradiation promotes proliferation and differentiation of human osteoblasts in vitro, Photomedicine and laser surgery, 23 (2005) 161-166.
[124] J.F. Hou, H. Zhang, X. Yuan, J. Li, Y.J. Wei, S.S. Hu, In vitro effects of low-level laser irradiation for bone marrow mesenchymal stem cells: proliferation, growth factors secretion and myogenic differentiation, Lasers in surgery and medicine, 40 (2008) 726-733.
[125] S. Bouvet-Gerbettaz, E. Merigo, J.P. Rocca, G.F. Carle, N. Rochet, Effects of low-level laser therapy on proliferation and differentiation of murine

bone marrow cells into osteoblasts and osteoclasts, Lasers in surgery and medicine, 41 (2009) 291-297.
[126] H.P. Wu, M.A. Persinger, Increased mobility and stem-cell proliferation rate in Dugesia tigrina induced by 880nm light emitting diode, Journal of photochemistry and photobiology. B, Biology, 102 (2011) 156-160.
[127] K.M. AlGhamdi, A. Kumar, N.A. Moussa, Low-level laser therapy: a useful technique for enhancing the proliferation of various cultured cells, Lasers in medical science, 27 (2012) 237-249.
[128] T. Yamaza, F.S. Alatas, R. Yuniartha, H. Yamaza, J.K. Fujiyoshi, Y. Yanagi, K. Yoshimaru, M. Hayashida, T. Matsuura, R. Aijima, K. Ihara, S. Ohga, S. Shi, K. Nonaka, T. Taguchi, In vivo hepatogenic capacity and therapeutic potential of stem cells from human exfoliated deciduous teeth in liver fibrosis in mice, Stem cell research & therapy, 6 (2015) 171.
[129] M.A. Aon, S. Cortassa, B. O'Rourke, Mitochondrial oscillations in physiology and pathophysiology, Adv Exp Med Biol, 641 (2008) 98-117.
[130] S. Sart, L. Song, Y. Li, Controlling Redox Status for Stem Cell Survival, Expansion, and Differentiation, Oxid Med Cell Longev, 2015 (2015) 105135.
[131] Y.Y. Jo, H.J. Lee, S.Y. Kook, H.W. Choung, J.Y. Park, J.H. Chung, Y.H. Choung, E.S. Kim, H.C. Yang, P.H. Choung, Isolation and characterization of postnatal stem cells from human dental tissues, Tissue Eng, 13 (2007) 767-773.
[132] S. Sundelacruz, M. Levin, D.L. Kaplan, Role of membrane potential in the regulation of cell proliferation and differentiation, Stem Cell Rev, 5 (2009) 231-246.
[133] S. Sundelacruz, M. Levin, D.L. Kaplan, Membrane potential controls adipogenic and osteogenic differentiation of mesenchymal stem cells, PloS one, 3 (2008) e3737.
[134] J.P. Miller, N. Yeh, A. Vidal, A. Koff, Interweaving the cell cycle machinery with cell differentiation, Cell Cycle, 6 (2007) 2932-2938.
[135] D. Pastore, M. Greco, S. Passarella, Specific helium-neon laser sensitivity of the purified cytochrome c oxidase, Int J Radiat Biol, 76 (2000) 863-870.
[136] M. van Kempen, A. van Ginneken, I. de Grijs, N. Mutsaers, T. Opthof, H. Jongsma, M. van der Heyden, Expression of the electrophysiological system during murine embryonic stem cell cardiac differentiation, Cellular physiology and biochemistry : international journal of experimental cellular physiology, biochemistry, and pharmacology, 13 (2003) 263-270.

[137] H. Beinert, R.W. Shaw, R.E. Hansen, C.R. Hartzell, Studies on the origin of the near-infrared (800-900 nm) absorption of cytochrome c oxidase, Biochim Biophys Acta, 591 (1980) 458-470.
[138] J.M. Suski, M. Lebiedzinska, M. Bonora, P. Pinton, J. Duszynski, M.R. Wieckowski, Relation between mitochondrial membrane potential and ROS formation, Methods Mol Biol, 810 (2012) 183-205.
[139] A.P. Kudin, G. Debska-Vielhaber, W.S. Kunz, Characterization of superoxide production sites in isolated rat brain and skeletal muscle mitochondria, Biomed Pharmacother, 59 (2005) 163-168.
[140] N. Urao, M. Ushio-Fukai, Redox regulation of stem/progenitor cells and bone marrow niche, Free Radic Biol Med, 54 (2013) 26-39.
[141] L. Miao, D.K. St Clair, Regulation of superoxide dismutase genes: Implications in disease, Free Radical Bio Med, 47 (2009) 344-356.
[142] Y.L. Guo, S. Chakraborty, S.S. Rajan, R. Wang, F. Huang, Effects of oxidative stress on mouse embryonic stem cell proliferation, apoptosis, senescence, and self-renewal, Stem Cells Dev, 19 (2010) 1321-1331.
[143] S. Suzuki, N. Haruyama, F. Nishimura, A.B. Kulkarni, Dentin sialophosphoprotein and dentin matrix protein-1: Two highly phosphorylated proteins in mineralized tissues, Arch Oral Biol, 57 (2012) 1165-1175.
[144] M. Pietila, S. Lehtonen, M. Narhi, I.E. Hassinen, H.V. Leskela, K. Aranko, K. Nordstrom, A. Vepsalainen, P. Lehenkari, Mitochondrial function determines the viability and osteogenic potency of human mesenchymal stem cells, Tissue Eng Part C Methods, 16 (2010) 435-445.
[145] P. Niethammer, C. Grabher, A.T. Look, T.J. Mitchison, A tissue-scale gradient of hydrogen peroxide mediates rapid wound detection in zebrafish, Nature, 459 (2009) 996-999.
[146] D. Barolet, F. Christiaens, M.R. Hamblin, Infrared and skin: Friend or foe, Journal of photochemistry and photobiology. B, Biology, 155 (2016) 78-85.
[147] S.R. Tsai, R. Yin, Y.Y. Huang, B.C. Sheu, S.C. Lee, M.R. Hamblin, Low-level light therapy potentiates NPe6-mediated photodynamic therapy in a human osteosarcoma cell line via increased ATP, Photodiagnosis Photodyn Ther, 12 (2015) 123-130.
[148] J. Liebmann, M. Born, V. Kolb-Bachofen, Blue-light irradiation regulates proliferation and differentiation in human skin cells, J Invest Dermatol, 130 (2010) 259-269.
[149] Y. Wang, Y.Y. Huang, Y. Wang, P. Lyu, M.R. Hamblin, Photobiomodulation

(blue and green light) encourages osteoblastic-differentiation of human adipose-derived stem cells: role of intracellular calcium and light-gated ion channels, Scientific reports, 6 (2016) 33719.

[150] A. Higuchi, P.Y. Shen, J.K. Zhao, C.W. Chen, Q.D. Ling, H. Chen, H.C. Wang, J.T. Bing, S.T. Hsu, Osteoblast differentiation of amniotic fluid-derived stem cells irradiated with visible light, Tissue engineering. Part A, 17 (2011) 2593-2602.

[151] A.N. Bashkatov, E.A. Genina, V.I. Kochubey, V.V. Tuchin, Optical properties of human skin, subcutaneous and mucous tissues in the wavelength range from 400 to 2000 nm, J Phys D Appl Phys, 38 (2005) 2543-2555.

[152] J.B. Lewis, J.C. Wataha, R.L. Messer, G.B. Caughman, T. Yamamoto, S.D. Hsu, Blue light differentially alters cellular redox properties, J Biomed Mater Res B Appl Biomater, 72 (2005) 223-229.

[153] M. Ohara, T. Fujikura, H. Fujiwara, Augmentation of the inhibitory effect of blue light on the growth of B16 melanoma cells by riboflavin, Int J Oncol, 22 (2003) 1291-1295.

[154] L.A. Gorgidze, S.A. Oshemkova, I.A. Vorobjev, Blue light inhibits mitosis in tissue culture cells, Biosci Rep, 18 (1998) 215-224.

[155] B.B. Aggarwal, A.T. Quintanilha, R. Cammack, L. Packer, Damage to mitochondrial electron transport and energy coupling by visible light, Biochim Biophys Acta, 502 (1978) 367-382.

[156] M. Pflaum, C. Kielbassa, M. Garmyn, B. Epe, Oxidative DNA damage induced by visible light in mammalian cells: extent, inhibition by antioxidants and genotoxic effects, Mutat Res, 408 (1998) 137-146.

[157] A.B. Stemer, B.N. Huisa, J.A. Zivin, The evolution of transcranial laser therapy for acute ischemic stroke, including a pooled analysis of NEST-1 and NEST-2, Curr Cardiol Rep, 12 (2010) 29-33.

[158] I. Baran, C. Ganea, A. Scordino, F. Musumeci, V. Barresi, S. Tudisco, S. Privitera, R. Grasso, D.F. Condorelli, I. Ursu, V. Baran, E. Katona, M.M. Mocanu, M. Gulino, R. Ungureanu, M. Surcel, C. Ursaciuc, Effects of menadione, hydrogen peroxide, and quercetin on apoptosis and delayed luminescence of human leukemia Jurkat T-cells, Cell Biochem Biophys, 58 (2010) 169-179.

[159] K.J. Campbell, N.R. Chapman, N.D. Perkins, UV stimulation induces nuclear factor kappa B (NF-kappa B) DNA-binding activity but not transcriptional activation, Biochem Soc T, 29 (2001) 688-691.

[160] P.E. Hockberger, T.A. Skimina, V.E. Centonze, C. Lavin, S. Chu, S. Dadras, J.K. Reddy, J.G. White, Activation of flavin-containing oxidases underlies light-

induced production of H2O2 in mammalian cells, Proceedings of the National Academy of Sciences of the United States of America, 96 (1999) 6255-6260.

[161] E.L. Hull, T.H. Foster, Cytochrome spectroscopy in scattering suspensions containing mitochondria and red blood cells, Appl Spectrosc, 55 (2001) 149-154.

[162] V. Massey, The chemical and biological versatility of riboflavin, Biochem Soc T, 28 (2000) 283-296.

[163] K.R. Pryde, J. Hirst, Superoxide Is Produced by the Reduced Flavin in Mitochondrial Complex I A SINGLE, UNIFIED MECHANISM THAT APPLIES DURING BOTH FORWARD AND REVERSE ELECTRON TRANSFER, Journal of Biological Chemistry, 286 (2011) 18056-18065.

[164] L.C. Shum, N.S. White, B.N. Mills, K.L. Bentley, R.A. Eliseev, Energy Metabolism in Mesenchymal Stem Cells During Osteogenic Differentiation, Stem Cells Dev, 25 (2016) 114-122.

[165] H.J. Niggli, C. Scaletta, Y. Yu, F.A. Popp, L.A. Applegate, Ultraweak photon emission in assessing bone growth factor efficiency using fibroblastic differentiation, J Photoch Photobio B, 64 (2001) 62-68.

[166] A. Scordino, A. Triglia, F. Musumeci, F. Grasso, Z. Rajfur, Influence of the presence of atrazine in water on the in-vivo delayed luminescence of Acetabularia acetabulum, J Photoch Photobio B, 32 (1996) 11-17.

[167] J.B. Lian, G.S. Stein, Development of the osteoblast phenotype: molecular mechanisms mediating osteoblast growth and differentiation, Iowa Orthop J, 15 (1995) 118-140.

[168] H.H. Ritchie, J.E. Berry, M.J. Somerman, C.T. Hanks, A.L. Bronckers, D. Hotton, P. Papagerakis, A. Berdal, W.T. Butler, Dentin sialoprotein (DSP) transcripts: developmentally-sustained expression in odontoblasts and transient expression in pre-ameloblasts, European journal of oral sciences, 105 (1997) 405-413.

[169] A.J. Smith, H. Lesot, Induction and regulation of crown dentinogenesis: embryonic events as a template for dental tissue repair?, Crit Rev Oral Biol Med, 12 (2001) 425-437.

[170] S.M. Baker, R.V. Sugars, M. Wendel, A.J. Smith, R.J. Waddington, P.R. Cooper, A.J. Sloan, TGF-beta/extracellular matrix interactions in dentin matrix: a role in regulating sequestration and protection of bioactivity, Calcif Tissue Int, 85 (2009) 66-74.

[171] A.J. Sloan, R. Moseley, K. Dobie, R.J. Waddington, A.J. Smith, TGF-beta latency-associated peptides (LAPs) in human dentin matrix and pulp,

Connect Tissue Res, 43 (2002) 381-386.
[172] A.J. Smith, J.B. Matthews, R.C. Hall, Transforming growth factor-beta1 (TGF-beta1) in dentine matrix. Ligand activation and receptor expression, European journal of oral sciences, 106 Suppl 1 (1998) 179-184.
[173] G.C. Gurtner, S. Werner, Y. Barrandon, M.T. Longaker, Wound repair and regeneration, Nature, 453 (2008) 314-321.
[174] H. Tuby, L. Maltz, U. Oron, Induction of autologous mesenchymal stem cells in the bone marrow by low-level laser therapy has profound beneficial effects on the infarcted rat heart, Lasers in surgery and medicine, 43 (2011) 401-409.
[175] P. Verma, R.M. Love, A Micro CT study of the mesiobuccal root canal morphology of the maxillary first molar tooth, Int Endod J, 44 (2011) 210-217.
[176] M. Terasawa, R. Shimokawa, T. Terashima, K. Ohya, Y. Takagi, H. Shimokawa, Expression of dentin matrix protein 1 (DMP1) in nonmineralized tissues, J Bone Miner Metab, 22 (2004) 430-438.
[177] H.B. Kim, K.Y. Baik, P.-H. Choung, J.H. Chung, Pulse frequency dependency of photobiomodulation on the bioenergetic functions of human dental pulp stem cells, Scientific reports, 7 (2017) 15927.
[178] G.T. Huang, T. Yamaza, L.D. Shea, F. Djouad, N.Z. Kuhn, R.S. Tuan, S. Shi, Stem/progenitor cell-mediated de novo regeneration of dental pulp with newly deposited continuous layer of dentin in an in vivo model, Tissue engineering. Part A, 16 (2010) 605-615.
[179] G.T. Huang, S. Gronthos, S. Shi, Mesenchymal stem cells derived from dental tissues vs. those from other sources: their biology and role in regenerative medicine, Journal of dental research, 88 (2009) 792-806.
[180] A.J. Smith, B.A. Scheven, Y. Takahashi, J.L. Ferracane, R.M. Shelton, P.R. Cooper, Dentine as a bioactive extracellular matrix, Arch Oral Biol, 57 (2012) 109-121.
[181] N. Cassidy, M. Fahey, S.S. Prime, A.J. Smith, Comparative analysis of transforming growth factor-beta isoforms 1-3 in human and rabbit dentine matrices, Arch Oral Biol, 42 (1997) 219-223.
[182] H.H. Sun, T. Jin, Q. Yu, F.M. Chen, Biological approaches toward dental pulp regeneration by tissue engineering, J Tissue Eng Regen Med, 5 (2011) e1-16.

Abstract in Korean

포토바이오모듈레이션은 가시광선 혹은 근적외선을 사용하여 생물체에 광반응을 유도하는 방법으로서, 근육통 완화 및 상처 치유, 조직 재생에 효과가 있는 것으로 알려져 있다. 이 광반응의 핵심은 광수용체로 알려진 세포내 소기관인 미토콘드리아 내에 있는 cytochrome c oxidase 이다. cytochrome c oxidase 가 빛을 흡수하면, 미토콘드리아 막전압 및 칼슘 및 산화질소 이온 농도가 상승하여 에너지원인 ATP 생성을 높이고, gene transcription 을 촉진하여 다양한 단백질을 합성하여 세포증식 및 세포분화를 촉진한다. 이 단백질 합성의 촉진은 빛을 연속 혹은 펄스방식으로 조사하는 것에 따라 다르며, 펄스방식이 효과적인 것으로 알려져 있다. 그러나 그 기전에 대해 불분명하고 펄스에 대해 특성화 되어 있지 않다. 따라서 본 연구에서는 치수줄기세포의 골분화에 대해 포토바이오모듈레이션의 기전과 펄스를 특성화 하였다. 먼저, 이를 위해서 delyed luminescence (DL)을 도입하여 근적외선을 이용하는 포토바이모듈레이션을 관찰한 결과, 연속방식보다 펄스방식에서 들뜬 상태가 높았고, 펄스방식의 300 Hz 가 높게 나타났다. 이에 따라 치수줄기세포의 분화를 살펴본 결과 펄스방식에서, 펄스방식에서는 300 Hz 에서 높은 골분화를 보였다. 이것은 줄기세포의 미토콘드리아의 수와 면적 및 길이의 증가와 미토콘드리아 내에서 생성된 유산소의 second messenger 역할에 기인한 것으로 밝혀졌다. 나아가, 펄스의 duty cycle 에 따른 줄기세포의 골분화를 살펴본 결과, 30%에서 치수줄기세포의 분화가 높게 나타났다. 이것은 줄기세포가 골분화를 진행함에 따라 세포막 전위가 낮아지는 과분극(hyperpolarization) 양상을 보이는 것과 일치하는 것으로, 1 ~ 3000 Hz 까지 10 단위로 증가하면서 살펴본 바에서도 이전과 같은 결과인

300 Hz 에서 이 양상을 보여 포토바이모듈레이션의 펄스방식이 분화에 적합함을 보였다.

한편, 치수 줄기세포의 골분화 효율을 높이기 위해서 UV 영역에 가까운 blue light 을 도입하였다. 기존 근적외선을 조사하기 전에 근적외선보다 파장은 짧지만 양자역학적인 관점에서 에너지가 두 배인 blue light 을 조사하면, 빛을 흡수하는 단백질을 더 높은 들뜬 상태로 만들 수 있어 줄기세포의 골분화를 근적외선의 단독 조사 때보다 높일 수 있다. Delayed luminescence 로 분석한 결과, 근적외선 단독 조사보다 blue light 을 먼저 조사하고 후에 근적외선을 조사한 것에서 들뜬 상태가 높게 나타났다. 초기 골분화 지표에서도 크게 나와 기존의 같은 에너지를 인가한 단독 근적외선 조사 결과에 비해 7 배 이상 증가한 것이 관찰되었다. 이 결과는 추후 논의 및 추가 실험이 필요한 상황이다. 세포실험에서 얻은 duty cycle 30%, 주파수 300 Hz 를 치아 관련 동물모델인 beagle 에 8 주 동안 매일 근적외선을 약 80 mJ/cm2 를 조사한 결과, dentin 의 생성율이 실험군에서 대조군에 비해 평균 15% 이상 증가한 것으로 나타났다. 이것은 치수줄기세포가 odontoblast 로 분화하고 이 odontoblast 가 dentin 을 생성한 것으로 보여진다. 따라서 본 연구에서는 포토바이모듈레이션을 치수줄기세포의 골분화에 적용하여 펄스방식에 대해 특성화하였고, 이 결과는 차후 포토바이모듈레이션을 임상에 적용하는데 있어 기초 데이터를 제공할 것으로 기대된다.

주요어 : 포토바이오모듈레이션, 펄스변조, delayed luminescence, 골분화, 치수줄기세포, cytochrome c oxidase

학 번 : 2014-30404